UNIVERSITY OF TURKISH AERONAUTICAL ASSOCIATION
INSTITUTE OF SCIENCE AND TECHNOLOGY

THE APPLICATION OF SPECTRAL ELEMENT METHOD TO MAGNETOSTATIC PROBLEMS

MASTER THESIS

Atakan ERCIYAS

Electrical and Electronics Engineering Department

Master Thesis Program

JANUARY 2017

UNIVERSITY OF TURKISH AERONAUTICAL ASSOCIATION
INSTITUTE OF SCIENCE AND TECHNOLOGY

THE APPLICATION OF SPECTRAL ELEMENT METHOD TO MAGNETOSTATIC PROBLEMS

MASTER THESIS

Atakan ERCIYAS

1303620001

Electrical and Electronics Engineering Department

Master Thesis Program

Supervisor: Assist. Prof. Dr. Ibrahim MAHARIQ

Atakan ERCIYAS, having student number 1303620001 and enrolled in the Master Program at the Institute of Science and Technology at the University of Turkish Aeronautical Association, after meeting all of the required conditions contained in the related regulations, has sucessfuly accomplished, in front of the jury, the presentation of the thesis prepared with the title of: The Application of Spectral Element Method to Magnetostatic Problems.

Supervisor : **Assist. Prof. Dr. Ibrahim MAHARIQ**
University of Turkish Aeronautical Assocation .....

Jurry Members : **Assist. Prof. Dr. Ozan KEYSAN**
Middle East Technical University .....

: **Assist. Prof. Dr. Hassan SHARABATY**
University of Turkish Aeronautical Assocation .....

: **Assist. Prof. Dr. Ibrahim MAHARIQ**
University of Turkish Aeronautical Assocation .....

Thesis Defense Date: 24.01.2017

STATEMENT OF NON-PLAGIARISM PAGE

I hereby declare that all information in this document has been obtained and presented in accordance with academic rules and ethical conduct. I also declare that, as required by these rules and conduct, I have fully cited and referenced all material and results that are not original to this work.

24.01.2017

Atakan ERCIYAS

ACKNOWLEDGEMENTS

I would like to thank my thesis advisor Asst. Prof. Dr. Ibrahim MAHARIQ for his patience, huge support and dedicating himself to help me for writing my thesis. He encouraged me to choose my thesis topic despite of the difficulties and he never gave up supporting me.

I would thank my mother Sevcihan Erciyas and my father Cihat Erciyas for their infinite tolerance and support.

January 2017 Atakan ERCIYAS

TABLE OF CONTENTS

LIST OF FIGURES

LIST OF SYMBOLS AND ABBREVIATIONS

∇^2	:	Laplacian Operator
Ω	:	Problem Domain
Γ	:	Boundary of Ω
Φ_i	:	Analytical trial function
N_{dof}	:	Number of global degrees of Freedom
v	:	Weight functions
$\oint_{\Gamma_h}$	:	Boundary integral of Neumann Boundary Condition
$\psi_p(\xi_1)\psi_q(\xi_2)$	:	Weight functions in two dimensions
$\psi_i(\xi_1)\psi_j(\xi_2)$	:	Trial functions in two dimensions
ξ_1 and ξ_2	:	Local Cartesian coordinates
Ω^e	:	Elemental region physical coordinates
$h_p(x)$	:	One-dimensional pth order Lagrangian polynomial
$\Phi_p^B(x)$	:	A nodal expansion
$\hat{u}_p$	:	Vector of pth degree expansion coefficient
$\hat{M}$ and $\hat{M}_{ij}$	:	1D mass matrix evaluated with GLL polynomials
$\hat{K}$	:	1D stiffness matrix evaluated with GLL polynomials
$\bar{H}$	:	Helmholtz operator
$\otimes$	:	Kronecker product
$x_1, x_2,$ x	:	Global cartesian coordinates
$f^A(\xi_1), f^B(\xi_1), f^C(\xi_2), f^D(\xi_2)$	:	The shape mapping functions of each edge of quadrilateral element
$\lvert J_{2D} \rvert$	:	Jacobian
$\mathcal{F}(v)$	:	Load vector
Γ_h	:	Neumann Boundary condition
$\Re$	:	Residual
ϕ_i	:	Truncated trial functions
χ	:	Space trial functions
$\mathcal{V}$	:	Space of weight functions
χ_N	:	Finite dimensional space of trial functions $\chi_N \subset \chi$ subspace of χ

$\mathcal{V}_N$	:	Finite dimensional space of trial solutions $\mathcal{V}_N \subset \mathcal{V}$
n	:	Unit outward normal
$\Phi_p^{\mathrm{A}}(x)$	:	Modal expansion
$\Phi_p^{\mathrm{C}}(x)$	:	Modal expansion with Legendre polynomials
δ_{pq}	:	Kronecker delta
$L_p(\xi)$	:	Lagrange interpolants through the zeros of the pth degree Gauss-Lobatto polynomials
L_1 and L_2	:	Lengths of rectangular domain
$D_{N,ij}^{(1)}$ and $D, \hat{D}$	:	The nodal values of the first derivative of the GLL Lagrangian polynomials are called one dimensional differentiation matrix
$\mathcal{L}$	:	Steady diffusion operator
x_i^e	:	Global Cartesian coordinates of the element
$J_{2D}(\xi_1, \xi_2)$	:	2D Jacobian matrix
$\frac{\partial}{\partial x_1}$ and $\frac{\partial}{\partial x_2}$	:	Partial derivatives of global coordinates
$J(\xi)$	:	Dimensionless Jacobian

Abbreviations

SEM	:	Spectral element method
FEM	:	Finite element method
GLL	:	Gauss Lobatto Legendre
GL	:	Gauss Legendre
CPU	:	Central processing unit
RAM	:	Random access memory

Subscripts

g	:	Dirichlet
h	:	Neumann
st	:	Standart (master) element in ξ_1 and ξ_2

ABSTRACT

THE APPLICATION OF SPECTRAL ELEMENT METHOD TO MAGNETOSTATIC PROBLEMS

ERCIYAS, Atakan

Master, Department of Electrical and Electronics Engineering

Thesis Supervisor: Asst. Prof. Dr. Ibrahim MAHARIQ

January 2017, 97 pages

Recently, we have observed good progress in our ability to simulate complex electromagnetic systems. Yet, there are still many challenges that have to be tackled for sake of computational electromagnetic field. One of these challenges is the constraint of accessible computational resources. The traditional techniques, such as finite element method, finite difference method and finite volume methods have been utilized for several decades. On the other hand, spectral element method has been recently applied in limited to some branches of electromagnetics such as photonic structures, waveguides. In this thesis, the numerical approximation to the set of partial differential equations which are governing a typical magnetostatic problem is obtained by spectral element method and simulation results are presented. Legendre polynomials and Gauss-Legendre-Lobatto grids are used in this thesis as test functions and discretization of problem domain.

Key words: Computational electromagnetics, finite element method, magnetostatics spectral element method.

ÖZET

SPEKTRAL ELEMAN YÖNTEMİNİN MANYETOSTATİK PROBLEMLERE UYGULANMASI

ERCIYAS, Atakan
Yüksek Lisans, Elektrik-Elektronik Mühendisliği Bölümü
Tez Danışmanı: Yrd. Doç. Dr. Ibrahim MAHARIQ
Ocak 2017, 97 sayfa

Son zamanlarda, kompleks elektromanyetik sistemleri simüle etme kabiliyetimizde iyi ilerlemeler kaydettik. Ancak, hesaplamalı elektromanyetik alanında halen aşılmayı bekleyen birçok zorluk bulunmaktadır. Bu zorluklardan bir tanesi kullanılabilir sistem kaynaklarındaki kısıtlamadır. Son on yılda, elektromanyetik alanında sonlu fark yöntemi, sonlu elemanlar yöntemi ve sonlu hacim yöntemlerinin yoğun olarak kullanılmıştır. Öte yandan, spektral eleman yöntemi yüksek doğrulukta sonuçlar verdiğinden dolayı son yıllarda dalga klavuzları ve fotonik yapılar alanlarına kısıtlı olmak üzere kullanılmaya başlanmıştır. Bu tezde, tipik bir manyetostatik problemini tanımlayan kısmi diferansiyel denklemlerin çözümü spektral eleman yöntemi ile çözülmüş ve simülasyon sonuçları paylaşılmıştır. Çalışmamızda probleme ait tanımlanan alan Gauss-Legendre-Lobatto ızgaraları ile ayrıştırılmış olup, Legendre polinomları test fonksiyonu olarak kullanılmıştır.

Anahtar Kelimeler: Hesaplamalı elektromanyetik, sonlu elemanlar yöntemi, manyetostatik, spektral eleman yöntemi.

CHAPTER ONE

INTRODUCTION

1.1 Electromagnetic Modeling

Electromagnetic modeling techniques are divided into two categories fundamentally by analytical and numerical. Analytical techniques start with the proper governing equations, such as Maxwell's equations, and utilize mathematical manipulations in order to acquire quantities of interest. Some problems consist of simple structures that can be studied by utilizing this method. However, for complex structures, some simplifying assumptions which limit the accuracy of the result should be made.

On the other hand, numerical methods, start with obtaining governing equations but put them in a discrete form so as to let them to be solved by a computer. In spite of numerical methods provide approximate solutions to problems, adjusting of modeling detail can reduce error to acceptable levels in terms of engineering point of view. Thanks to improvements of technology, there are more processing power and memory resources available with affordable prices which makes numerical methods more attractive [1].

1.2 Literature Review

In literature, there have been many researchers involved in computational electromagnetics. However, there are still many existing challenges that have to be dealt with. One of these challenges is constraints on computational resources. For several decades, the conventional computational techniques such as finite element method, finite difference method and finite volume method that have been widely utilized in the electromagnetics. Yet, spectral element method has been recently

applied in some branches of electromagnetics such as waveguides and photonic structures for improved accuracy.

To illustrate that, Biro O. and Preis K. [2] published a paper about vector potential formulations for the problem consists of eddy currents in three dimensions. They presented how they obtained the uniqueness of the vector potential. Their study proved that the advantage of setting the normal component of the magnetic potential to zero on the interfaces between regions having different vector potentials.

Lee J. et al. [3] published a paper which presents three dimensional spectral element method efficiently by utilizing the mixed order curl so as to obtain solutions of vector wave equations. They employed lookup tables corresponding to stiffness matrix in order to reduce CPU usage while assembling system matrices. The represented method provides higher accuracy with increased order of interpolation. Based on their study, spectral element method is more efficient when it is compared to conventional finite element method.

In Ref. [4], a novel method, which combines both analytical and numerical solutions is introduced by Chau K, et al. in order to solve magnetic field in electrical machines for rotor and stator regions. The chief goal of study was to naturally couple the analytical solution with the FEM equations consisting of the continuity of vector potentials across the problem boundary. As a result, the stiffness matrix was obtained. Their results and experiments represent that computational time is nearly same because of analytical computation due to the fact that there are less nodes which was obtained in finite elements.

In Ref. [5], Sjögren M. presented a study which consists of utilization of finite difference and spectral element methods on the material discontinuity problem. Based on the results, finite difference method and spectral element method can simulate simple case of wave reflection and refraction in 2D rectangular geometry accurately. Although finite difference method was better fitted and provided higher accuracy for specific geometry, spectral element method has more advantages in complex geometries because of the fact that it is easier to construct unstructured grid. In addition to that, spectral element method provided parallel implementation opportunity for large scale computations. Similar studies were presented by Airiau [6] and Christoph [7] by utilizing discontinuous Galerkin spectral element method and both results confirmed Sjögren's study.

To extent of our knowledge, when literature is searched, one can infer that spectral element method has not been utilized in magnetostatic or quasi-magnetostatic problems. It is important to note that, spectral methods (but not SEM) were introduced in 1983 by Steele C. [8]. In the method introduced by the author, magnetic fields are evaluated by denoting them as a linear combination of a set of orthogonal functions. The only advantage of this method as it is pointed by the author is the reduction of linear equations defining the system compared to finite element method. However, spectral methods are not successful in solving complex domain problems and/or nonhomogeneous materials. Therefore, people did not extend Steele's study.

Park I. et al [9] presented a sensitivity analysis for the shape design problems consisting of two dimensional nonlinear magnetostatic system. To obtain the design sensitivity, the authors utilized the algebraic equation obtained by finite element method and adjoint variable method. They applied this algorithm to the sample problem of a quadrupole magnet operating in the saturation region. As a result, they obtained the optimal pole shape with a tolerable deviation after they had applied several iterations.

An article about three dimensional magnetostatic field analysis by utilizing finite element method is provided by Chari K. et al [10]. They presented the requirement of choosing the vector potential function in order to make its divergence zero. Implementation of this requirement consists of an energy-related functional associated with the Poisson equation. They created the mesh corresponding to the field region by first order finite elements, and then the solution by minimizing the functional with respect to values of vector potential at the nodes of each element and evaluating linear algebraic equations is obtained. In order to accelerate convergence, they utilized an iterative solution method which is also known as the conjugate gradient technique. In the paper, they employed three-dimensional field analysis to the sample illustrative problems. When they compared the results, they observed that flux density results corresponding to a three-dimensional field analysis was perfectly matched with the two-dimensional solution.

Penman J. and Fraser J. R. [11] outlined a method which provides bounded solutions to magnetostatic problems in a wide range. The method expands complementary and dual energy variational principles to include the T-Ω formulation of electromagnetic field problems by finite element method. In the paper, they

presented examples showing that the bounded nature of the procedure, and pointed how it can be utilized so as to reduce computational requirements for specific accuracy. Consequently, by the method that they presented in the article, it is possible to reduce computational effort significantly in order to obtain relatively accurate values of parameters depending on field in magnetostatic problems.

Imhoff J.F., et al. [12], presented a finite element modeling consisting of open boundary 2D and 3D problems. In the article, they obtain finite element solution for unbounded electromagnetic problem. The results shown that obtained electromagnetic field values were highly accurate. Despite of utilizing the method in magnetostatic problem for its simplicity, it can be applied on different types of problems. As a result, the technique that they utilized is highly performant when it is compared to other methods. In addition, the chief advantage of the technique is drastically reduced computational time.

1.3 Contribution of Thesis

As it is presented in the literature review section, the computational methods are extensively utilized in electromagnetic problems, thanks to improvements of technology. Many of researchers applied finite element method, finite difference method and spectral element methods in electromagnetic problems especially in electromagnetic wave problems. However, spectral element method in particular has not been investigated in magnetostatic or quasi-magnetostatic problems. In this thesis, the numerical approximation to the set of the partial differential equations defining the typical magnetostatic problem is utilized by applying spectral element method for the first time. In this thesis, simulation results obtained by the spectral element method for a sample magnetostatic problem compared with finite element method corresponding to same problem. As it is presented in the results chapter, spectral element method provides higher accuracy than finite element method. This is in addition to all research paper where the accuracy of spectral element method is proven to be dominant. For instance, but not limited to, Mahariq et al. [13] provided a comparison amongst the spectral element method, the finite difference method, and the finite element method. For the sake of consistency, the comparison is carried out on one dimensional and two-dimensional problems based on the same measure of error in order to emphasize on the high accuracy gained by the SEM.

1.4 Arrangement of Thesis

In this chapter, the literature search is presented. Electromagnetic modelling process is described briefly, and the importance of utilizing spectral element method to magnetostatic problems is pointed.

In Chapter 2, Maxwéll's equations are discussed, types of electromagnetic problems are shortly introduced. In magnetostatic subsection, governing Maxwéll equations defining the sample problem is obtained. The importance of boundary conditions is discussed and the commonly used methods in electromagnetics are introduced. In Section 2.4, finite difference method is introduced. Advantages and disadvantages of this method is discussed in terms of accuracy, and domain complexity. In Section 2.5, finite element method is introduced, Galerkin and variational approaches are briefly described. The advantages of this method over finite difference method are discussed.

In Chapter 3, the fundamentals of spectral element method are introduced. The formulation of spectral element method is presented for Maxwell's equations defining the problem. The process of evaluation the corresponding stiffness and mass matrices is also formulated for rectangular and quadrilateral elements. The formulation of load vector and Helmholtz operator is obtained by utilizing the mass matrix formulas.

In Section 4.1, two dimensional time-invariant magnetostatic problem is defined. In Section 4.2, problem discretization (which is also called meshing) and element numbering are presented. In Section 4.3, the boundary conditions and interface conditions which are utilized in the problem are presented. The vector potential results are re-evaluated by changing various parameters such as number of nodes, magnetic permeability, injected current density and corresponding values are discussed in terms of accuracy, computational time, memory usage, CPU usage. In Section 4.5, same magnetostatic problem is implemented in a computational software called as "FEMM" and created by David Meeker [14]. The obtained finite element method results are compared with spectral element results. The results corresponding to the comparison are discussed, advantages and disadvantages of two methods are presented.

In Chapter 5, the thesis is ended up by appending some comments, and some discussions are provided for future works.

CHAPTER TWO

MAGNETOSTATICS

2.1 Maxwell Equations

Thanks to James Maxwell (b. 13th June 1831, d. 5th October 1879) who simplified and combined the laws of electromagnetism to give the complete picture describing all the phenomena that humans knew in that branch of physics. Maxwell re-expressed those governing laws into a much compact and generalized form known as Maxwell's equations.

Electric and magnetic phenomena study electromagnetic fields which are caused by electric charges in steady state or in motion. There are two types of electric charges in nature which are positive and negative. These types of charges are basically the source of electric field intensity, E. Moving electric charges produce current which also produces a magnetic field intensity, H. Spatial distribution of a vector quantity defines a vector field which may be time varying or may not. Time-varying electric and magnetic field intensities are always followed by each other. That is, time varying electric field intensities and time varying magnetic fields are essentially coupled and produce electromagnetic field intensity.

As it is mentioned, time-varying electric fields are accompanied by magnetic fields and vice versa. In Maxwell's Equations, it is explained how electric and magnetic fields are generated and effect on each other. The first law of Maxwell's Equations is Faraday's law of induction, the second is Ampére's law which is modified by Maxwell in order to include displacement current $\partial D / \partial t$, the last two equations belong to Gauss's law for electric and magnetic field [15].

$$\nabla \times \mathrm{E} = -\frac{\partial \mathrm{B}}{\partial t} \tag{2.1}$$

$$\nabla \times \mathrm{H} = \mathrm{J} + \frac{\partial \mathrm{D}}{\partial t} \tag{2.2}$$

$$\nabla \cdot \mathrm{D} = \rho \tag{2.3}$$

$$\nabla \cdot \mathrm{B} = 0 \tag{2.4}$$

The displacement current term $\partial D / \partial t$ in Ampére's law is essential in predicting the existence of propagating electromagnetic waves. The quantities E and H are electric and magnetic field and measured in units of [volt/meter] and [ampere/m] respectively. The quantities D and B are electric and magnetic flux densities and are measured in units of [coulomb/m^2] and [weber/m^2], or tesla. D is also called the electric displacement, and B, the magnetic induction.

The charge and current densities ρ, J may be thought as the sources of electromagnetic fields. For wave propagation problems, these densities are localized in space; for example, they are restricted to flow on an antenna. The generated electric and magnetic fields are radiated away from these sources and can propagate to large distances to the receiving antennas. Away from sources, that is, in source free regions of space, Maxwell's equations take the simpler form [15].

$$\nabla \times \mathrm{E} = -\frac{\partial \mathrm{B}}{\partial t} \tag{2.5}$$

$$\nabla \times \mathrm{H} = \frac{\partial \mathrm{D}}{\partial t} \tag{2.6}$$

$$\nabla \cdot \mathrm{D} = 0 \tag{2.7}$$

$$\nabla \cdot \mathrm{B} = 0 \tag{2.8}$$

2.2 Types of Electromagnetic Problems

2.2.1 Magnetostatic Fields

Analytical and numerical methods which have been developed for solution of electrostatic field problems are also applied grandly to the magnetostatic field problems. Identically structured electrostatic fields which is produced by dipole

distributions and fictive double layers can represent magnetostatic fields. Free charges do not exist in magnetostatics, and the surface singularity which is generated by electric charges does not really exist. A double layer causes a multivalued potential and as a result non-conservative field. It is important to note that the physical structure of field owing to stationary distributed current varies essentially from any configuration of electric charges.

The equations correspond to stationary fields are obtained by setting time derivatives to zero in Maxwell's Equations.

$$\nabla \times \mathrm{H} = \mathrm{J} \tag{2.9}$$

$$\nabla \cdot \mathrm{B} = 0 \tag{2.10}$$

Equation of continuity must be appended to these which reduces to;

$$\nabla \cdot \mathrm{J} = 0 \tag{2.11}$$

Assume that flux density which is produced by current filament $\mathbf{I_1}$ is $\mathbf{B_1}$. $\mathbf{I_1}$ is linked by all lines belonging to this field. However, a fraction of $\mathbf{B_1}$ may also pass on second current filament $\mathbf{I_2}$. The "flux linkage" concept is utilized to make practical analysis of electromagnetic problems that of the solenoidal features in terms of stationary state current and flux [16].

When Stokes' theorem is applied to (I), the equivalent integral equation is obtained below,

$$\int_C \mathrm{H} \cdot ds = \int_S \mathrm{J} \cdot n da = I \tag{2.12}$$

S is the surface which is bounded by the contour C, and I is the total current flowing through the surface. The linked current I equals to the integral of H around a closed path.

Every solenoidal field can be represented in terms of vector potential. So the equation which is defined in (2.10) can identically satisfy the equation defined below;

$$\mathrm{B} = \nabla \times \mathrm{A} \tag{2.13}$$

The vector A is selected to satisfy equation (2.13), so that the relationship between magnetic vectors must be specified ($\mathrm{H}=H(\mathrm{B})$). If B is substituted with $\mathrm{B}=\mu\mathrm{H}$ in equation (2.13), the following equation is obtained;

$$H=\frac{\nabla\times A}{\mu} \tag{2.14}$$

When the magnetic vector H defined in (2.9) is substituted with H obtained in (2.14), we arrive at,

$$\nabla\times\nabla\times A=\mu J \tag{2.15}$$

which can also be written as,

$$\nabla\nabla\cdot A-\nabla^2 A=\mu J \tag{2.16}$$

for vector potential. According to the Helmholtz theorem, if divergence and curl of a vector function is specified, it is determined to within an additive constant. Because of that, to determine A, its divergence must be specified. In order to be simplified, it has been chosen as,

$$\nabla\cdot A=0 \tag{2.17}$$

In xy coordinates, the equation which is defined in (2.15) is now reduced to,

$$\nabla^2 A=-\mu J \tag{2.18}$$

which is also known as Poisson's equation [16].

2.2.2 Quasi-Magnetostatic Fields

The previous section discussed the static magnetic field which is produced by the time invariant sources. In the case where the current distribution is slowly time varying, displacement current can be omitted that is, we can neglect the $\partial E/\partial t$ term in Maxwell's equations. Therefore, the following equations are obtained;

$$\nabla\cdot E=\frac{\rho}{\varepsilon_0} \tag{2.19}$$

$$\nabla\cdot B=0 \tag{2.20}$$

$$\nabla\times E=-\frac{\partial B}{\partial t} \tag{2.21}$$

$$\nabla\times B=\mu_0 J \tag{2.22}$$

Due to $\nabla \cdot \nabla \times \mathrm{B} \equiv 0$, it is required to neglect also $\mathrm{J_D}$, hence,

$$\nabla \cdot \mathrm{J} = 0 \tag{2.23}$$

The existence of static charge density is not prevented by equations (2.19), (2.20) and (2.21), (2.22). However, it is not reliable with the previous statement that the limit of source is constant current. Because of that reason, in case we choose $\rho(\mathrm{r},t) = 0$, generality will be valid.

The Helmholtz theorem gives the following for $\mathrm{B}(\mathrm{r},t)$,

$$\mathrm{B}(\mathrm{r},t) = \nabla \times \mathrm{A}(\mathrm{r},t) = \nabla \times \frac{\mu_0}{4\pi} \int d^3 r' \frac{\mathrm{j}(\mathrm{r}',t)}{|\mathrm{r}-\mathrm{r}'|} \tag{2.24}$$

Consequently, the quasi-electrostatic electric field is obtained as,

$$\mathrm{E}(\mathrm{r},t) = -\frac{\mu_0}{4\pi} \int d^3 r' \frac{\partial j(\mathrm{r}',t)/\partial t}{|\mathrm{r}-\mathrm{r}'|} \tag{2.25}$$

One can verify that Equations (2.23) and (2.24) are engaged to Faraday's law, that is, divergence of Equation (2.25) is zero in case constant current condition is applied [17].

2.2.3 Time Harmonic Electromagnetic Fields

Many problems in electrical engineering consist of time harmonic fields. Fortunately, the differentiation of time can be calculated and the time variable can be omitted to reduce Maxwell's equations to be limited to its three spatial dimensions. In this section, the special case of time-harmonic fields will be introduced.

$$E(x,y,x,t) = \mathrm{Re}[E_s(x,y,z)e^{jwt}] \tag{2.26}$$

where $E_s(x,y,z)$ is space dependent, vector phasor containing information corresponding to direction, magnitude and phase. Therefore, the time harmonic Maxwell's equations can be re-arranged as follows,

$$\nabla \times E_s = -j\omega\mu H_s \quad (\partial/\partial t \rightarrow j\omega) \tag{2.27}$$

$$\nabla \times H_s = J_s + j\omega\varepsilon E_s \tag{2.28}$$

$$\nabla \cdot E_s = \frac{\rho_s}{\varepsilon} \tag{2.29}$$

$$\nabla \cdot B_s = 0 \tag{2.30}$$

In case of source free condition which is characterized by $J = 0$, $\rho_v = 0$ and $\sigma = 0$, the time harmonic $(\partial / \partial t \rightarrow j\omega)$ Maxwell's equations can be modified as,

$$\nabla \times E_s = -j\omega\mu H_s \tag{2.31}$$

$$\nabla \times H_s = j\omega\varepsilon E_s \tag{2.32}$$

$$\nabla \cdot E_s = 0 \tag{2.33}$$

$$\nabla \cdot B_s = 0 \tag{2.34}$$

In this special case, there are not any sources existing, that is, there are not any particular solution that can be obtained. However, most general solutions which are obtained for the problems are combinations of the two independent solutions corresponding to homogeneous equations [15].

2.2.4 Electrostatic Fields

Electromagnetism is a science that utilizes ways of understanding mutual interactions between electric charges in steady state or motion. Electrostatic which is branch of electromagnetism deals with interactions of steady state charges.

Coulomb successfully discovered the fundamental law of electrostatics in 1785. During his study, he achieved in building a highly sensitive and accurate torsion balance in order to measure relative repulsion force between two lights. Based on that study, he clearly proved that, electrostatic forces follow along the line through the particle. Besides that, electrostatic forces are proportional to each electrical charges' magnitude and it decreases inversely depending on the distance between charges. The equation which is stated by Coulomb is defined as,

$$F_1 = K \frac{q_1 q_2}{r_{12}^2} \hat{\mathrm{r}}_{12} \tag{2.35}$$

$$K = \frac{1}{4\pi\varepsilon_0} = 10^{-7} c^2 \tag{2.36}$$

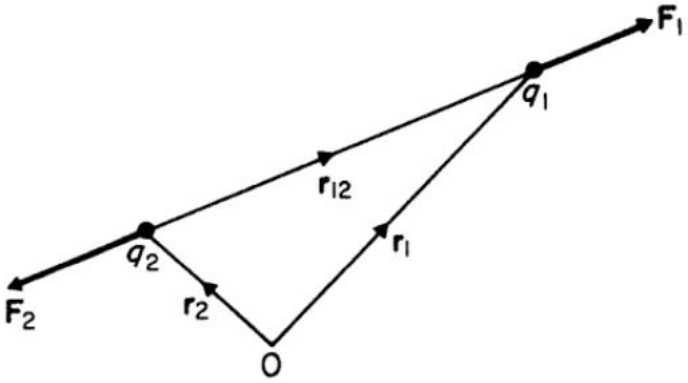

Figure 2.1: Forces between charges.

where the electric constant is ε_0, c is the speed of light. K is the constant which is obtained by experiments and its value is $K = 9\times10^9\,\mathrm{Nm^2C^{-2}}$. But it is important to note that these values are defined in SI units.

Gauss's law explains us the behavior of electric flux. It is well-known fact that if the angle between flux lines and surface arises, the magnitude of field vector increases up to angle of surface's normal. In other words, it is maximum when the angle between flux lines and surface is 90° and it is minimum when the angle between flux lines and surface is 0 and that also means that flux lines and surface in parallel. The point charge is defined as,

$$E \cdot dS = \frac{q}{4\pi\varepsilon_0 r^2}\hat{r} \cdot dS \tag{2.37}$$

where $E \cdot \hat{\mathrm{n}} dS$ is flux of vector E from the element dS. $\hat{\mathrm{n}}$ is unit vector which defines the surface orientation. When the vector equation stated in (2.37) is calculated, we obtain,

$$\int_S E \cdot dS = \frac{1}{\varepsilon_0}\int_V \rho d\tau \tag{2.38}$$

and it defines that the total flux leaving out of any surface equals to the enclosed total charge which is divided by the electric constant [18].

2.2.5 Transient Electromagnetic Fields

It is important to separate the moment of switching on the field and instant of non-stationary behavior starts in many cases. The non-stationary points a moment

which is accompanied by existence of transient (non-harmonic) field. These transient fields can be significant part of total field.

A mathematical approach which is applied to transient electromagnetic fields must contain a description of continuous and instant changes which is belonging with field functions and the medium parameters. This approach should also consider the correlation between spatial and temporal changes in the media. Uniformly continuous and discontinuous functions which are belonging with field and media parameters are described by the generalized functions. Application of this theory to electromagnetic equations means using generalized derivatives instead of utilizing conventional derivatives with corresponding modification of Maxwell's equation [19].

2.3 Boundary Conditions

In computational electromagnetics, boundary conditions are required to be applied so as to be ensured of obtaining unique solutions. There are some various types of boundary conditions can be utilized on computational methods however, there are five of them commonly used in computational electromagnetics.

In Dirichlet boundary condition, the value belongs to vector potential is defined explicitly on boundary. In most cases, A is defined zero on boundary in order to prevent magnetic flux to leave outside boundary.

In Neumann boundary condition, normal derivative of potential is defined along boundary. In other words, $\partial \mathrm{A} \diagup \partial n = 0$ is defined in order to force magnetic flux to pass the boundary perpendicularly.

Robin boundary condition utilizes features of Dirichlet and Neumann boundary conditions. In other words, it can be considered as a composition of Dirichlet and Neumann boundary conditions. Thus, Robin boundary condition states that,

$$\frac{\partial \mathrm{A}}{\partial n} + c\mathrm{A}=0 \tag{2.39}$$

In periodic boundary conditions, two boundaries are joint together. This type of boundary condition provides boundary values to be equal on corresponding points with same sign. The same rules are applied for anti-periodic boundary conditions. However, the boundary values on corresponding points are same but with opposite sign [20].

2.4 Finite Difference Method

Finite difference method is one of the techniques of numerical analysis methods utilized for approximation of solutions by dealing with partial differential equations [21].

2.4.1 Intuitive Derivation

The approximate solutions are obtained by substituting derivative expressions with approximately equivalent difference quotients. In other words, the first derivative of a function is,

$$f'(a) = \lim_{h \to 0} \frac{f(a+h) - f(a)}{h} \tag{2.40}$$

then the approximation to first derivative would be,

$$f'(a) \approx \frac{f(a+h) - f(a)}{h} \tag{2.41}$$

for small values of h. Although, it is the first derivation of a function, one can utilize this formula to substitute derivative expressions in differential equations [21].

2.4.2 Derivation by Utilizing Taylor's Polynomial

If the function is to be approximated is well-behaved, by Taylor's theorem we obtain,

$$f(x_0 + h) = f(x_0) + \frac{f'(x_0)}{1!}h + \frac{f^{(2)}(x_0)}{2!}h^2 + \ldots + \frac{f^{(n)}(x_0)}{n!}h^n + R_n(x) \tag{2.42}$$

where $n!$ is represented as the factorial of n, and $R_n(x)$ is represented for reminder. By utilizing the same function as an example, we obtain the following by Taylor's theorem,

$$f(x_0 + h) = f(x_0) + f'(x_0)h + R_1(x), \tag{2.43}$$

which is equals to,

$$f'(a) = \frac{f(a+h) - f(a)}{h} - \frac{R_1(x)}{h} \tag{2.44}$$

Therefore, $R_1(x)$ is small enough,

$$f'(a) \approx \frac{f(a+h) - f(a)}{h} \tag{2.45}$$

2.4.3 Accuracy

The error in the finite difference method computation is defined as the difference between analytical and approximate results. There are two error sources in finite difference method which are truncation and round-off errors. The loss of precision (round-off) error occurs due to rounding action of decimal quantities made by computers. Truncation error which is also called as discretization error, is the difference between exact solution and exact quantity of nodes [21].

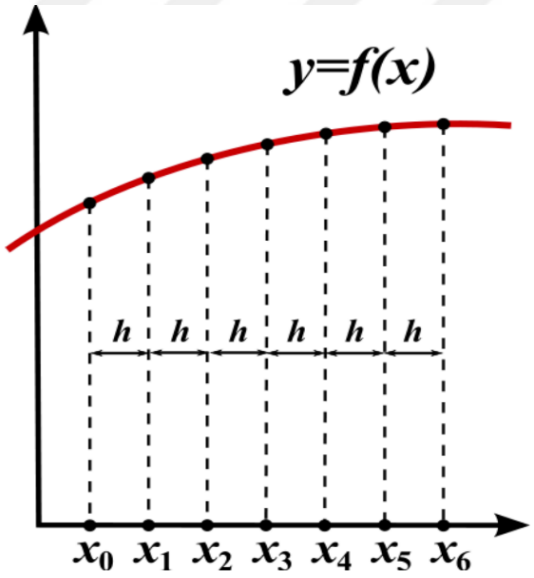

Figure 2.2: The finite difference method depends on discretizing a function on a grid.

To utilize FDM, the problem domain must be discretized first. This is usually achieved by dividing the problem domain into a grid created uniformly. It is important to note that, FDM provides sets of discrete numerical approximations [21].

Local truncation error is typically expressed in Big-O notation. Since local truncation error is referring to the single application of a method. Therefore, the quantity of error is $f'(x_i) - f_i'$ where $f'(x_i)$ refers to exact value and f_i refers to numerical approximation. It is appropriate to use the reminder term of a Taylor

polynomial so as to analyze discretization (truncation) error. By utilizing the Lagrange form of the reminder term in the Taylor polynomial $f(x_0+h)$, which is;

$$R_n(x_0+h)=\frac{f^{(n+1)}(\xi)}{(n+1)!}(h)^{n+1} \tag{2.46}$$

the predominant term of discretization error can be obtained where $x_0<\xi<x_0+h$.

2.5 Finite Element Method

The Finite element method is also a numerical method which is utilized to the problems governed by differential equations. The fundamental principle of this method is to represent the problem domain in smaller subdomains which is called the finite elements. In Figure 2.3, the discretization of a two dimensional problem is illustrated. The distributed primary unknown quantities inside an element are interpolated by using the values of nodal elements or the values which are obtained in the edges. The interpolation which is also known as shape functions are obligated to be a complete set of polynomials. The accuracy corresponding to the obtained solution depends on the order of these polynomials. The numerical solution depends on the quantity of primary unknowns at the nodes of discretized domain. In order to obtain solution, system of linear equations must be solved. To construct such a linear system of equations, conversion corresponding to governing differential equation and boundary conditions to integro-differential formulation must be made by minimizing a functional or utilizing Galerkin approach (also known as weighted-residual method). This formulation is applied to a single element by using proper weight and interpolation functions. As a result, all elements are assembled which represents the entire domain in a global matrix system [22].

As it is mentioned earlier in the previous paragraph, there are two methods which are commonly utilized to obtain FEM equations; the variational method and weighted-residual method. It is required by the variational technique to construct a functional which denotes the energy associated with the boundary value problem. A functional is a function which is denoted in an integral form and takes arguments which are also functions themselves. As it is referred from the most of the engineers, functional is a function of functions. A stable or stationary solution of boundary value problem can be evaluated by minimizing or maximizing governing functional. Such a solution

corresponds to a point of minimum, maximum or saddle. Nearby such a point, the solution is stable which means

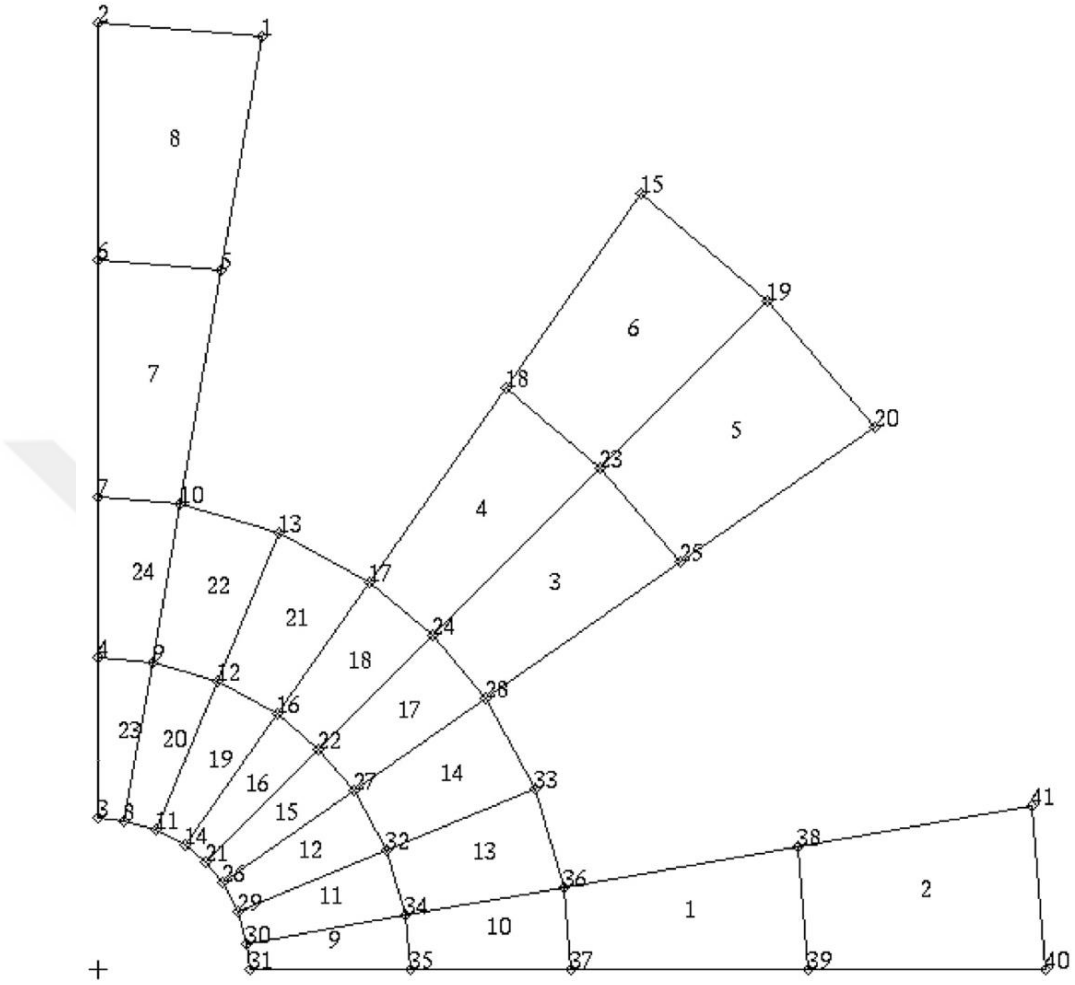

Figure 2.3: An example for 2D discretization of a problem domain by assigning unique numbers.

that it is not sensitive to small changes of dependent parameters. This results a smaller numerical error comparing with a solution evaluated for any other point. Minimizing or maximizing of a functional is of a process obtaining partial derivatives of the function with respect to each variables and setting result of the derivation to zero. As a result, this constructs a set of equations which can be discretized by choosing appropriate interpolation functions so as to obtain FEM equations [22].

The second technique is weighted-residual method which is also known as Galerkin method. This method starts by constructing a residual directly form the partial differential equations which is related boundary value problem. It is important to note that, this function does not need to utilize the functional. The residual is of a method

transferring all items of partial differential equation on one side. Then, the residual is multiplied by a weight function and integration is obtained over the domain of an element. This is the reason of calling this method as a weighted-residual. The shape functions which are employed to interpolate the primary unknown quantity are obligated to be twice differentiable in case of usage second order differential equation. This requirement is debilitated by utilizing integration by parts and allocating the second derivative to the weight functions and shape functions. By utilizing that, related weight and shape functions are needed to be differentiable only for once. Due to this requirement, this formulation is denoted as the weak formulation. In addition to that, if the weight functions are selected from the same function set as the interpolation functions, the weighted-residual method is referred as Galerkin method [22].

In many cases, it is much easier to utilize Galerkin method due to the fact that the variational methods require strong knowledge of its principles so as to utilize it to construct functional. To prevent compelling procedure of utilizing a functional and involving related mathematical complexities, it is often considered to choose Galerkin approach instead of the variational approach.

The most important steps should be followed on applying the Galerkin approach are; Discretizing the problem domain by utilizing finite elements, choosing the appropriate interpolation (shape) functions, obtaining the linear equations corresponding to single element, constructing the global matrix system, imposing the boundary conditions, solving the linear equations by utilizing linear algebra methods, post processing the results [22].

CHAPTER THREE

SPECTRAL ELEMENT METHOD

3.1 Spatial Discretization

In order to represent the fundamentals of SEM formulation, strong formulation corresponding to magnetic vector potential will be introduced at the beginning.

$$\nabla^2 \mathrm{A} = -\mu \mathrm{J} \text{ on } \Omega \tag{3.1}$$

$$\mathrm{A} = g \text{ on } \Gamma_g \text{ Dirichlet boundary conditions} \tag{3.2}$$

$$\mathrm{n}.(\frac{1}{\mu}\nabla A) = h \text{ on } \Gamma_h \text{ Neumann boundary conditions} \tag{3.3}$$

∇^2, refers to an operator which is applied on partially differential equations. It is also called as Laplacian operator. A is representing the vector field. Ω refers to a domain of the problem, and as it is stated in the equations (3.2), (3.3), Γ_g and Γ_h refer to boundary of the domain. The normal unit vector n points out from Γ_h, and g and h refer to known functions.

The Poisson equation is governed in residual form as follows by assigning left hand-side of the function to zero [23].

$$\Re = \nabla^2 \mathrm{A} - \mu \mathrm{J} = 0 \tag{3.4}$$

3.1.1 Weighted Residual Formulation

It is assumed by the weighted residuals that approximate solution (3.5) can provide an accurate solution for A,

$$\mathrm{A}_N = \sum_{i=1}^{N_{dof}} \mathrm{A}_i \Phi_i \tag{3.5}$$

where Φ_i is of an analytical function which is called trial or expansion functions, A_i , N_{dof} are unknown coefficients. Φ_i equals to zero on Dirichlet boundaries in order to satisfy requirements of homogeneous boundary conditions by definition.

The residual is multiplied by a weight function w to create weighted residual function. The approximate solution is compelled so as to fulfill the residual equation in aspect of weighted integral. The formulation stated below is the same as forcing residual to be vanished when it is projected on to test space.

$$\int_{\Omega} \left(\nabla^2 \mathrm{A} - \mu \mathrm{J} \right) v d\Omega = 0 \tag{3.6}$$

The A is approximate solution and v is weighted function. They belong to Hilbert space. Hilbert space is also called as trial space which is denoted by χ and where trial(approximate) solutions exist.

$$\chi = \left\{ \mathrm{A} : \mathrm{A} \in H^1(\Omega), \mathrm{A} = \mathrm{g} \text{ on } \Gamma_g \right\} \tag{3.7}$$

$$\mathcal{V} = \left\{ w : w \in H^1(\Omega), \mathrm{v} = 0 \text{ on } \Gamma_g \right\} \tag{3.8}$$

The Hilbert (trial) and test spaces which are stated in (3.7) and (3.8), represented as χ and $\mathcal{V}$ respectively, contain infinite number of functions which makes it an infinite dimensional problem. χ_N, v_N are trial and test subspaces respectively and are chosen to contain finite number of functions. They are considered as approximation spaces which are finite dimensional and belong to $\chi_N \subset \chi$ and $v_N \subset v$. The test space $v_{N,0}$ belongs to $v_N \subset v_{N,0}$. It can be inferred from the subscript 0 that test space satisfies the boundary conditions on Γ_g. This means that the test function v is zero on all Dirichlet boundaries [23].

The approximate solution $u_N \subset \chi_N$ is modified as follows,

$$\mathrm{A}_N = \sum_{i=0}^{N} \mathrm{A}_i \phi_i \tag{3.9}$$

The trial functions ϕ_i are utilized as basis functions corresponding to an expansion of truncated series of the solution. For generalization purposes, we denote our unknown function that is to be solved by u, i.e., let A=u.

3.1.2 Weak Formulation

In order to construct weak form, integration by parts method is employed to the first term of the Equation (3.6).

$$\int_{\Omega} \nabla u.\nabla v d\Omega = \int_{\Omega} f.v d\Omega + \oint_{\Gamma_A} hv ds \tag{3.10}$$

In order to impose Neumann boundary conditions naturally and reduce the order of the first term, integration by part method is utilized. As a result, to precondition the mesh, linear order polynomials can be utilized.

Domain discretization is the process in which weak formulation is applied into all individual elements [23].

$$\int_{\Omega} \nabla u^e.\nabla v^e d\Omega^e = \int_{\Omega} f^e.v^e d\Omega^e + \oint_{\Gamma_h^e} h^e v^e ds \tag{3.11}$$

3.1.2.1 Weak formulation for one element

The Equation (3.11) becomes,

$$\int_{\Omega} \frac{\partial v}{\partial x}\frac{\partial u}{\partial x} dxdy + \int_{\Omega} \frac{\partial v}{\partial y}\frac{\partial u}{\partial y} dxdy = \int_{\Omega} f(x,y).v(x,y) dxdy + \oint_{\Gamma_h^e} h^e v^e ds \tag{3.12}$$

In case of treatment of whole domain as a single element, p-type method is converted to spectral method. There are lot of methods can be obtained if the trial function ϕ_i and test function v are chosen. For instance, least squares and collocation. The main consideration is Galerkin method which is also known as Bubnov-Galerkin [23, 24].

The last term of Equation (3.12) refers to boundary term. It is chosen zero to satisfy Neumann boundary conditions $\mathrm{n}.(\frac{1}{\mu}\nabla A) = 0$ on Γ_h. Thus, Equation (3.12) transforms to;

$$\int_{\Omega} \frac{\partial v}{\partial x}\frac{\partial u}{\partial x} dxdy + \int_{\Omega} \frac{\partial v}{\partial y}\frac{\partial u}{\partial y} dxdy = \int_{\Omega} f(x,y).v(x,y) dxdy \tag{3.13}$$

3.2 Two Dimensional Element Discretization

Tensor product forms are employed to create steady diffusion operator and other special element operators used in elliptic problems. For instance, vector potential equation in a rectangular domain. By mapping all elements one by one in physical coordinate (x, y) to a master element $(\xi_1, \xi_2) \in [-1,1]^2$, u is obtained approximately in the element Ω^e. The typical function $u(x, y) \in \mathcal{V}_N$ is represented as follows,

$$u(\xi_1, \xi_2) = \sum_{i=0}^{N} \sum_{j=0}^{N} u_{ij} \psi_i(\xi_1) \psi_j(\xi_2) \tag{3.14}$$

3.2.1 2D differentiations in the computational domains

The differentiations with respect to ξ_1 and ξ_2 are defined in reference coordinate as follows,

$$\frac{\partial u}{\partial \xi_1} = \sum_{i=0}^{N} \sum_{j=0}^{N} u_{ij} \frac{\partial \psi_i(\xi_1)}{\partial \xi_1} \psi_j(\xi_2) \tag{3.15}$$

$$\frac{\partial u}{\partial \xi_2} = \sum_{i=0}^{N} \sum_{j=0}^{N} u_{ij} \psi_i(\xi_1) \frac{\partial \psi_i(\xi_2)}{\partial \xi_2} \tag{3.16}$$

3.3 Galerkin Methods

The test functions are selected to be identical with trial (expansion) functions. Consequently, the spaces χ and v are selected to also be the same, the Equation (3.11) is utilized as an initial point of the method. That is called Galerkin weighted-residual method. Thus, weight(test) function v is presented as,

$$v = \phi_{pq}(\xi_1, \xi_2) = \sum_{p=0}^{N} \sum_{q=0}^{N} \psi_p(\xi_1) \psi_q(\xi_2) \tag{3.17}$$

3.4 Rectangular Geometries

In this section, the evaluation corresponding to two dimensional rectangular stiffness matrix and mass matrix are formulated. In addition to that, Helmholtz operator and variable coefficient case are also formulated.

3.4.1 Evaluation of Two Dimensional Mass Matrix

The two dimensional mass matrix is obtained by evaluating (u,v) as given in Equation (3.18) for all u, $v \in v_N$ for rectangular domains. Mass matrix is employed in order to evaluate load vector with force function [23].

$$(u,v) = \int_{\Omega} vudV = \sum_{pj}\sum_{ij} v_{pq}\left(\int_{\Omega} \psi_p(\xi_1)\psi_q(\xi_2)_q\psi_i(\xi_1)\psi_j(\xi_2)dx_1dx_2\right)u_{ij} \qquad (3.18)$$

For rectangular domain $[x,y] \in [0,L_1]\times[0,L_2]$

$$M_{\hat{k}k} = \int_{-1}^{1}\int_{-1}^{1} \psi_p(\xi_1)\psi_i(\xi_1)\psi_j(\xi_2)\psi_q(\xi_2)\frac{L_1}{2}d\xi_1\frac{L_2}{2}d\xi_2 \qquad (3.19)$$

$$M = \frac{L_1L_2}{4}\hat{M}\otimes\hat{M} \qquad (3.20)$$

L_1 and L_2 refer to the lengths of the edges of domain.

Because of inverting the mass matrix is an important issue in aspects of computational costs, the usability of diagonal mass matrix is advantageous feature in unsteady or temporal discretization problems requiring frequent application of M^{-1}. Nevertheless, the primary cost is computational cost which is spent on constructing the matrix system involving numerical integration.

$\hat{M}$ will be diagonal in case of basis functions are orthogonal in respect of inner product. One option is to select $\{\psi_p\}_{i=0}^{N}$ in order to be an array of orthogonal functions like Legendre polynomials but this expansion will not fulfill automatically the required boundary conditions. The difficulty appears in cases where the degree of continuity is tried to be ensured in the global expansion. For a domain having a single element, element and domain boundaries are identical. To obtain accurate results, it is enough to guarantee u_N. In typical, this is fulfilled in finite element methods by setting a C_0 continuity between elemental regions that is to say, in spite of derivatives may not be continuous everywhere in the solution domain, the global expansion modes are continuous.

Instead of utilizing fully orthogonal basis, localized Lagrangian interpolants can be employed. These interpolants can be used in conjunction with mass lumping. To

apply that, the mass matrix can be substituted with a diagonal matrix with an identical row sum.

The SEM is not defined only by depending on its Lagrangian basis functions choice. It is defined by also the associated quadrature rule which is also known as inner product that is given by Gauss Lobatto quadrature in each spatial direction. The integral of $g(\xi)$ is defined as follows for a single coordinate direction and in which $\{\xi_0, \xi_1, ..., \xi_N\}$ and $\{w_0, w_1, ..., w_N\}$ are denoting the quadrature nodes [23].

$$\int_{-1}^{1} g(\xi) d\xi \approx \sum_{k=0}^{N} w_k g(\xi_k) \tag{3.21}$$

In order to compute each inner product in SEM, integrand is evaluated first. Then, quadrature (3.21) is substituted for integration. Thus, $\hat{M}$ becomes,

$$\hat{M}_{ij} = \sum_{k=0}^{N} w_k L_i(\xi_k) L_j(\xi_k) \tag{3.22}$$

However, due to the fact that the basis is Lagrangian $\left[\text{i.e.,} L_i(\xi_j) = \delta_{ij}, \text{where } \delta_{ij} \text{ is the Kronecker Delta}\right]$, it is obvious that because of cardinality property of Lagrangian basis on the GLL grid, $\hat{M}$ is diagonal,

$$\hat{M} = diag(w_i) \tag{3.23}$$

The stiffness matrix K is obtained in same a manner. p(x) and q(x) are defined as constant first. It is led to especially simple form that is proper to both fast evaluation and inversion [23].

3.4.2 Stiffness Matrix Evaluation for Rectangular Element

In $\mathbb{R}^2$, the energy product is defined as,

$$\mathcal{A}(\text{u,v}) = \int_{\Omega} \left(p \frac{\partial v}{\partial x} \frac{\partial u}{\partial x} + p \frac{\partial v}{\partial y} \frac{\partial u}{\partial y} + qvu \right) dx \tag{3.24}$$

By using the expansions defined in Equations (3.14), (3.15), (3.16) for u and v, the first term on the RHS of Equation (3.24) will be,

$$\int_{\Omega} p \frac{\partial v}{\partial x} \frac{\partial u}{\partial x} dx = \sum_{pq} \sum_{ij} v_{pq} p \frac{L_2}{L_1} \left(\int_{-1}^{1} \psi_q \psi_j d\xi_2 \right) \left(\int_{-1}^{1} \frac{\partial \psi_p}{\partial \xi_1} \frac{\partial \psi_i}{\partial \xi_1} d\xi_1 \right) u_{ij}$$

$$\int_{\Omega} p \frac{\partial v}{\partial x} \frac{\partial u}{\partial x} dx = \sum_{pq} \sum_{ij} v_{pq} p \frac{L_2}{L_1} \hat{M}_{qj} \hat{K}_{pi} u_{ij} \tag{3.25}$$

where $\hat{K}$ is one-dimensional stiffness matrix on [-1,1]. By using tensor notation in Equation (3.20) gives,

$$\int_{\Omega} p \frac{\partial v}{\partial x} \frac{\partial u}{\partial x} dx = p \frac{L_2}{L_1} \underline{v}^T \left(\hat{M} \otimes \hat{K} \right) \underline{u} \tag{3.26}$$

By using the expansions with same equations above, second term on the RHS of Equation (3.24) will be,

$$\int_{\Omega} p \frac{\partial v}{\partial y} \frac{\partial u}{\partial y} dx = \sum_{pq} \sum_{ij} v_{pq} p \frac{L_1}{L_2} \left(\int_{-1}^{1} \frac{\partial \psi_q}{\partial \xi_2} \frac{\partial \psi_j}{\partial \xi_2} d\xi_2 \right) \left(\int_{-1}^{1} \psi_p \psi_i d\xi_1 \right) u_{ij}$$

$$\int_{\Omega} p \frac{\partial v}{\partial y} \frac{\partial u}{\partial y} dx = \sum_{pq} \sum_{ij} v_{pq} p \frac{L_1}{L_2} \hat{K}_{qj} \hat{M}_{pi} u_{ij} \tag{3.27}$$

where $\hat{K}$ is one-dimensional stiffness matrix on [-1,1]. By using tensor notation in Equation (3.20) gives,

$$\int_{\Omega} p \frac{\partial v}{\partial y} \frac{\partial u}{\partial y} dx = p \frac{L_1}{L_2} \underline{v}^T \left(\hat{K} \otimes \hat{M} \right) \underline{u} \tag{3.28}$$

Numerical quadrature can also be utilized to evaluate $\hat{K}$

$$\hat{K}_{ij} = \sum_{k=0}^{N} w_k \psi_i'(\xi_{1k}) \psi_j'(\xi_{1k}) = \sum_{k=0}^{N} w_k \frac{\partial \psi_i(\xi_{1k})}{\partial \xi_1} w_k \frac{\partial \psi_j(\xi_{1k})}{\partial \xi_1}$$

$$\hat{K}_{ij} = \sum_{k=0}^{N} w_k \frac{\partial L_i(\xi_{1k})}{\partial \xi_1} \frac{\partial L_j(\xi_{1k})}{\partial \xi_1} \tag{3.29}$$

ξ_{1k} is the tensor product matrix corresponding to ξ_1 coordinates of the element. Considering the number of nodes in the direction of x and y equals to each other, $\hat{K}_{pi}$ equals to $\hat{K}_{qj}$. This equation is recalled as one dimensional stiffness matrix and its implementation is also comparable.

More accurate evaluation can performed for one dimensional stiffness matrix if exact evaluation of mass matrix is obtained ($\psi_i'\psi_j'$ has got a degree of 2N-2). Because Gauss-Lobatto-Legendre rule which is applied for N+1 points, is applied also for all polynomials of degree 2N-1 or less [23].

$\frac{\partial L_i(\xi_{1k})}{\partial \xi_1}$ is the derivative of the Lagrangian polynomials. $D_{N,ij}^{(1)}$ will be the differentiation matrix and can be represented as follows;

$$D_{N,ij}^{(1)} := \left.\frac{dL_j}{d\xi}\right|_{\xi=\xi_i} = \begin{Bmatrix} \frac{L_N(\xi_i)}{L_N(\xi_i)}\frac{1}{\xi_i-\xi_j}, \to i \neq j \\ -\frac{(N+1)N}{4}, \to i=j=0 \\ \frac{(N+1)N}{4}, \to i=j=N \\ 0, i=j=1,...,N-1 \end{Bmatrix} \tag{3.30}$$

The matrix elements are represented as the nodal values of first derivative corresponding to Gauss-Lobatto-Legendre Lagrangian polynomials.

By combining Equations (3.26) and (3.28) with similar expression for derivatives of y, Equation (3.20) becomes,

$$A(u,v) = \underline{v}^T \left(p\frac{L_2}{L_1}\left(\hat{M}\otimes\hat{K}\right) + p\frac{L_1}{L_2}\left(\hat{K}\otimes\hat{M}\right) + p\frac{L_1L_2}{4}\left(\hat{M}\otimes\hat{M}\right)\right)\underline{u} \tag{3.31}$$

At the RHS of Equation (3.13), In case there is no force equation for load matrix, it is required to be calculated for all of the PDE's.

$$F(v) = \int_\Omega f(x,y).v(x,y)dxdy = \frac{L_1L_2}{L_4}\underline{v}^T\left(\hat{M}\otimes\hat{M}\right)\underline{f} \tag{3.32}$$

The second expression is obtained by the insertion of the interpolant of $f(x)$ into the RHS of Equation (3.13) [23].

3.4.3 Helmholtz (Neumann) Operator for a Single Element

Equations from (3.20) to (3.32) explain the essential procedures for evaluation of the bilinear form $(u,v), A(u,v)$ and $F(v)$ for any element pair ($u,v \in V_N$). The discrete Helmholtz operator,

$$\bar{H} := p\left[\frac{L_2}{L_1}\left(\hat{M}\otimes\hat{K}\right)+p\frac{L_1}{L_2}\left(\hat{K}\otimes\hat{M}\right)+q\frac{L_1L_2}{4}\left(\hat{M}\otimes\hat{M}\right)\right] \tag{3.33}$$

is sometimes called as the Neumann operator. Because, it is the system obtaining the homogeneous Neumann problem. It is positive and symmetric. It is also definite unless q=0, if it has one dimensional nullspace of the constant mode.

3.4.4 Laplacian Operator for a Single Element

For q=0, the Laplacian operator, which is also named as Steady diffusion operator will be,

$$\mathcal{L} := p\left[\frac{L_2}{L_1}\left(\hat{M}\otimes\hat{K}\right)+p\frac{L_1}{L_2}\left(\hat{K}\otimes\hat{M}\right)\right] \tag{3.34}$$

For Laplacian problem,

$$\mathcal{L}u = \mathcal{F}(v) \tag{3.35}$$

Here, the local stiffness matrix is evaluated. The local stiffness matrix is of a rectangular element on reference coordinates and it is calculated for steady diffusion operator. Sometimes K is called by its symbol, because it is name is stiffness matrix.

All of the stiffness matrices corresponding to the square element which are located on different coordinates with same degree, are identical. $\mathcal{F}(v)$ will be different regardless of the dependency of force function on x and y coordinates.

For non-zero Neumann boundary condition, in case of square domain, poldif.m can be utilized in order to find the differentiation matrix in respect of x or y of element [23, 24].

3.4.5 The Variable-Coefficient Case

In order to develop the system matrices, it is required to perform the evaluation of integrals once again in the first term at RHS of Equation (3.24) for the case of variable p(x,y). The reference coordinate and physical coordinate are same. For 2D domains, the first term corresponding to Equation (3.24) is written as,

$$\mathcal{A}_x(u,v) := \int_{-1}^{1}\int_{-1}^{1} p(\xi_1,\xi_2)\frac{\partial v}{\partial \xi_1}\frac{\partial u}{\partial \xi_1}d\xi_1 d\xi_2 \tag{3.36}$$

which establishes a single term in the energy inner product $\mathcal{A}_x(u,v)$. To produce discrete operators, the expansion equations corresponding to (3.14), (3.15), (3.16), (3.17) for u, v and p are inserted into Equation (3.36):

$$\mathcal{A}_x(u,v)\sum_{pq}\sum_{ij}v_{pq}\sum_{mn}p_{mn}\left(\int_{-1}^{1}\psi_q\psi_j\psi_n d\xi_2\right)\left(\int_{-1}^{1}\frac{\partial\psi_p}{\partial\xi_1}\frac{\partial\psi_i}{\partial\xi_1}\psi_m d\xi_1\right)u_{ij} \qquad (3.37)$$

If left in this form, tensor product form is destroyed by p_{mn} which makes an unacceptable fill in stiffness matrix.

$$\mathcal{A}_y(u,v)\sum_{pq}\sum_{ij}v_{pq}\sum_{mn}p_{mn}\left(\int_{-1}^{1}\frac{\partial\psi_q}{\partial\xi_2}\frac{\partial\psi_j}{\partial\xi_2}\psi_n d\xi_2\right)\left(\int_{-1}^{1}\psi_p\psi_j\psi_m d\xi_1\right)u_{ij} \qquad (3.38)$$

The Spectral element method avoids this difficulty by employing a high order quadrature rule. This rule is based on Gauss Lobatto Legendre points and it is coupled with Lagrangian basis functions. The first integral which is defined in the right side of the Equation (3.38) is approximated as,

$$\sum_{k=0}^{N}\frac{dL_p(\xi_{1k})}{d\xi_1}\frac{dL_i(\xi_{1k})}{d\xi_1}L_m(\xi_{1k})w_k=\frac{dL_p(\xi_{1m})}{d\xi_1}\frac{dL_i(\xi_{1m})}{d\xi_1}w_m=\hat{D}_{mp}\hat{D}_{mi}\hat{D}_m \qquad (3.39)$$

where $\hat{D}_{mp}:=\frac{dL_p(\xi_{1m})}{d\xi_1}$. The second integral which is defined in Equation (3.38) is approximated as,

$$\sum_{k=0}^{N}L_q(\xi_{1k})L_j(\xi_{1k})L_n(\xi_{1k})w_{1k}=\delta_{qn}\delta_{jn}w_n \qquad (3.40)$$

Let $P:=\mathrm{diag}(p_{\dot{m}})$ and $W:=\mathrm{diag}(w_{\dot{m}})$ diagonal matrices. This matrices have entries $p_{\dot{m}}=p_{mn}$ and $w_{\dot{m}}:=p_{mn}w_m w_n$ where $\hat{m}=1+m+(N+1)n$ corresponding to natural ordering of the nodes [23]. W can be represented regarding tensor product forms where $\hat{M}=\mathrm{diag}(w_i)$.

$$W=P(\hat{M}\otimes\hat{M}) \qquad (3.41)$$

and the integral expression in Equation (3.36) is altered regarding W,

$$\mathcal{A}_x(u,v)=\underline{v}^T\left(I\otimes\hat{D}^T\right)W\left(I\otimes\hat{D}\right)\underline{u} \qquad (3.42)$$

From this expression, the spectral element stiffness matrix can be finalized for Equation (3.24) for q=0.

$$\bar{K} = \left(I \otimes \hat{D}^T\right) W \left(I \otimes \hat{D}\right) + \left(\hat{D}^T \otimes I\right) W \left(\hat{D} \otimes I\right) \tag{3.43}$$

The appearance of matrix P in Equation (3.41) is not in tensor form. Because of that, the fast diagonalization method cannot be utilized to invert $\bar{K}$. However, the order of complexity of forward application is obtained by the differentiation regarding with matrices D and D^T which is $O\left(N^{d+1}\right)$. Because, the cost of applying the diagonal matrix to a vector is $O\left(N^d\right)$. It is important to note that, if W were full instead of being diagonal, the cost of applying $\bar{K}$ would be $O\left(N^{2d}\right)$ [23].

3.5 Local Elemental Procedures for Quadrilateral Elements

It is important to remember that, it is required to evaluate the inner products of the form for every elemental region to solve Galerkin formulation of the Laplace equation which is defined for deformed geometries. The Equation (3.24) for q=0 can be re-arranged as follows;

$$\mathcal{A}(u,v) = \int_{\Omega^e} p(x) \nabla v . \nabla u dx = \int_{\Omega_M} p(x) \nabla v . \nabla u J(\xi) d\xi \tag{3.44}$$

where Ω^e represents the element region. Ω_{st} represents the computational domain. x represents the Cartesian coordinates and J represents the Jacobian of the mapping between two regions. There are three important notions based on the structure of inner product. First, integration within Ω_{st}. Second, differentiation in the problem domain Ω_{st}. Last, differentiation in the elemental region Ω^e. In order to differentiate and integrate the elemental region, between these regions, elemental mapping is defined.

The Local Cartesian coordinates $\left(\xi_1, \xi_2\right)$ which are denoted by,

$$x = x_1^e\left(\xi_1, \xi_2\right), \quad y = x_2^e\left(\xi_1, \xi_2\right) \tag{3.45}$$

are defined in 2D so that consider these cases a one to one mapping amongst Cartesian coordinates $\left(x_1, x_2\right)$. Likewise,

$$x = x_1^e\left(\xi_1, \xi_2, \xi_3\right), \quad y = x_2^e\left(\xi_1, \xi_2, \xi_3\right), \quad z = x_3^e\left(\xi_1, \xi_2, \xi_3\right) \tag{3.46}$$

are defined in three dimensions [23].

3.5.1 Elemental Mappings for General Straight-Sided Elements

In order to produce a simple mapping for elemental shapes with no curved edges, linear vertex modes of a modified modal expansion can be utilized.

Due to linear order elements, it is named as bilinear mapping for a random-shaped straight-sided quadrilateral where only the Cartesian coordinates of the vertices required to be prescribed.

For the straight-sided quadrilaterals,

$$x_i = x_i^A \frac{(1-\xi_1)}{2}\frac{(1-\xi_2)}{2} + x_i^B \frac{(1-\xi_1)}{2}\frac{(1-\xi_2)}{2} + x_i^D \frac{(1-\xi_1)}{2}\frac{(1-\xi_2)}{2} + x_i^C \frac{(1-\xi_1)}{2}\frac{(1-\xi_2)}{2},\ \mathrm{i}=1,2 \tag{3.47}$$

The equation (3.47) is sub parametric for high-order element matrices. It is important to underline that the Jacobian of the mapping to the standard region should be non-zero when developing a mapping. It should also be of the same sign. To meet these requirements, all elemental regions need to have internal corners with angles less than 180 degrees. Similarly, if the quadrilaterals are concave, it would not be possibly to generate local stiffness matrix with an interior angle wider than 180 degrees, so they are required to be convex shaped [23].

3.5.2 Elemental Mappings for General Curvilinear Elements

From Equation (3.47), it can be inferred that this includes the vertex modes corresponding to modified hierarchical expansion basis. The mapping formula above can also be represented as:

$$x_1 = x_1^e(\xi_1,\xi_2) = \sum_{p=0}^{N_1}\sum_{q=0}^{N_2}(x_1)_{pq}\phi_{pq}(\xi_1,\xi_2) \tag{3.48}$$

$$x_2 = x_2^e(\xi_1,\xi_2) = \sum_{p=0}^{N_1}\sum_{q=0}^{N_2}(x_2)_{pq}\phi_{pq}(\xi_1,\xi_2) \tag{3.49}$$

where $\phi_{pq} = \psi_p^a(\xi_1)\psi_q^a(\xi_1)$ and $x_{pq}^i = 0$, apart from vertex modes which are exception and having values,

$$\begin{aligned} (x_1)_{0,0} &= x_1^A \qquad (x_1)_{N_1,0} = x_1^B \\ (x_1)_{N_1,N_2} &= x_1^c \qquad (x_1)_{0,N_1} = x_1^D \end{aligned} \tag{3.50}$$

Creating a mapping using the expansion modes in this form allows us to include curved-sided regions by representing them isoparametrically. The geometric representations consist of an expansion of the same and polynomial order as the variables.

Defining and representing a curved region is more complex than representing a straight-sided region, which only requires the values of the vertex locations. Mesh generation process of the isoparametric quadrilateral, involves the process of defining the mapping functions. A definition of mapping with edges represented in Cartesian coordinates can be shown as: $f_i^A(\xi_1)$, $f_i^B(\xi_1)$, $f_i^C(\xi_2)$, and $f_i^D(\xi_2)$. The definition process of mapping functions is thought as a part of mesh generation process corresponding to isoparametric quadrilateral [23].

If definition of the edges is known, a mapping for curvilinear domains can be utilized. To achieve that, isoparametric form of equation should be employed so that include more non-zero expansion coefficients. In case of existence of a polynomial in wrong order, the approximation of shape mapping is required $f_1(\xi)$.

This can be achieved by utilizing an approximation of the edge function in aspects of the Lagrange polynomial. The approximation for $f_i^A(\xi_1)$ is utilized as,

$$f^A(\xi_1) \simeq \sum_{p=0} f^A(\xi_i, i) h_p(\xi_1) \tag{3.51}$$

$$\simeq \sum_{p=0} \hat{x}_{p_0}^i \psi_p(\xi_1) \tag{3.52}$$

Coincidence of each element corresponding to the vertices provides the elements remain continuous and this is one important feature for approximation. One way to assure that is to utilize collection projection. The collection points should include the endpoints $\xi_1 \pm 1$. A coherent way to approximate $f_i^A(\xi_1)$ is represented in (3.51). Utilizing the Gauss-Lobatto-Legendre quadrature points are useful for the collocation projection. Applying collocation projections to nodal points series, f^A can approximately represented in aspects of a hierarchical expansion $\psi_p(\xi)$ so that obtain

the coefficients $\hat{x}_{p_0}^i$ in Equation (3.52). In case the polynomials span has same space, the final modification can be applied by collocation or Galerkin projection. Modified Galerkin projection can be employed in case of usage corresponding to more collocation points. If the coordinate expansion coefficients are determined, $\hat{x}_{p_0}^i$, (3.48) , (3.49), and (3.50) can be calculated in order to govern the isoparametric mapping from standard region [23].

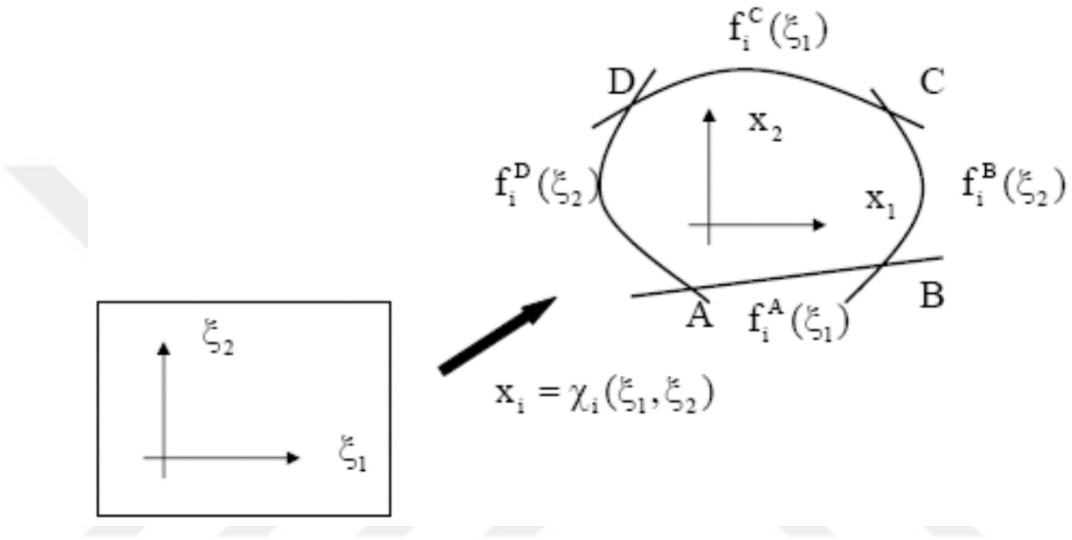

Figure 3.1: A general curved quadrilateral element can be expressed in terms of series of parametric functions. $f^A(\xi_1)$, $f^B(\xi_1)$, $f^C(\xi_2)$, and $f^D(\xi_2)$ (Adopted from [24]).

For the quadrilateral region which is illustrated in Figure 3.1 the linear blending function can be represented as,

$$\begin{aligned}\mathcal{X}_i(\xi) = {} & f^A(\xi_1)\frac{(1-\xi_2)}{2} + f^C(\xi_1)\frac{(1-\xi_2)}{2} + f^D(\xi_2)\frac{(1-\xi_1)}{2} + \\ & f^B(\xi_2)\frac{(1-\xi_1)}{2} - \frac{(1-\xi_1)}{2}\frac{(1-\xi_2)}{2} f^A(-1) - \frac{(1+\xi_1)}{2}\frac{(1-\xi_2)}{2} f^A(1) \\ & - \frac{(1-\xi_1)}{2}\frac{(1+\xi_2)}{2} f^C(-1) + \frac{(1+\xi_1)}{2} f^C(1)\end{aligned} \tag{3.53}$$

where the vertex points are not discrete. If $f^A(\xi_1)$, $f^B(\xi_1)$, $f^C(\xi_2)$, and $f^D(\xi_2)$ are substituted in Equation (3.51) and reorganized, the expansion of the form which is given by (3.48) and (3.49) can be achieved. The Equation (3.53) which is a blending function has been utilized in spectral element methods with approximation of an

Equation (3.51) to the mapped edges. Local collapsed coordinates should not be employed to generate a non-smooth Jacobian. Continuity of C^0 can be lost [23].

3.5.3 Integration Inside of an Element Region

After the coordinates are governed corresponding to element's inner and surface nodes, all partial derivatives required to be determined. $\frac{\partial \xi_1}{\partial x_1}, \frac{\partial \xi_2}{\partial x_1}, \frac{\partial \xi_1}{\partial x_2}, \frac{\partial \xi_2}{\partial x_2}$ must be obtained in order to find Laplacian operator.

$$\left|J_{2D}\right| = \begin{vmatrix} \frac{\partial x_1}{\partial \xi_1} & \frac{\partial x_1}{\partial \xi_2} \\ \frac{\partial x_2}{\partial \xi_1} & \frac{\partial x_1}{\partial \xi_2} \end{vmatrix} = \frac{\partial x_1}{\partial \xi_1}\frac{\partial x_2}{\partial \xi_2} - \frac{\partial x_1}{\partial \xi_2}\frac{\partial x_2}{\partial \xi_1} \tag{3.54}$$

3.5.4 Differentiation Inside of an Elemental Region

The chain rule is utilized for the 2D case so that differentiate a function inside the random elemental region Ω^e

$$\nabla = \begin{bmatrix} \frac{\partial}{\partial x_1} \\ \frac{\partial}{\partial x_2} \end{bmatrix} = \begin{bmatrix} \frac{\partial \xi_1}{\partial x_1}\frac{\partial}{\partial \xi_1} + \frac{\partial \xi_2}{\partial x_1}\frac{\partial}{\partial \xi_2} \\ \frac{\partial \xi_1}{\partial x_2}\frac{\partial}{\partial \xi_1} + \frac{\partial \xi_2}{\partial x_2}\frac{\partial}{\partial \xi_2} \end{bmatrix} \tag{3.55}$$

To evaluate partial derivatives in form of $\frac{\partial \xi_1}{\partial x_1}$, they are represented in aspects of ξ_1, ξ_2

The total change follows as; ($x_1 = x_1^e(\xi_1, \xi_2), x_2 = x_2^e(\xi_1, \xi_2)$)

$$\begin{bmatrix} dx_1 \\ dx_2 \end{bmatrix} = \begin{bmatrix} \frac{\partial x_1}{\partial \xi_1} & \frac{\partial x_1}{\partial \xi_2} \\ \frac{\partial x_2}{\partial \xi_1} & \frac{\partial x_2}{\partial \xi_2} \end{bmatrix} \begin{bmatrix} d\xi_1 \\ d\xi_2 \end{bmatrix} \tag{3.56}$$

In order to obtain, it can be inverted [23].

$$\begin{bmatrix} d\xi_1 \\ d\xi_2 \end{bmatrix} = \underbrace{\frac{1}{|J_{2D}|}\begin{bmatrix} \frac{\partial x_2}{\partial \xi_2} & -\frac{\partial x_1}{\partial \xi_2} \\ -\frac{\partial x_2}{\partial \xi_1} & \frac{\partial x_1}{\partial \xi_1} \end{bmatrix}}_{J^{-1}} \begin{bmatrix} dx_1 \\ dx_2 \end{bmatrix} \tag{3.57}$$

However, since mapping is considered to be one to one. And it has an inverse,

$$\xi_1 = (x_1^e)^{-1}(x_1, x_2), \qquad \xi_2 = (x_2^e)^{-1}(x_1, x_2) \tag{3.58}$$

and consequently, it is achieved that,

$$\begin{bmatrix} d\xi_1 \\ d\xi_2 \end{bmatrix} = \begin{bmatrix} \frac{\partial \xi_1}{\partial x_1} & \frac{\partial \xi_1}{\partial x_2} \\ \frac{\partial \xi_2}{\partial x_1} & \frac{\partial \xi_2}{\partial x_2} \end{bmatrix} \begin{bmatrix} dx_1 \\ dx_2 \end{bmatrix} \tag{3.59}$$

which by evaluation, finally gives,

$$\begin{aligned} \frac{\partial \xi_1}{\partial x_1} &= \frac{1}{|J_{2D}|}\frac{\partial x_2}{\partial \xi_2} & \frac{\partial \xi_1}{\partial x_2} &= -\frac{1}{|J_{2D}|}\frac{\partial x_1}{\partial \xi_2} \\ \frac{\partial \xi_2}{\partial x_1} &= -\frac{1}{|J_{2D}|}\frac{\partial x_2}{\partial \xi_1} & \frac{\partial \xi_2}{\partial x_2} &= \frac{1}{|J_{2D}|}\frac{\partial x_1}{\partial \xi_1} \end{aligned} \tag{3.60}$$

The 2D gradient operator can be obtained as whole partial derivatives are represented in terms of differentials respected to ξ_1, ξ_2

3.6 Implementation of Spectral Element Method

High order FEM was not well-known until 1980. Because high order means increased size of the element matrix. If size of element matrix is increased, the computational time is also increased. Decreasing the band size corresponding to the assembled stiffness matrix was a problem consists of the earliest times of FEM. Hence, diagonal mass matrix is the great asset for whom involves in Finite element method. Since Gauss-Lobatto-Legendre Lagrangian polynomials equal to kronecker delta at Gauss-Lobatto-Legendre nodes, GLL Lagrangian polynomials and quadrature are utilized. The matrix will be filled, If the same polynomials and quadrature are not utilized [23].

3.7 Vector Potential Equation with Single Rectangular Spectral Element

Rectangular element stiffness matrix is achieved by utilizing the Equation (3.34). Global stiffness matrix is equivalent to rectangular element stiffness matrix. Consequently, numbering local nodes equals to numbering global nodes.

3.7.1 Evaluation of Gauss Lobatto Legendre Nodes and Weights

The Lobatto function implemented in Lobatto.m is utilized as `[w, y] = Lobatto(N)` in order to find Gauss Lobatto Legendre weights and nodes in range 1, -1. The row vector x is also represented as the roots of Gauss Lobatto Legendre Lagrangian polynomials. The function is implemented by Tarman [24] and is given in Appendix A.

3.7.2 Evaluation of Mass Matrix and One Dimensional Stiffness Matrix

As it was mentioned before, $L_i(\xi_j) = \delta_{ij}$, where δ_{ij} is the Kronecker Delta. There is no doubt that $L_i(\xi_j)$ equals to `I = eye(N+1);` In Fig. 2, Gauss Lobatto Legendre polynomials within the degree of N=6 are illustrated.

The function which is expressed as `D = poldif(x,1);` evaluates the differentiation matrix. It is element in first row and the first column is the derivative of $L_1(\xi_1)$ at $x = 1$, $L_1(\xi_1 = 1)$. D(:, p) is the derivative of $L_i(\xi_1)$ whole points in range [1, -1] which means the matrix's pth column. The initial collocation point is 1. It can be inferred from the graph corresponding to lagrangian polynomials. The derivative of pth lagrangian polynomials equal to zero at pth collocation point except the points of first and last. For instance, the function `D = poldif(x, 2);` finds the differentiation matrix in second order [23].

3.7.2.1 Evaluation of one dimensional mass matrix

Equations (3.22) and (3.23) can be both utilized. Equation (3.23) is defined as `RH2 = diag(w);` Equation (3.22) is defined as;

Mathematical Expression	MATLAB implementation

$\hat{M}_{ij} = \sum_{k=0}^{N} w_k L_i(\xi_k) L_j(\xi_k)$	`for p=1:N+1`
	`  for q=1:N+1`
	`  L=I(:,q).*I(:,p)`
	`  RHS2(p,q)=dot(w,L);`
	`  end`
	`end`

$\hat{M} = diag(w_i)$	`RHS2=diag(w)`

`w` is the w_k and `L` is the $L_i(\xi_k)L_j(\xi_k)$. `w` and `k` are same dimensioned vectors. In order to achieve multiplication of array ".*" operators are utilized. The line which is implemented as `L=I(:,q).*I(:,p)` represents point by point product of `I(:,q)` and `I(:,p)`. The dot product is achieved by the following piece of code;

`dot(w,L)=w(1)*L(1)+w(2)*L(2)+...+w(N+1)*L(N+1)`

The fourth order of Lagrangian polynomial is illustrated in Figure 3.2. It can be inferred that it oscillates less than fourth equispaced Lagrangian polynomial at the boundaries [23].

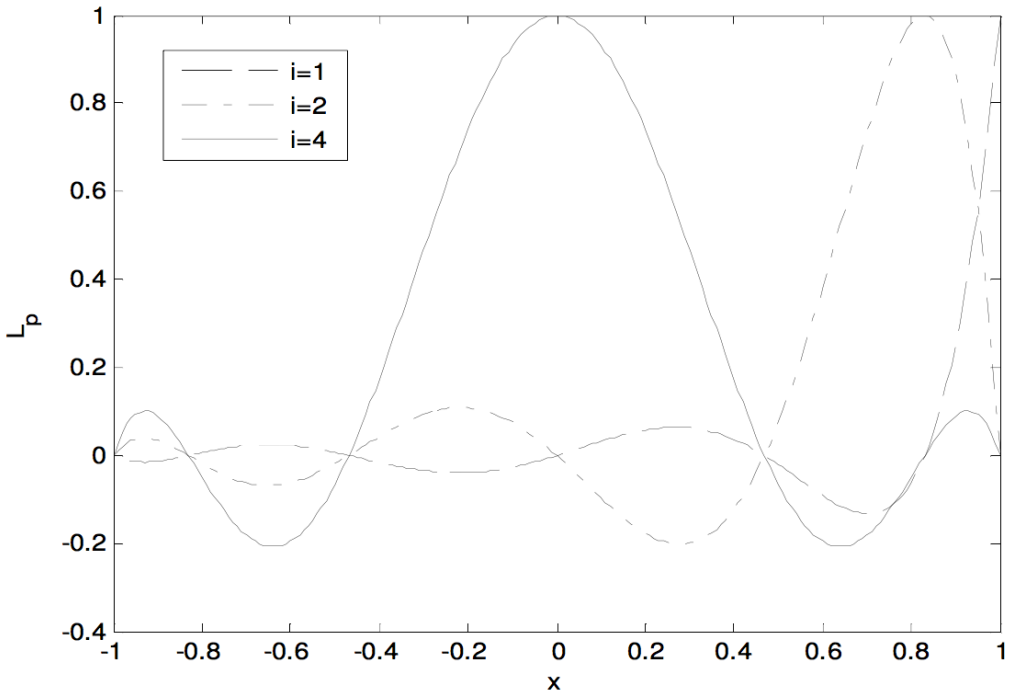

Figure 3.2: The plot of GLL Lagrangian polynomials obtained for 6th degree. There are 7 collocation points between [1, -1]. p = i. (Adopted from [23]).

3.7.2.2 Evaluation of two dimensional mass matrix

Equation (3.20) is defined as,

Mathematical Expression | MATLAB implementation

$$M = \frac{L_1 L_2}{4} \hat{M} \otimes \hat{M}$$

```
s=kron(RHS2, RHS2);
```

The two dimensional matrix is diagonal. L_1 and L_2 represent the length of standard element and are equal to 2. The kronecker product of A and B matrices is represented by $A \otimes B$ [23]. The computation of kronecker product is achieved by MATLAB with built-in function `kron(A,B)`. If $p \times q$ and $r \times s$ represent the dimensions corresponding to A and B respectively, $A \otimes B$ becomes a matrix with a dimension $pr \times qs$ with $p \times q$ block and arranged as follows,

$$\begin{pmatrix} 1 & 2 \\ 3 & 4 \end{pmatrix} \otimes \begin{pmatrix} a & b \\ c & d \end{pmatrix} = \begin{pmatrix} a & b & 2a & 2b \\ c & d & 2c & 2d \\ 3a & 3b & 4a & 4b \\ 3c & 3d & 4c & 4d \end{pmatrix} \tag{3.61}$$

3.7.2.3 Evaluation of one dimensional stiffness matrix

Equation (3.29) is utilized to obtain one dimensional stiffness matrix. It is implemented as follows,

Mathematical Expression | MATLAB implementation

$$\hat{K}_{ij} = \sum_{k=0}^{N} w_k \frac{\partial L_i(\xi_{1k})}{\partial \xi_1} \frac{\partial L_j(\xi_{1k})}{\partial \xi_1}$$

```
for p=1:N+1
  for q=1:N+1
      Ae=D(:,q).*D(:,p);
      df2(p,q)=dot(w,Ae);
  end
end
```

3.7.3 Construction of the Grid

Local coordinates corresponding to the master elements are obtained by `Lobatto.m`. The collocation points which is located in x and y direction are same for N=21. However, it is not compulsory to have same degree for all directions.

`[xx,yy] = meshgrid(x(1:N+1), y(1:N+1));` gives the local coordinates corresponding to each node which is presented in Figure 3.3 of the master element [23].

3.7.3.1 Obtaining the plot of grid

The plot of master element grid can obtained by the command `plot(xx,yy,xx',yy')`. As it can be inferred from the Figure 3.3, the grid is denser near edges. Due to orthogonality feature of Gauss-Lobatto-Legendre polynomials the distance between nodes which are located near the edges is less than the nodes which are located near the intersection of midlines [23].

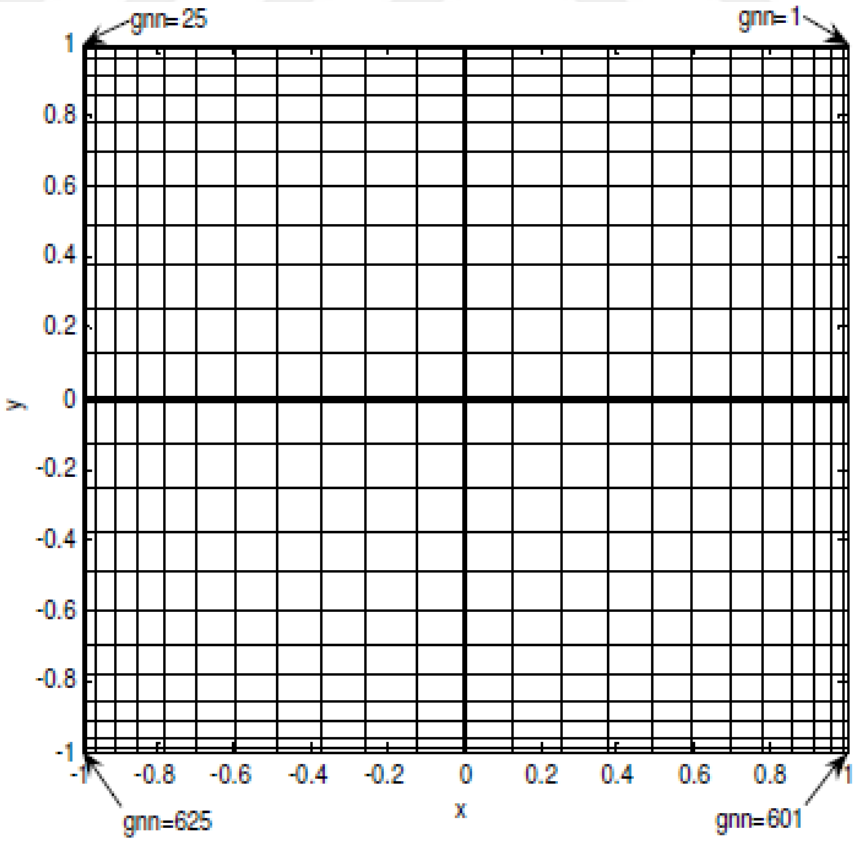

Figure 3.3: Single spectral element pilot obtained for degree of N=24. The bold lines represent the axis of the reference coordinates. There is an existing node at each intersection point. (Adopted from [23]).

3.7.4 Evaluation of Load Vector

The both equations (3.20) and (3.32) are identical but the force function included in Equation (3.32). The force function is evaluated at `xx = xx(:); yy = yy(:);` . Two dimensional mass matrix (M) is utilized to be implemented as s. Therefore, Equation (3.32) is implemented as,

Mathematical Expression

$$\mathcal{F}(v) = \frac{L_1 L_2}{4} \underline{v}^T \left(\hat{M} \otimes \hat{M} \right) \underline{f}$$

MATLAB implementation

```
for p=1:(N+1)^2
  for q=1:(N+1)^2
    if (p==q)
      RHS(q)=s(p,q).*f(q);
    end
  end
end
```

3.7.5 Evaluation of Steady Diffusion Operator

One dimensional stiffness and mass matrices $\hat{M}, \hat{K}$ was evaluated so as to implement the Equation (3.34). The Equation can be re-arranged for MATLAB implementation as follows,

Mathematical Expression

$$\mathcal{L} := p \left[\frac{L_2}{L_1} \left(\hat{M} \otimes \hat{K} \right) + p \frac{L_1}{L_2} \left(\hat{K} \otimes \hat{M} \right) \right]$$

MATLAB implementation

```
delta=kron(RHS2,df2)+kron(df2,RHS2);
```

Two dimensional rectangular element stiffness matrix is equal to steady diffusion operator in case of application for single element [23].

3.7.6 Imposing the Dirichlet Boundary Condition

Dirichlet BC can be utilized for a single rectangular spectral element by removing either first and last rows both or first and/or last rows corresponding to $\hat{K}$. The one dimensional stiffness matrix is evaluated by employing the Equation (3.29) and $\hat{M}$. One dimensional mass matrices are calculated by using Equation (3.22). The Equation (3.34) is defined in MATLAB as follows,

```
delta=kron(RHS2, df2(2:N, 2:N)+kron(df2(2:N,2:N), RHS2);
```

In Figure 3.4, the sparsity graph corresponding to the obtained delta is illustrated. As it is shown in the Figure 3.4, dimension of `delta` is 11200x11200. As it shown in the figure, black regions are of non-zero matrix elements and there are 5244760 elements having non-zero values in `delta` [23].

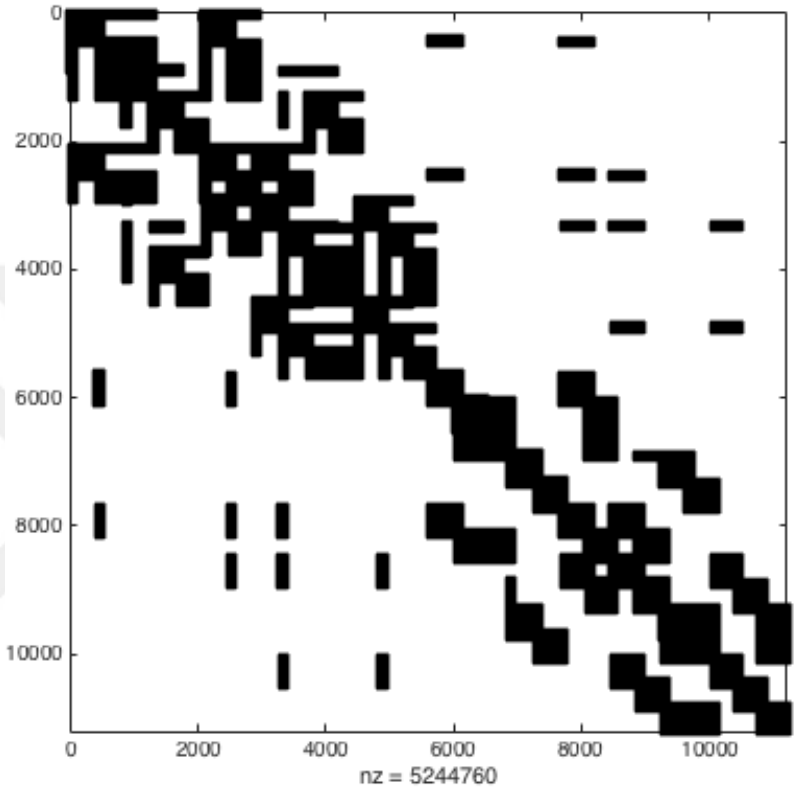

Figure 3.4: Sparsity plot of the element stiffness matrix.

3.7.7 Imposing the Neumann Boundary Conditions

For Neumann boundary condition, there is a method can be utilized on two dimensional rectangular elements so as to alter the related row in element stiffness matrix (steady diffusion operator) with related row corresponding to two dimensional 1st order differentiation matrix.

```
DNBC=kron(I, D)+kron(D, I);
```

The calculation of domain corresponding to square element stiffness and master element matrices which spans the area bounded by $-1 \le x \le 1,\ -1 \le y \le 1$ can obtained by same equations (3.22), (3.29), (3.34). If domain is not bounded by [1, -1], D must be obtained at one dimensional mapped nodes (from [1, -1] to [0, 1]). The D

differentiation matrix is utilized to evaluate steady diffusion operator. In addition to that, two dimensional first order differentiation matrix has to be same.

The related components which belong to the column vector `RHS'` is altered with u at the Neumann boundary condition.

```
RHS(c)=h;
```

c represents the node number corresponding to node numbers of Neumann boundary condition.

3.7.8 Evaluation of the u Values in Vector Potential Equations

```
un=-delta\RHS';
```

Backslash operator is employed to execute matrix left division. For the problem defined in thesis, delta is a matrix having size of 11200 by 11200. The elapsed time is 3.800713 seconds during calculation. If `inv()` command is executed to evaluate left division, 885.586415 seconds required for calculation which proves that the command is much slower than backslash. Besides that, MATLAB warns us not to use this command [23].

3.7.9 Plotting the Three Dimensional Graph of the Solution

In thesis, to represent the vector potential values surf and contour plots are created. In MATLAB, there are two built-in commands which provides a user to create contour and surf pilots which are `surf()` and `contour()`.

As it specified by MATLAB and stated in the manual, `contour()` command can take from 1 to N arguments. In our problem, we have two axis and vector potential values corresponding to these coordinates. Hence, we implemented the following code,

```
for elmt=1:28
  contour(X(:,:,elmt),Y(:,:,elmt),(uL(:,:,elmt))); hold on;
  contour(X(:,:,elmt),-Y(:,:,elmt),(uL(:,:,elmt))); hold on;
end
```

Due to the symmetry on the x axis, the contour plot is mirrored along the x.

For `surf()` command, the same procedure is applied and it takes some additional arguments for face color, edge color and face lighting. It is implemented as follows,

```
 for elmt = 1:28
 surf(X(:,:,elmt),Y(:,:,elmt),(uL(:,:,elmt)),'FaceColor','interp',...
 'EdgeColor','none',...
 'FaceLighting','phong')    ; hold on;
surf(X(:,:,elmt),-Y(:,:,elmt),(uL(:,:,elmt)),'FaceColor','interp',...
 'EdgeColor','none',...
 'FaceLighting','phong')    ; hold on;
 end
```

CHAPTER FOUR

RESULTS

4.1 Sample Problem

In this thesis, a typical magnetic problem is considered in time-invariant domain to verify the formulation of SEM which is presented in the previous chapter. The structure shown in Figure 4.1 is consists of an iron core which has three legs and two windows inside it. As it is shown in Figure 4.1, the coil, which provides the magnetizing current to the core, is placed along the middle leg. The resultant magnetic flux is divided equally between the left and right legs of iron core.

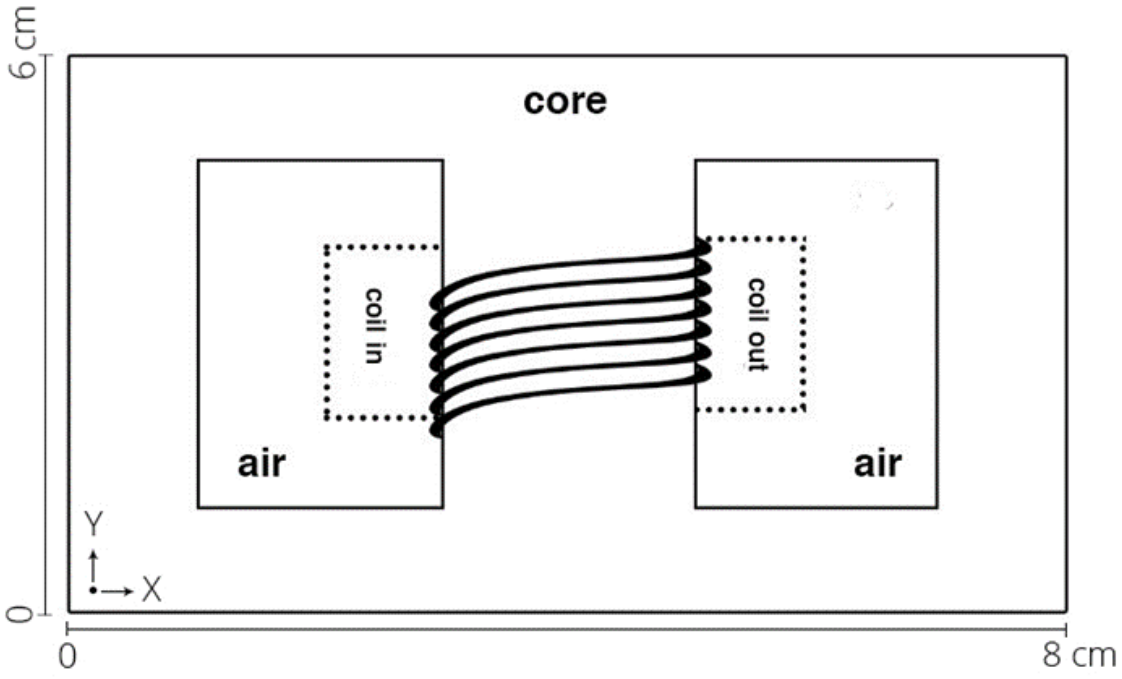

Figure 4.1: The structure of the problem.

The problem is defined in two dimensions on xy plane and as anyone can notice from Figure 1, the iron core is 8 cm wide and 6 cm high. The current injected through coil is 10 A/m^2. The permeability of the iron core is selected as 200000 times of permeability of air μ_0 which is represented in textbooks. It should be noticed that in simulation results, the flux density in air is almost zero due to selection of relatively high permeability of material.

In addition, it is important to note that the computational domain of the problem is reduced to half due to the fact that our problem is symmetrical around x-axis.

4.2 Meshing

As it is discussed in the spectral element method chapter, the computational domain has to be discretized into elements in order to be solved. The elements which are used for discretizing the computational domain is composed of Gauss-Legendre-Lobatto grids. Possible geometries of some elements that can be utilized by SEM are shown in Figure 4.2. As it is discussed earlier, like finite element methods, discretization of domains which are composed of deformed shapes can be handled by spectral element method.

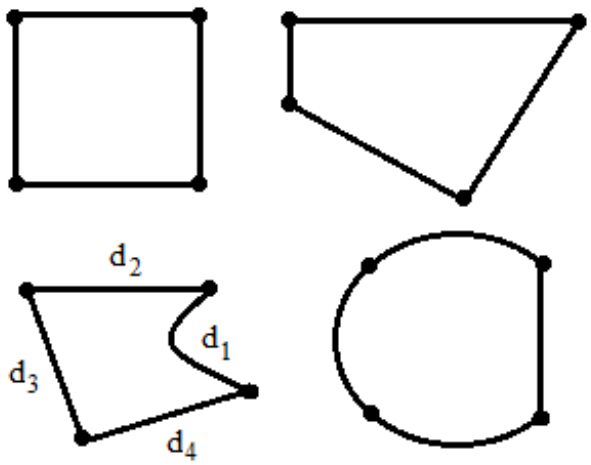

Figure 4.2: Representation of formed and deformed elements utilized by SEM.

Figures 4.3 and 4.4 show, respectively, the GLL node distributions in a regular element and a deformed element.

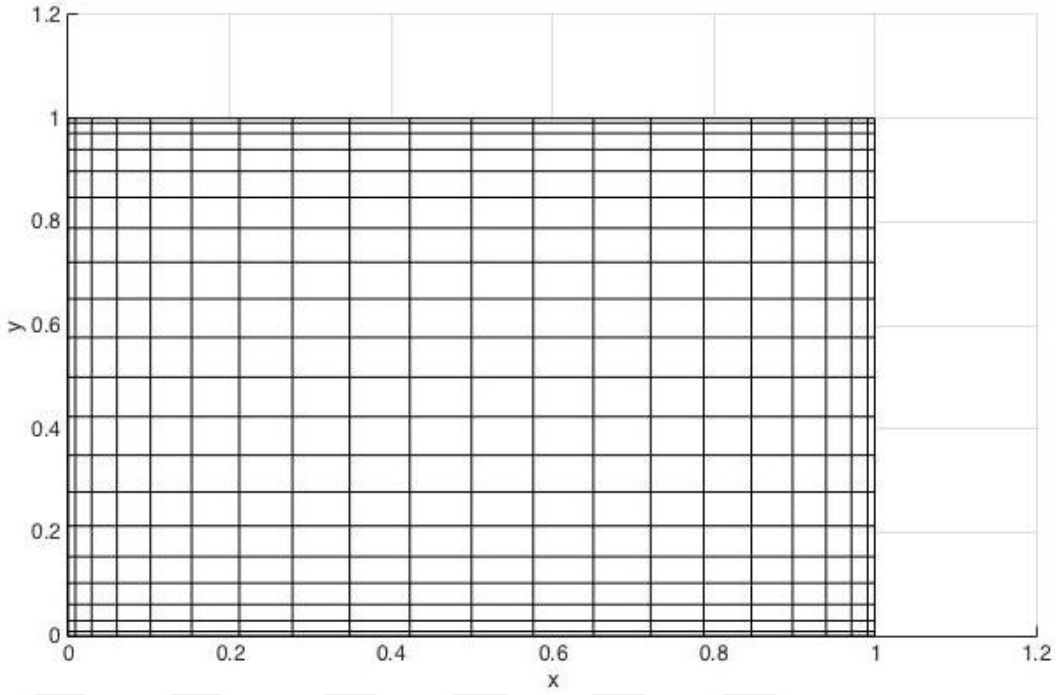

Figure 4.3: GLL grid in a regular square element (21x21 nodes).

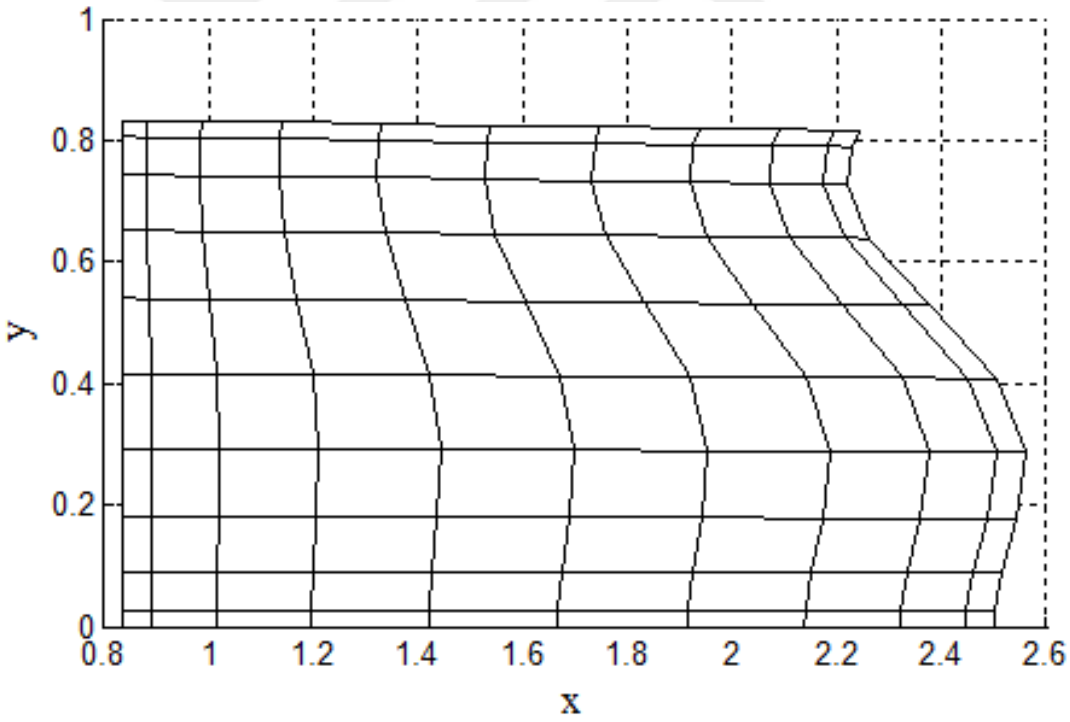

Figure 4.4: Discretized deformed element plot.

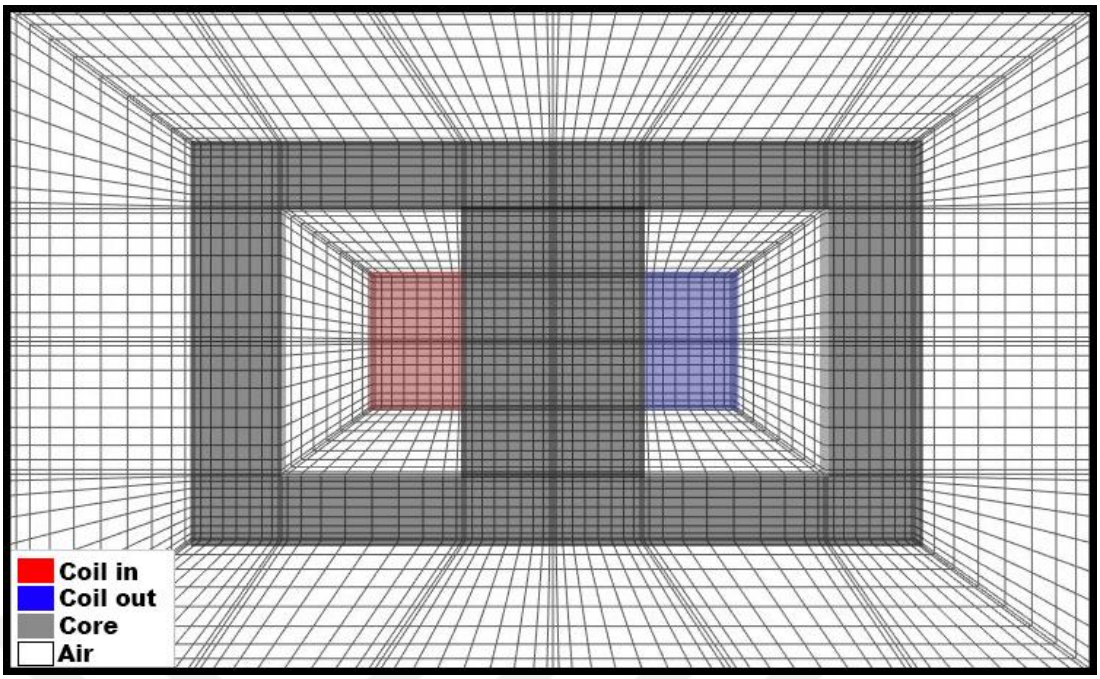

Figure 4.5: Gauss-Legendre-Lobatto grids in the elements forming the computational domain.

In Figure 4.5, complete meshing belongs to the computational domain is illustrated. As it can be noticed from the figure, spectral element discretization is similar to finite element discretization. In other words, elements are getting larger as we move farer from the region of interest.

Assignment of numbers to elements is vital for initialization of computational process. Because, before start computing, each individual element should be represented on the coordinates system. As it is illustrated in Figure 4.6, the assignment of numbers is started from 1 and ended up with 56. As anyone can infer from the figure, there is a symmetry on the x axis. Due to the symmetry, the difference between element numbers corresponding to mutual elements is 28. For instance, as an element's number at the upper side of x axis is 1, the element number corresponding to its mutual element is 29.

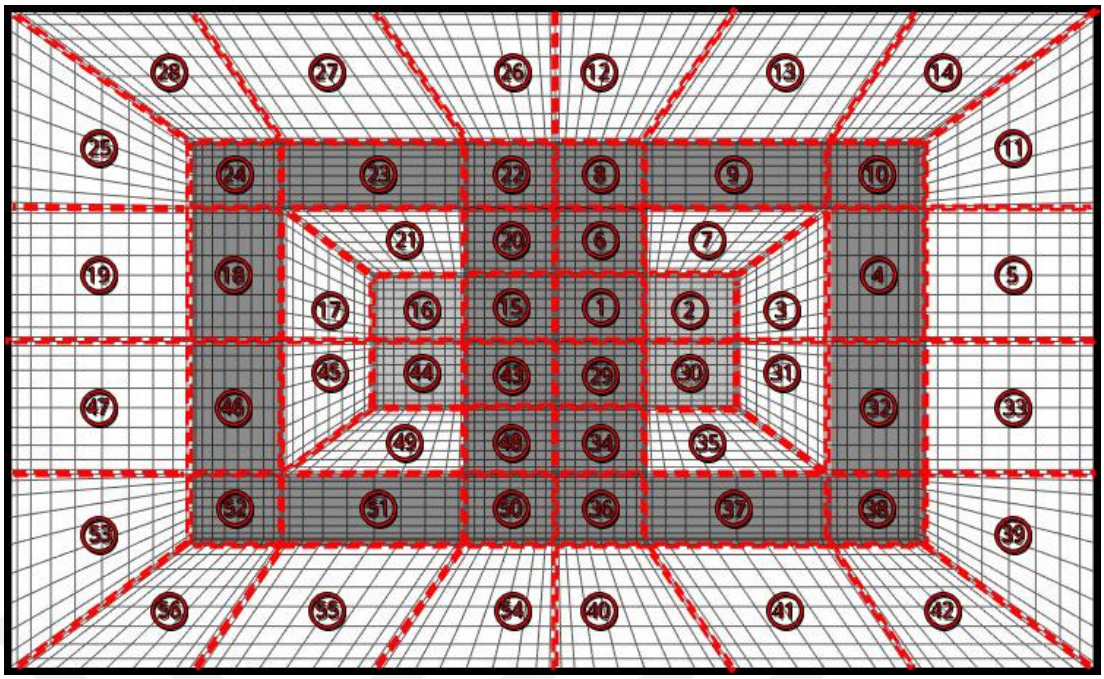

Figure 4.6: Element numbering corresponding to problem domain.

4.3 Boundary Conditions

Boundary conditions' definition is given in the second chapter and as it is mentioned, it is important to apply them on spectral element formulation in order to provide unique solution.

In this thesis, two types of boundary conditions are employed. Dirichlet boundary condition is applied along exterior boundaries so as to enforce zero vector potential values. In fact, choosing A = 0 will not affect the result due to the fact that most of the flux will flow in the core. Neumann boundary condition is applied along x axis (axis of symmetry). As it is stated in the definition corresponding to Neumann boundary condition, it provides us to ensure that zero tangential magnetic flux densities are guaranteed. In other words, the application of Neumann boundary condition along the x axis means that the derivative of vector potential values along the x axis is zero.

After obtaining the numerically solved vector potential, one can compute the magnetic flux density as follows:

$$B_x = \frac{\partial A}{\partial y}, \text{ and } B_y = \frac{\partial A}{\partial x}. \qquad (4.3.1)$$

The governing differential equations defining each region have derived in Chapter 2. But in order to solve those partial differential equations, the problem requires interface conditions to be defined on adjacent regions. This condition can be satisfied by defining the normal component of

$$\mathrm{n}.(\frac{1}{\mu}\nabla A) \tag{4.3.2}$$

on the boundary. The definition introduced in (4.3.2) provides us to define tangential value of electromagnetic field intensity on boundary.

4.4 Vector Potential Results

The aim of this thesis is to solve the partial differential equations which are derived from Maxwell's equations by applying the spectral element method to the problem explained in section 4.1. In this section, vector potential results are obtained and presented. In addition to that, vector potential values will be re-evaluated by changing one of the parameters such as magnetic permeability, injected current density or number of nodes whereas keeping rest of the parameters constant. Also, the results will be compared in terms of accuracy, computation time, memory consumption and CPU load.

Based on injected current and permeability specified as $J = 10\mathrm{A/m}^2$ and $\mu = 2\times10^5\mu_0$ in the problem definition section, vector potential result is obtained and illustrated in Figure 4.7. As it is shown in the figure, vector potential values reach maximum 0.3 T.m approximately.

It is well known fact that the derivative of magnetic vector potential equals to magnetic flux density. As it is illustrated in the figure, the derivation of vector potential value along green plane which represents outside of core is zero. That is to say, the magnetic flux density at outside the core equals to zero. On the other hand, the slope of vector potential is different than zero in the range [0, 1], [3, 4] and [-1 0], [-3,-4] on the x axis which proves that the vector potential values are varying across that range. Therefore, it can be said that the magnetic flux density values are different than zero and is directly proportional to slope of A.

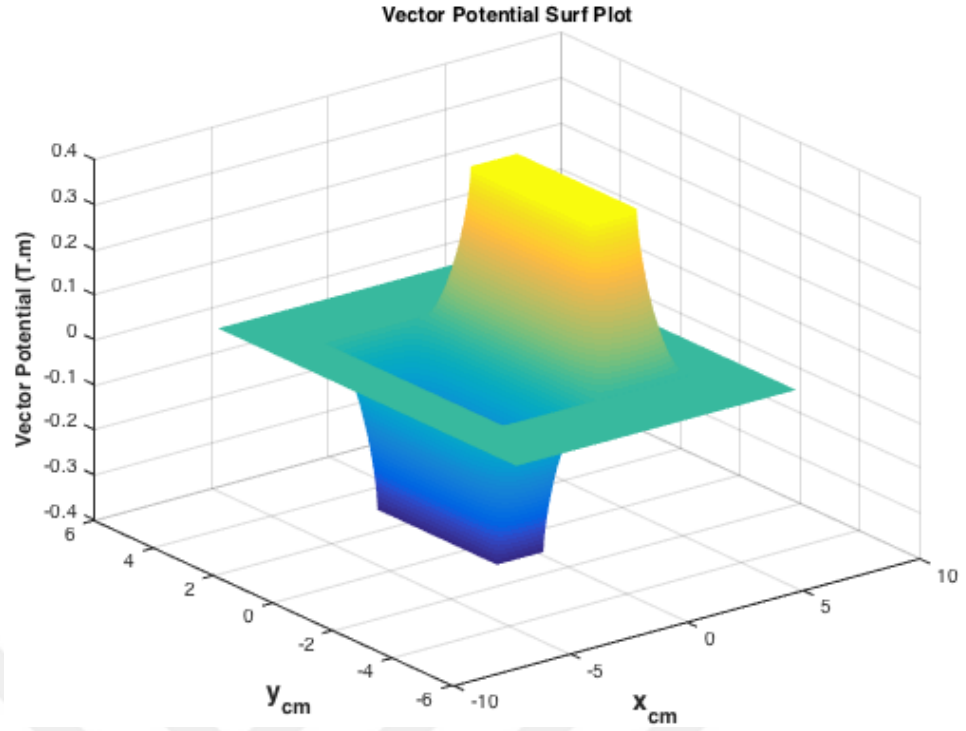

Figure 4.7: Vector potential result surface plot obtained for permeability of $\mu = 2\times10^5 \mu_0$ and injected current $J = 10\text{A/m}^2$ with 21 nodes.

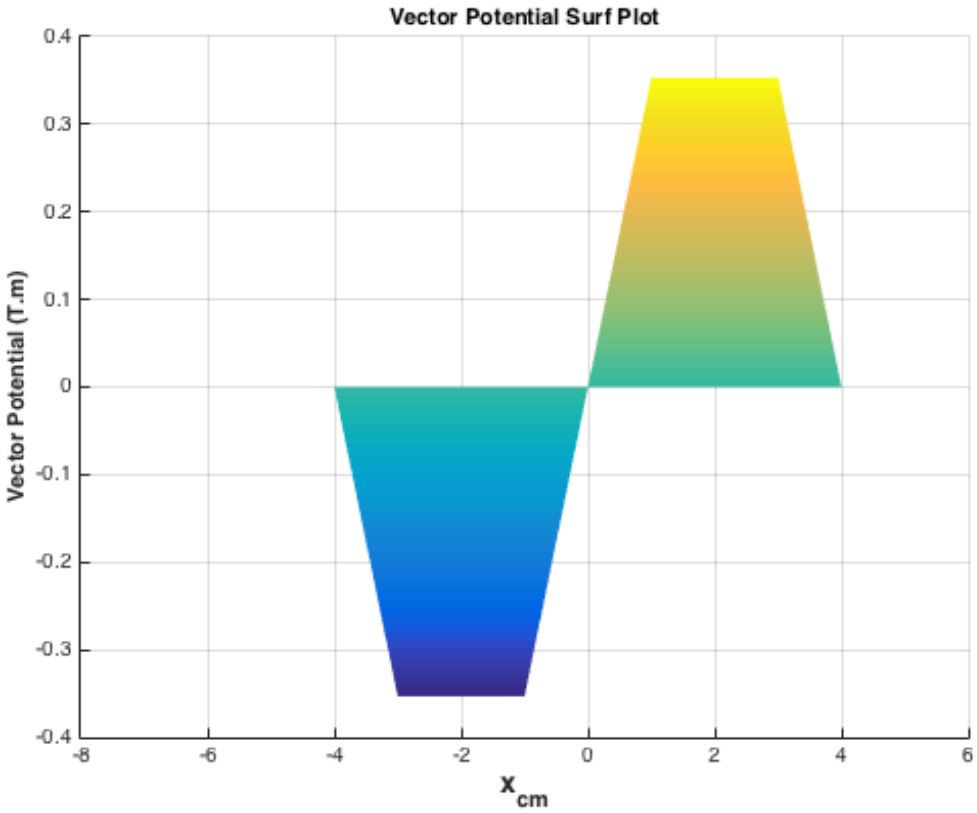

Figure 4.8: Vector potential surface plot in X-Z view obtained for paramters of number of nodes 21, permeability $\mu = 2\times10^5 \mu_0$ and injected current $J = 10\text{A/m}^2$

In Figure 4.8, the vector potential values are re-illustrated in X-Z view to show the slope clearly. As it can be clearly seen from the figure, the slope of the vector potential only exists in the core which is bounded by the coordinates [-4, -3], [-1 0] and [0, 1], [3, 4]. The magnetic flux density is zero at outside of the core and the area of elements forming the coils. All of the magnetic flux is flowing through the iron core as the magnetic permeability of iron is much higher than the permeability of air.

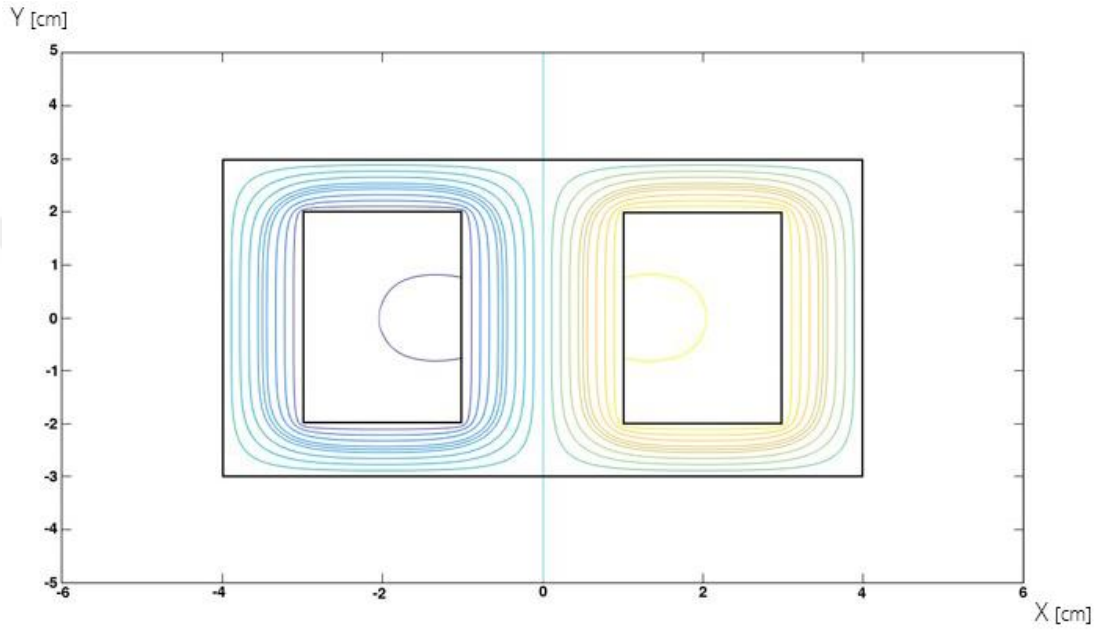

Figure 4.9: Vector potential contour plot a permeability of $\mu = 2\times10^5 \mu_0$ and injected current $J = 10\text{A/m}^2$.

In Figure 4.9, the magnetic flux isolines are illustrated in form of contour plot. There is almost no leakage magnetic flux flowing outside from the iron core except leakages around the coils.

As it is mentioned at the beginning of the section, the parameters that are used to evaluate vector potential and magnetic flux density such as magnetic permeability, number of nodes and injected current density should be changed and obtained results should be compared in order to interpret results more accurately. To achieve that, the magnetic permeability is set to a value of steel which is $\mu = 100\mu_0$ at constant injected current density and number of nodes in order to understand the effect of permeability on vector potential results.

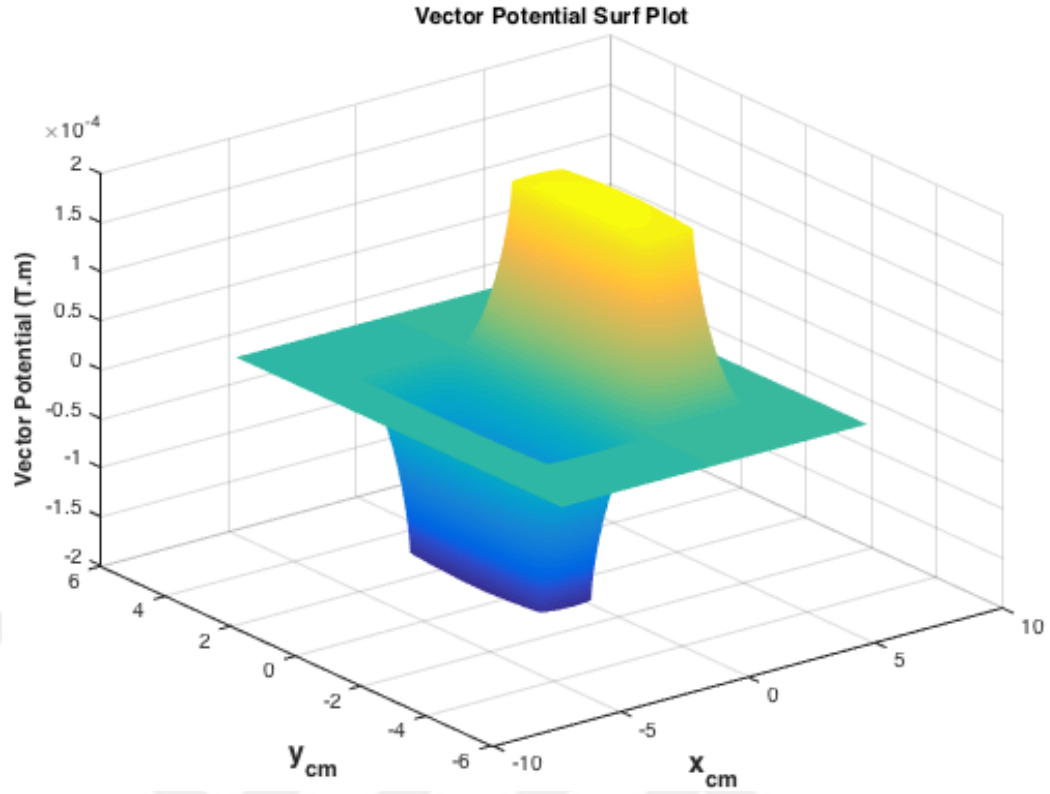

Figure 4.10: Vector potential surface plot obtained for permeability of $\mu = 100\mu_0$, and injected current $J = 10\text{A/m}^2$.

In Figure 4.10, magnetic vector potential values are illustrated in the form of surface plot. As it is shown in the figure, the slope is not equal to zero at the outside of the core and also it is not zero around coils. As it was stated earlier in this section, in order to interpret the magnetic flux density, the slope of magnetic vector potential should be analyzed. If one considers the slope of magnetic vector potential one can inferred that there is too much leakage flux flowing outside from the iron core when it is compared to results obtained for higher magnetic permeability. In other words, due to reduced magnetic permeability of iron core, the magnetic flux can leak from the iron core easily.

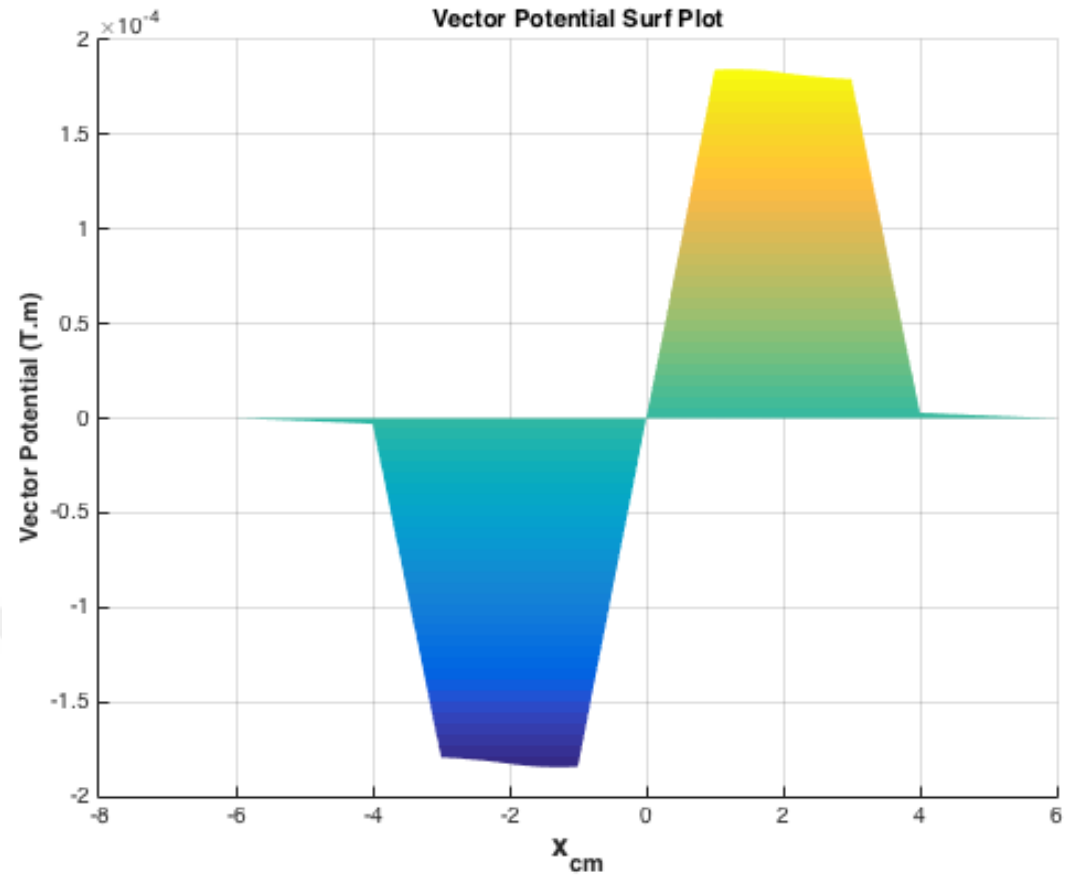

Figure 4.11: Vector potential surface plot obtained in X-Z view for magnetic permeability of $\mu = 100\mu_0$, injected current $J = 10\text{A/m}^2$ and number of nodes 21.

The Figure 4.11, vector potential is illustrated to interpret magnetic flux density more accurately due to the fact that the slope of magnetic vector potential can be noticed easily in X-Z view. As it is shown in the figure, the magnetic vector potential values are varying across the domain.

If magnetic permeability is changed, the magnitude of magnetic vector potential will also change based on Maxwell's equations. That is to say, if the value of magnetic permeability is increased, it is expected to see that the evaluated value of magnetic vector potential will also increase or vice versa. In this problem, the magnetic permeability was reduced to $\mu = 100\mu_0$.

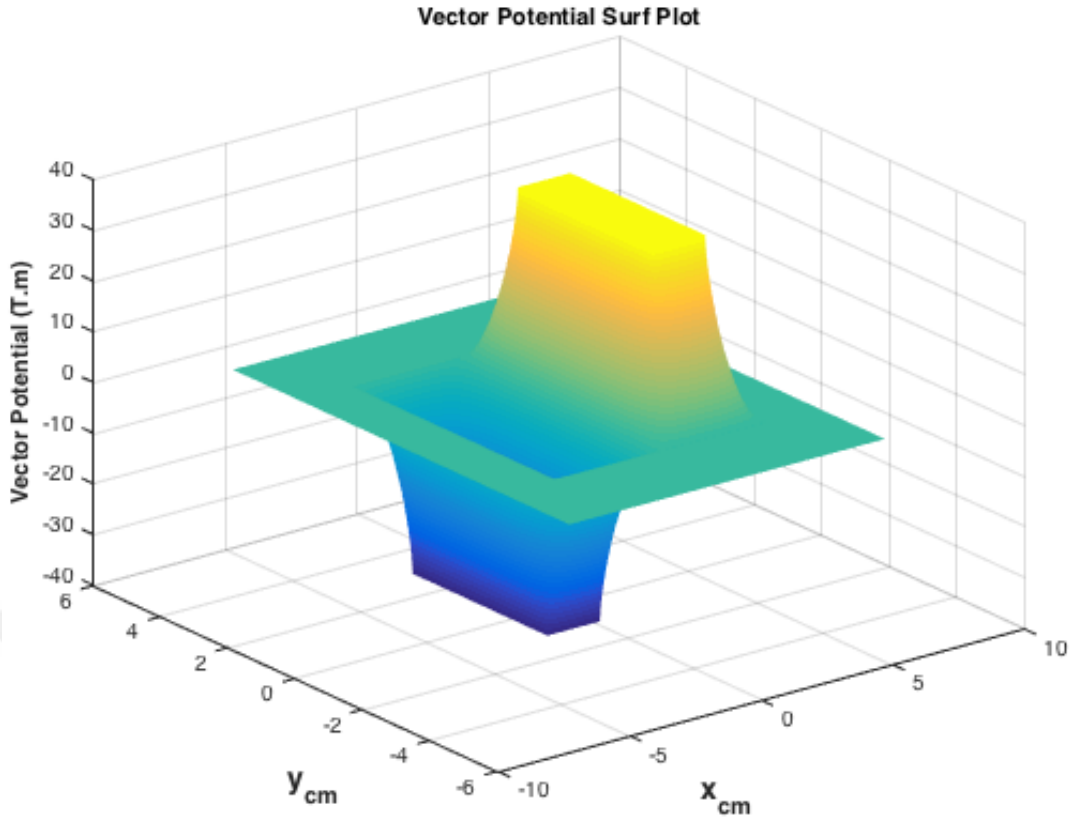

Figure 4.12: Vector potential surface plot obtained for magnetic permeability of $\mu = 2\times10^5\,\mu_0$, injected current $J = 10^3\,\mathrm{A/m^2}$ and number of nodes 21.

In Figure 4.12, magnetic vector potential values are illustrated and evaluated for the injected current density 1kA/m^2, magnetic permeability $\mu = 2\times10^5\,\mu_0$ and number of nodes 21. If Figure 4.12 and Figure 4.7 are compared, one can notice that both figures are almost identical. In Figure 4.7, the parameters of magnetic permeability and injected current density were set to 10 A/m^2 and $\mu = 2000\mu_0$ respectively. On the other hand, in Figure 4.12, the injected current density is increased to 1000 A/m^2 as the magnetic permeability is kept at $\mu = 2\times10^5\,\mu_0$. As it can be inferred from Figure 4.12, it can be said that only amplitude of magnetic vector potential is increased to approximately 30 T.m.

As it was previously mentioned, in order to utilize spectral element method, the problem should be discretized into elements. The elements which are obtained have nodes and these nodes are used for evaluation individually. Therefore, the number of nodes employed by the evaluation process plays a role for accuracy and time being consumed during computation. There is always a trade-off between accuracy and

consumed time. If higher number of nodes are defined, it is expected to see that there will be more computational time consumed. In other words, higher number of nodes means that more processing time and memory resources are required.

In order to verify relationship between accuracy of obtained magnetic vector potential value and elapsed time during computation, the number of nodes is changed to 6 while keeping the other parameters constant. In this case, it is expected to see less accurate values of magnetic vector potential and fewer consumed computational time. It is important to set a reference point to compare results. The reference point is selected as following values, X = 2 cm, Y = 1 cm.

The magnetic flux density results are employed to investigate the effects of number of nodes on accuracy. In Figure 4.13, magnetic flux density is illustrated which is calculated for 6 nodes, magnetic permeability $\mu = 2\times10^5 \mu_0$ and injected current density $10 A/m^2$. As it is shown in the figure, magnetic flux density varies between 0T to 0.16T. It can be said that, the magnetic flux lines are following the path which is closest to the interior edges in the core as it is expected. On the other hand, one can claim that the density of magnetic flux inside the core is homogeneous.

In Figure 4.14, the output of information corresponding to the elapsed time during computation of the problem is given. As it can be inferred from the figure, the computational time is 3.48 seconds.

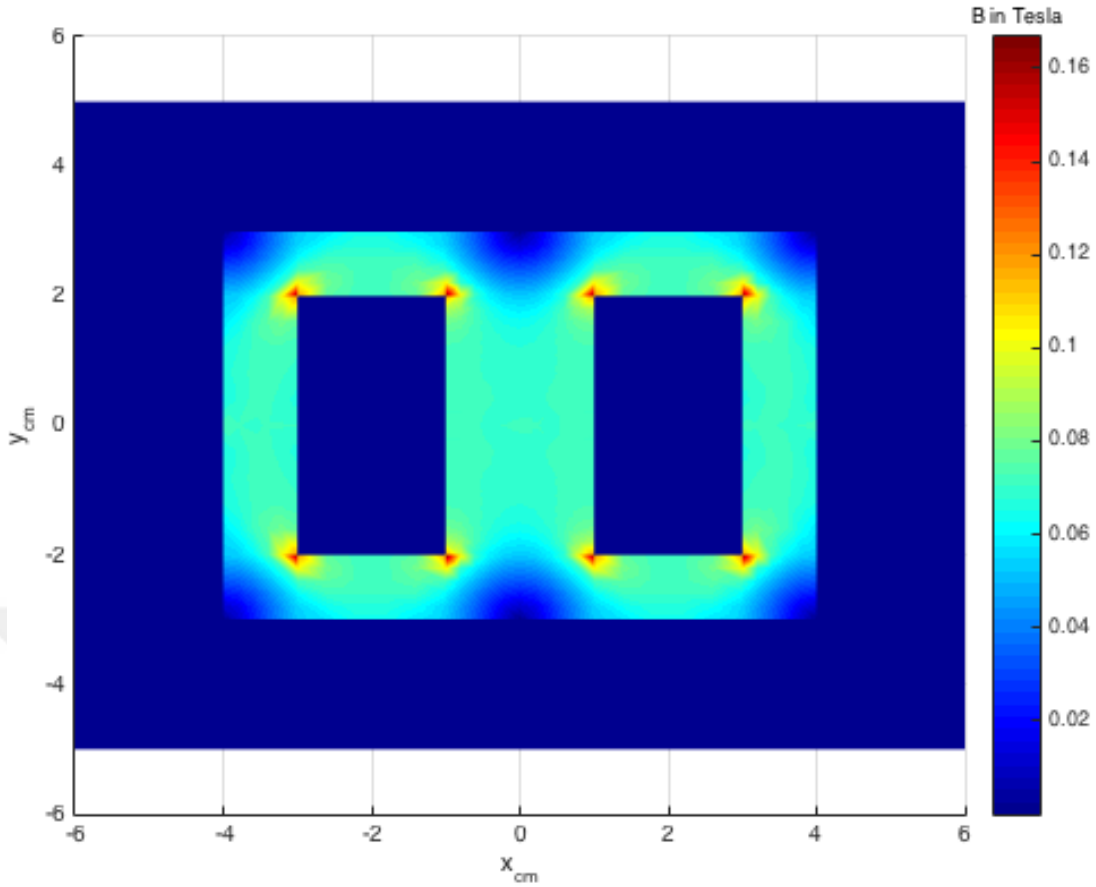

Figure 4.13: Magnetic flux density plot obtained for magnetic permeability of $\mu = 2\times10^5 \mu_0$, injected current density $J = 10\text{A/m}^2$ and number of nodes 6.

Figure 4.14: Elapsed time measured during calculation 6 nodes, $\mu = 2\times10^5 \mu_0$, injected current density $J = 10\text{A/m}^2$.

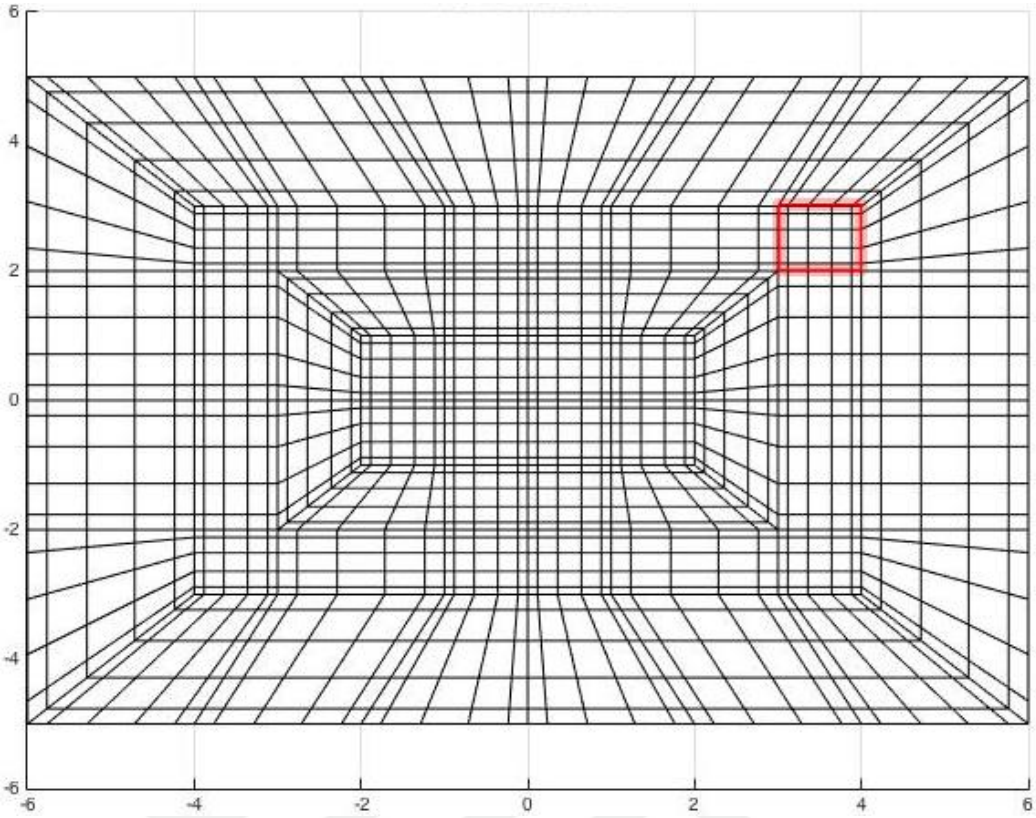

Figure 4.15: Representation of an element highlighted for 6 nodes, $\mu = 2\times10^5 \mu_0$ with an injected current $J = 10\text{A/m}^2$.

In Figure 4.15, the created nodes corresponding to each element in the problem are illustrated and one of the element belonging to the domain is highlighted. As it can be seen from the figure, each element has 36 nodes and totally the domain has 2016 nodes.

In Figure 4.16, magnetic flux density is shown which is calculated for the parameters of magnetic permeability $\mu = 2\times10^5 \mu_0$, injected current density 10A/m^2 and number of nodes 21. It can be clearly inferred from the figure; the magnetic flux density values are not homogeneous inside of the iron core. The magnetic flux density values are differentiating while it was keeping constant in the previous calculation which was made for 6 number of nodes. The reason is that there are more calculation points in the domain due to increased number of nodes to 21 which provides us higher accuracy. The elapsed time is given in the Figure 4.17, and it is increased to 97.842964 seconds as it is expected.

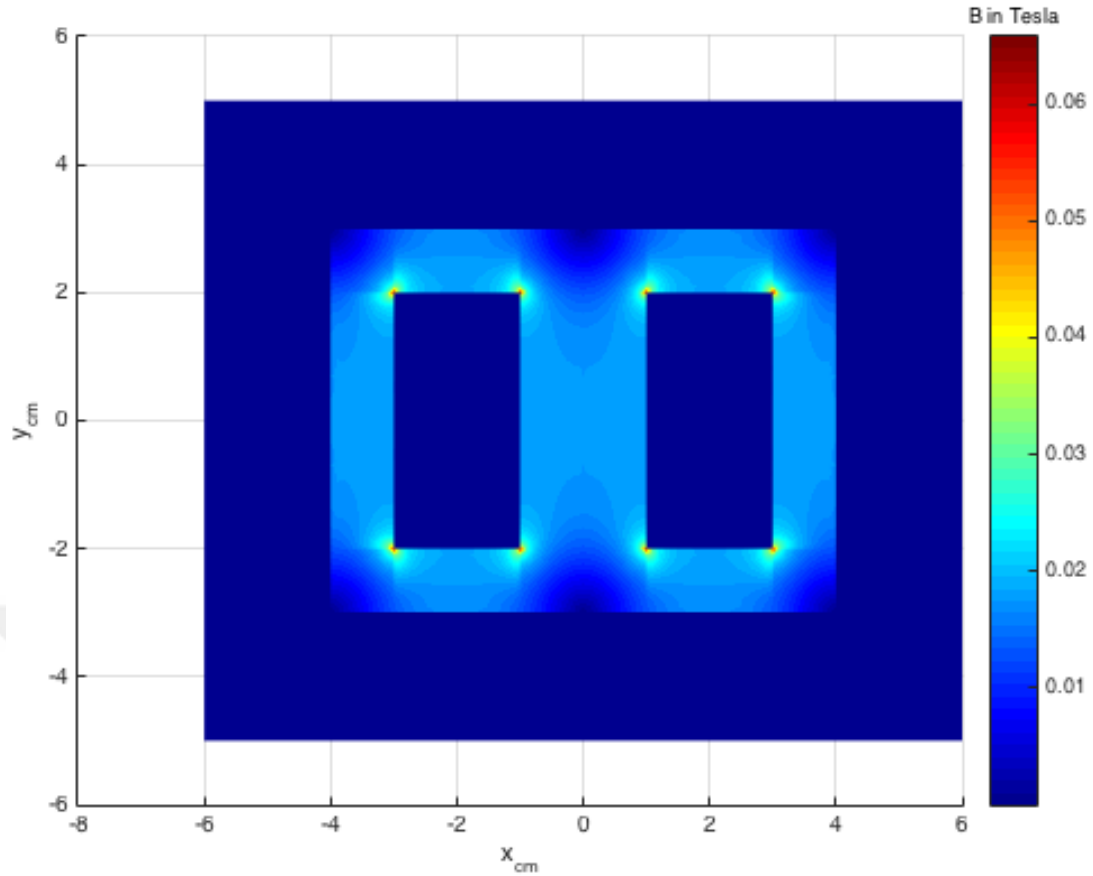

Figure 4.16: Magnetic flux density plot obtained for parameters of magnetic permeability $\mu = 2\times10^5 \mu_0$, injected current density $J = 10\text{A/m}^2$ and number of nodes 21.

Figure 4.17: Elapsed time measured during calculation for parameters of number of nodes 21, $\mu = 2\times10^5 \mu_0$, injected current density $J = 10\text{A/m}^2$

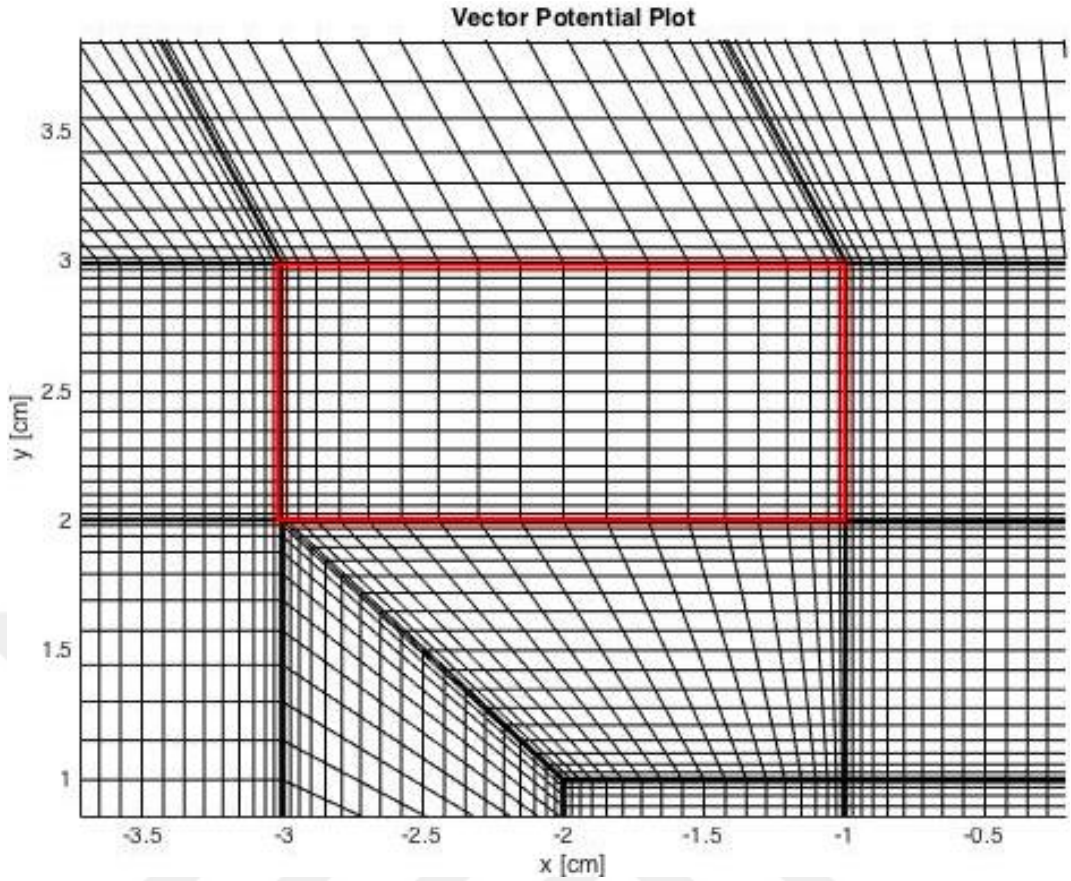

Figure 4.18: Representation of an element having 21x21 nodes.

In Figure 4.18, part of the created nodes in the problem domain are shown and one of the element belonging to the domain is highlighted. As it is shown in the figure, each element has 441 nodes and totally the domain has 24696 nodes. Based on the results obtained in different number of nodes configuration, 21 number of nodes is accurate and efficient enough to produce reliable solutions.

It is previously mentioned that the accuracy highly depends on defined number of nodes for each element. In thesis, two different number of nodes configuration are applied to each element in order to compare results and element 8 is chosen to be a reference.

In Figure 4.19, the vector potential is presented for different number of nodes corresponding to the reference point. The vector potential value along the x axis which is highlighted in blue line for 21 nodes, varies in range starting from zero to approximately 0.34 T.m. On the other hand, the vector potential value which is highlighted in red-color line for 6 nodes, varies from 0 T.m to nearly 0.28 T.m. When

it comes to comparison, the difference between those values as it was previously mentioned that caused by number of nodes created for problem domain elements.

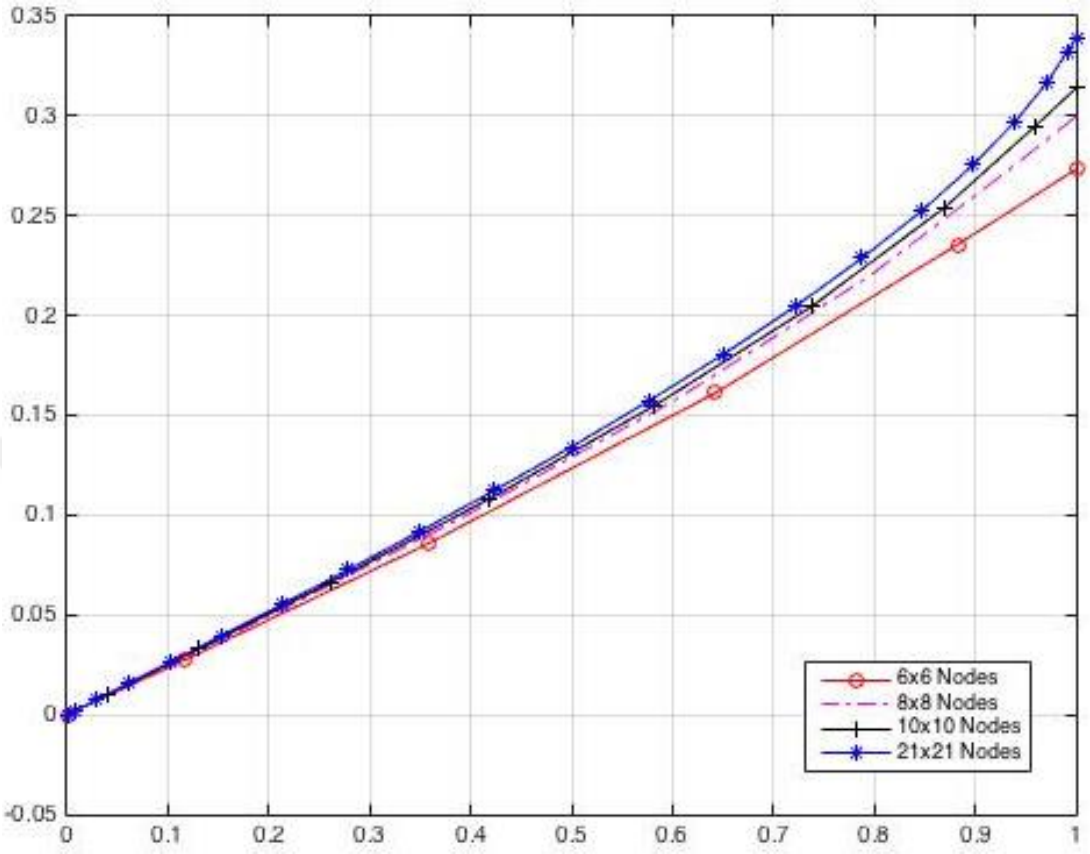

Figure 4.19: Comparison of magnetic vector potential values corresponding to reference element.

Memory usage is one of the important parameters that should be taken into account while utilizing spectral element method. It is well-known fact that defining number of nodes plays key role on the accuracy of results. If number of nodes is too low, it is nearly impossible to obtain accurate results. If number of nodes is too high however, the accurate results is guaranteed but the resources, especially RAM to be assigned for calculation process are increased dramatically.

In Figure 4.20, the memory usages are represented for different number of node configurations. The line which is highlighted in red color represents the usage belonging with the calculation made for 21 nodes and the blue highlighted line represents the values belonging with calculation made for 6 nodes. The memory values are presented in terms of gigabytes. As it is represented in the figure, the difference between memory usages in both cases is too much. The average memory values of

calculation made for 21 number of nodes and 6 number of nodes are 2.0131 gigabytes and 0.1022 gigabytes, respectively.

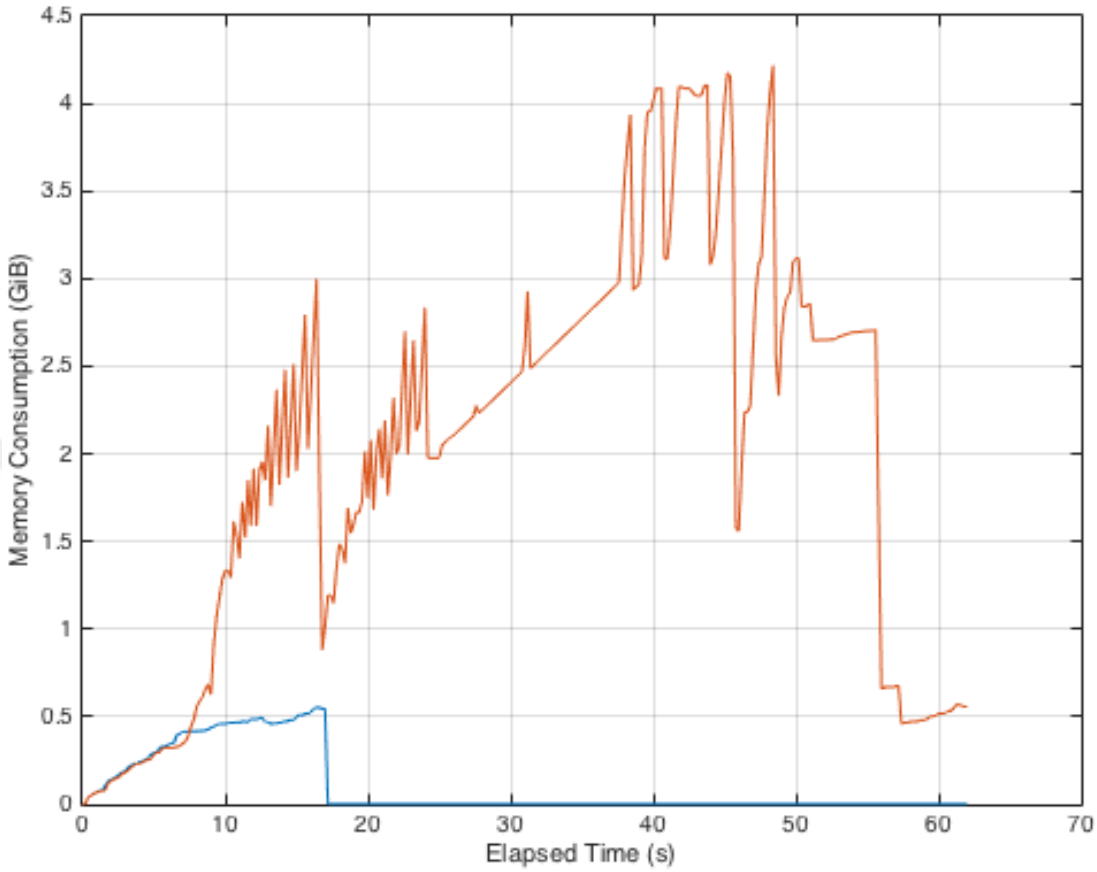

Figure 4.20: Consumed RAM results during execution of script for 21 and 6 nodes.

Figure 4.21 illustrates the consumed processor resources which is required by the computational process. The red line presents CPU activity corresponding to script executed by the 21 nodes and blue line represents CPU activity corresponding to 6 number of nodes configuration. As it is illustrated in the figure, all processor resources are allocated during computation for each number of nodes configuration. However, due to lower accuracy, the process configured with 6 number of nodes finishes its job faster than other's. Besides, it is important to note that, two of executions overshoots the 100% which means that more than one CPU core is allocated for execution.

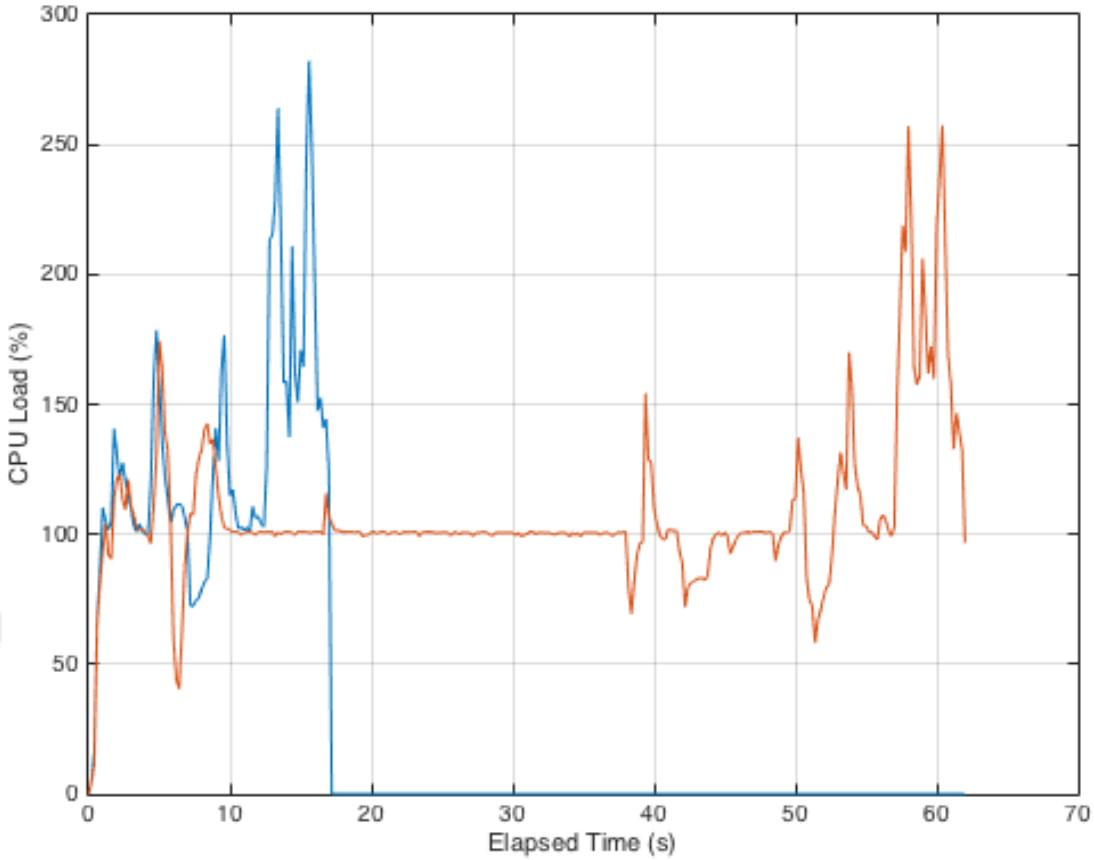

Figure 4.21: CPU load results during execution of the script for the number nodes 6 and 21.

4.5 Comparison Between SEM and FEM

In this thesis, spectral element method is utilized to solve the present problem because of its high accuracy and ability of calculation on deformed elements efficiently and requiring low computational resources. In order to prove that, finite element method is utilized to solve the same problem for verification purposes.

In order to utilize finite element method on our problem, it is required to discretize the problem domain into elements. Figure 4.22 illustrates the problem definition involving several subdomains. For instance, “u1” represents the outer boundary and “air” represents outside and partially inside of iron core, “Positive” and “Negative” labels represent coils attached to core.

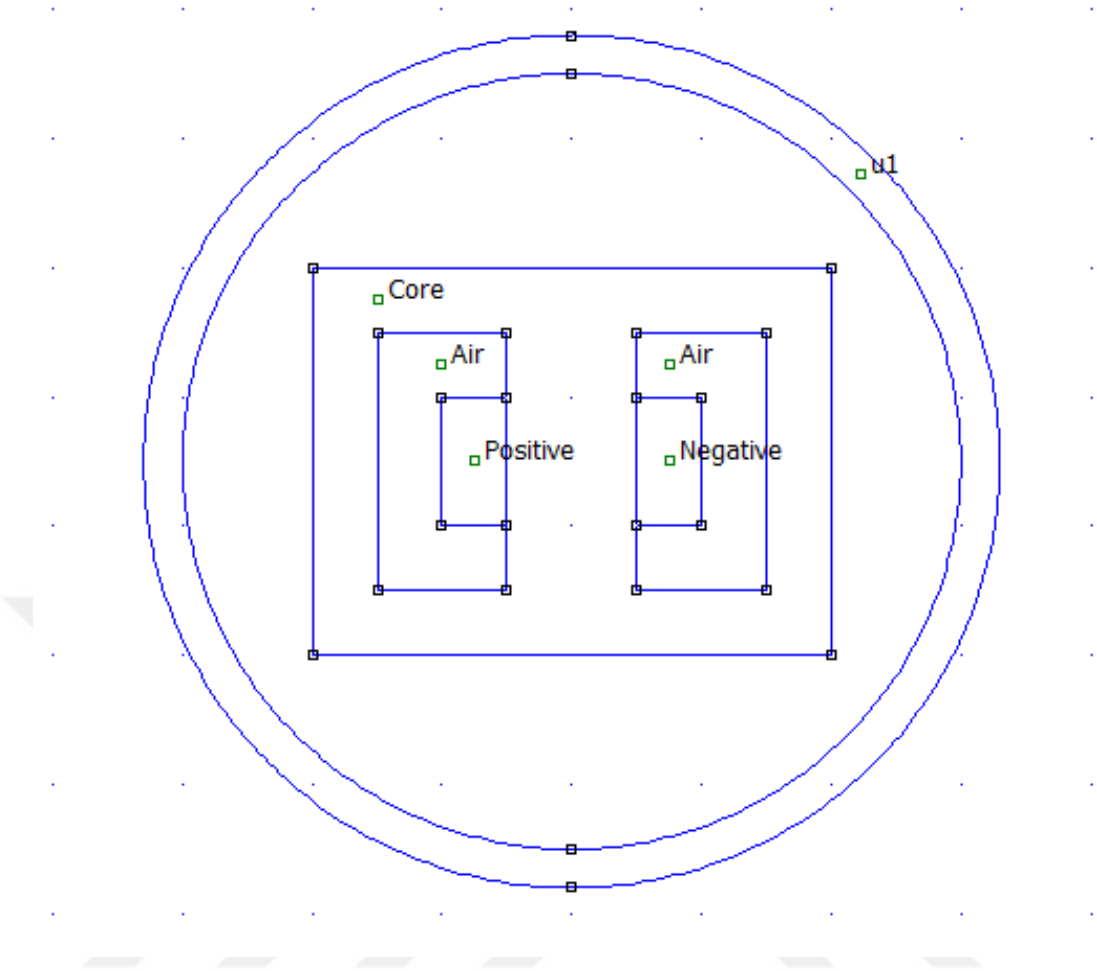

Figure 4.22: Problem definition for FEM.

The discretization of problem domain is illustrated in the Figure 4.23. As it can be shown in the figure, triangular elements used for discretization. Besides that, it can be also inferred that the number of elements is denser in corners and sparser in middle. It is important to note that, outer boundary of problem domain was not used in spectral element method.

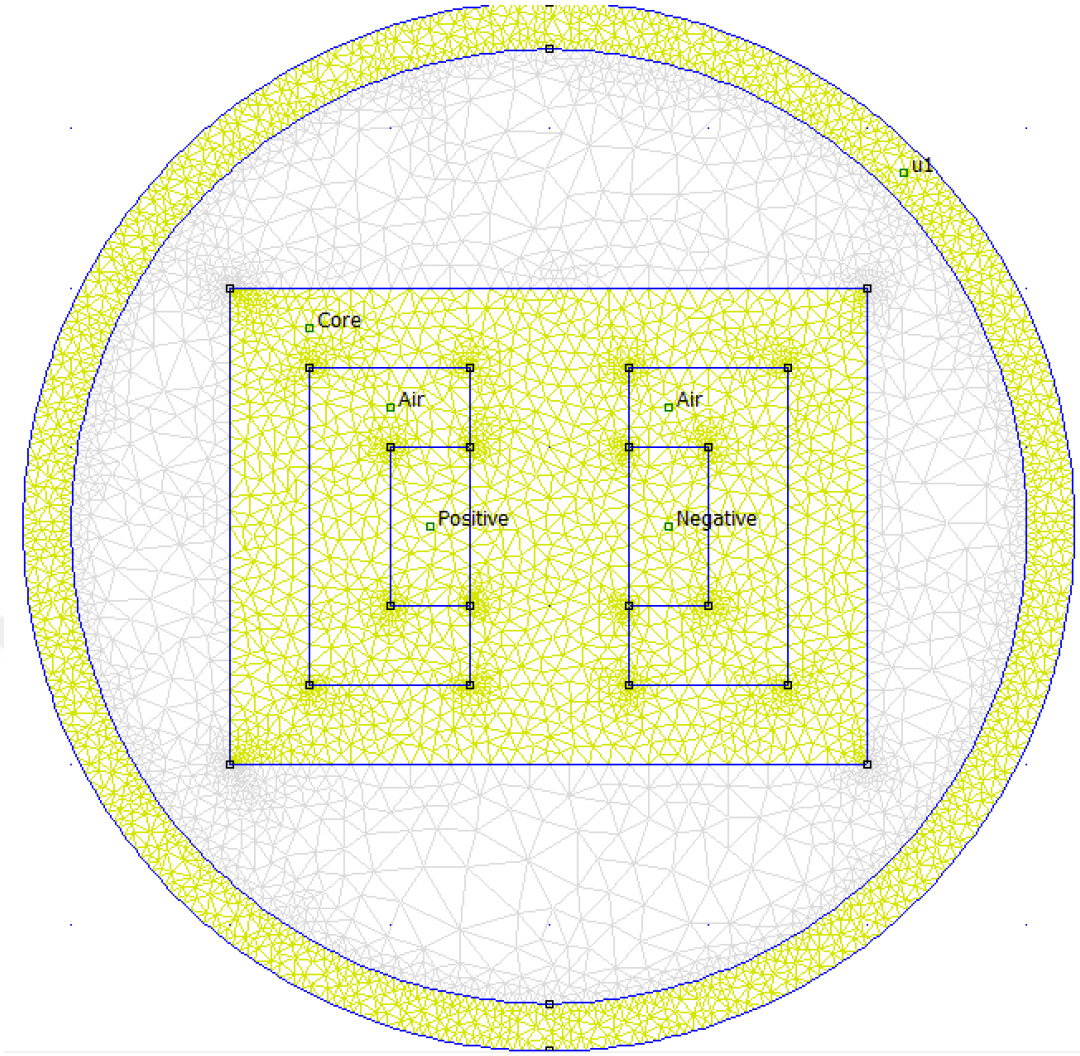

Figure 4.23: Meshing the problem domain in FEM.

In order to compare the results which is obtained by spectral element method and finite element method, a reference line on the problem domain is chosen. As it can be seen in Figure 4.24, the reference line is defined as “ab” in the middle leg of iron core.

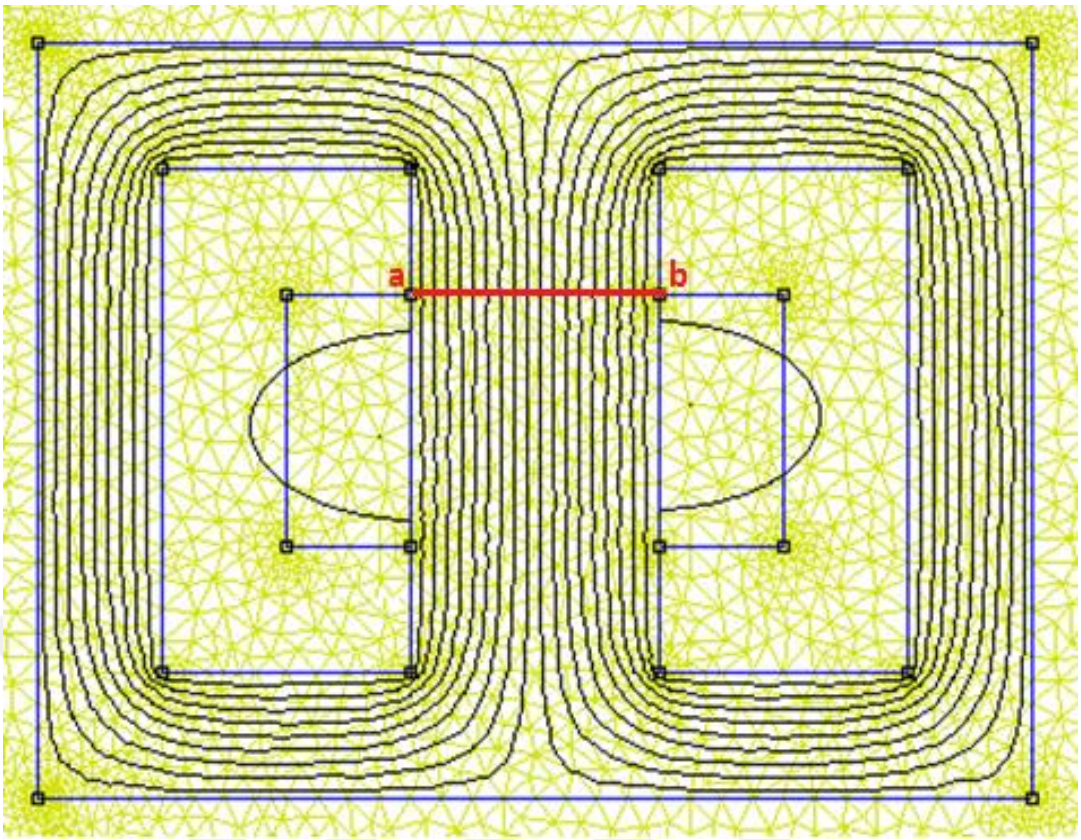

Figure 4.24: Vector potential contour plot obtained by FEM.

Figure 4.25 shows the magnetic flux density values corresponding to finite element method and spectral element method results along the defined reference line drawn from a to b. As it shown in the figure, the average value of magnetic field density (B) is 35.4 T. Besides, SEM shows smoother form of variation compared to FEM and as it is shown in the figure, SEM is more symmetrical around x axis (x=0).

The maximum difference between results corresponding to SEM and FEM is approximately 1.12%. It can be considered small amount of difference and FEM can also be seemed as accurate as SEM and yet this amount of difference can be acceptable in aspects of engineering. However, the other features of spectral element method like low dependency on computational resources make it more feasible to be used.

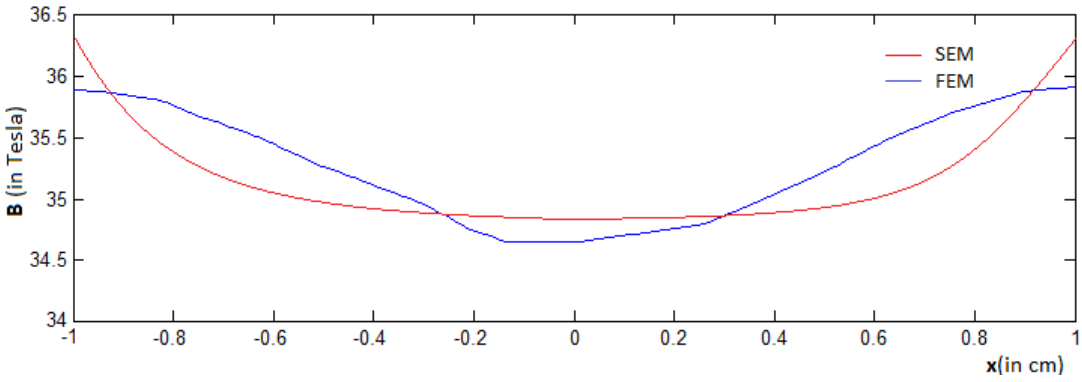

Figure 4.25: Accuracy comparison between FEM and SEM.

4.6 Summary

In this chapter, the simulation results corresponding to the formulation of a typical magnetostatic problem by spectral element method are presented. In order to simulate results of the problem, the following steps are followed; defining typical magnetostatic problem, obtaining governing partial differential Maxwell's equations, discretization of problem domain, defining boundary conditions and the utilization of spectral element method respectively. The problem defined in thesis is time-invariant and two dimensional. And, the problem is symmetrical around x axis(x=0). Due to the symmetry, computational time of the problem is reduced and also memory usage is reduced to half as it is expected. Adapted formulation by spectral element method is based on the continuous galerkin approach, however discontinuous approach can also be used.

Number of nodes created for domain elements effects on the accuracy of results as it is previously mentioned in thesis. In order to prove that, more than one number of nodes configuration has been used and the corresponding results are presented.

In order to show memory usage effect, simulation process has repeated several times with different number of nodes configuration. It is expected to see that lower number of nodes configuration is associated with less memory usage. The results proved our expectations by presenting higher memory consumption on higher number of nodes configuration.

As it is proved by results, the spectral element method is feasible to use in magnetostatic problems due to its high accuracy.

CHAPTER FIVE

CONCLUSION & FUTURE WORK

Electromagnetic modeling is handled by techniques; analytical modeling, and numerical modeling. Numerical modeling is utilized in electromagnetic problems by discretizing the problem domain into elements while analytical modeling begins with governing differential equations and solve them by some mathematical manipulations. Due to the complexity of electromagnetic problems, numerical methods became more popular recently thanks to the advent of technology.

There are several numerical methods that can be utilized in computational electromagnetics. However, some of them such as finite element and finite difference methods have been extensively applied. After Patera [25] had introduced spectral element method in the article, spectral element method began to be applied in various branches of engineering problems by many researchers. The chief advantage of spectral element method is that it offers high accuracy and low computational resource requirements. Despite of these advantages, this method has not been used in magnetostatic or quasi-magnetostatic problems. When literature is searched, we confirmed that there are several studies have been made based on the application of spectral element method in the wave theory and photonics structure.

In this thesis, we applied the spectral element method in sample magnetostatic problem. The sample problem is time invariant and defined in two-dimensions. The magnetic permeability is assumed as a different constant value in each region such as air, iron core and current injected coil. After vector potential results had been obtained, the problem was re-evaluated in order to realize the effects of parameters defining our problem. First, we created sparser mesh, we obtained less accurate results in contrast with denser mesh. Then, we reduced the permeability of the core and we observed more leakage flux as it is expected. Last but not least, when the injected current was increased, we observed higher vector potential values.

In addition, we also modeled and simulated the same problem by a freely available software which is created by Meeker, D [14]. Consequently, the results proved that spectral element method provides accuracy with less computational resources when it is compared to finite element method.

In our future work, we are planning to study the following topics;

1. Quasi-magnetostatic problems
2. Discontinuous Galerkin approach
3. Since we assumed that the permeability (μ) is linear, it may become non-linear under high excitation conditions. In future works, nonlinear permeability can be considered.
4. Solving problems involving permanent magnets.
5. Investigation of solving the resultant system of equations $\mathrm{A}\,\mathrm{x} = \mathrm{b}$ by different iterative methods.

REFERENCES

[1] Wallace, J. W. (2002). *Modeling electromagnetic wave propagation in electrically large structures* (Unpublished PhD thesis). Brigham Young University/Utah.

[2] Biro, O., & Preis, K. (1989). On the use of the magnetic vector potential in the finite-element analysis of three-dimensional eddy currents. *IEEE Transactions on magnetics*, *25*(4), 3145-3159.

[3] Lee, J. H., Xiao, T., & Liu, Q. H. (2006). A 3-D spectral-element method using mixed-order curl conforming vector basis functions for electromagnetic fields. *IEEE transactions on microwave theory and techniques*, *54*(1), 437-444.

[4] Zhang, Y., Chau, K. T., Jiang, J. Z., Zhang, D., & Liu, C. (2006). A Finite Element- Analytical Method for Electromagnetic Field Analysis of Electric Machines with Free Rotation. *IEEE transactions on magnetics*, *42*(10), 3392-3394.

[5] Sjogren, M. (2002). Comparison of Spectral Element and Finite Difference Methods for Electromagnetic Wave Propagation over a Material Discontinuity.

[6] Airiau, S., Azaïez, M., Belgacem, F. B., & Guivarch, R. (2002, June). Parallelization of spectral element methods. In *International Conference on High Performance Computing for Computational Science* (pp. 392-403). Springer Berlin Heidelberg.

[7] Kramer, R. K. D., & Weiss, J. P. Facing the Multicore-Challenge III. Springer Berlin.

[8] Steele, C. (1983). A spectral method for field computation. *IEEE Transactions on Magnetics*, *19*(6), 2296-2299.

[9] Park, I. H., Lee, B. T., & Hahn, S. Y. (1992). Design sensitivity analysis for nonlinear magnetostatic problems using finite element method. IEEE transactions on magnetics, 28(2), 1533-1536.

[10] Chari, M. V. K., Csendes, Z. J., Silvester, P., Konrad, A., & Palmo, M. A. (1981). Three-dimensional magnetostatic field analysis of electrical machinery by the finite-element method. IEEE Transactions on Power Apparatus and Systems, (8), 4007-4019.

[11] Penman, J., & Fraser, J. (1982). Complementary and dual energy finite element principles in magnetostatics. IEEE Transactions on Magnetics, 18(2), 319-324.

[12] Imhoff, J. F., Meunier, G., Brunotte, X., & Sabonnadiere, J. C. (1990). An original solution for unbounded electromagnetic 2D-and 3D-problems throughout the finite element method. IEEE Transactions on Magnetics, 26(5), 1659-1661.

[13] Mahariq, I., Kurt, H., & Kuzuoğlu, M. (2015). Questioning degree of accuracy offered by the spectral element method in computational electromagnetics. Applied Computational Electromagnetics Society Journal, 30(7).

[14] IEEE, D. M. (n.d.). Finite Element Method Magnetics (Version 4.2) [Computer software]. Retrieved from http://www.femm.info/wiki/Download

[15] Huray, P. G. (2011). *Maxwell's equations*. John Wiley & Sons.

[16] Stratton, J. A. (2007). *Electromagnetic theory*. John Wiley & Sons.

[17] Hwang, C. C. (1997). Numerical computation of eddy currents induced in structural steel due to a three-phase current. *Electric power systems research*, *43*(2), 143-148.

[18] Dobbs, E. R. (2013). *Basic electromagnetism*. Springer Science & Business Media.

[19] Nerukh, A., Sakhnenko, N., Benson, T., & Sewell, P. (2012). *Non-stationary electromagnetics*. CRC Press.

[20] Meeker, D. (2010). Finite element method magnetics. *FEMM*, *4*, 32.

[21] J. B., & L. C. (2012). Finite Difference Method. In *Analysis of Numerical Differential Equations and Finite Element Method* (1st ed., pp. 71-74). Delhi: College Publishing House.

[22] Polycarpou, A. C. (2005). Introduction to the finite element method in electromagnetics. *Synthesis Lectures on Computational Electromagnetics*, *1*(1), 1-126.

[23] MARAL, T. (2006). *Spectral (hp) Element Methods Approach to The Solution of Poisson and Helmholtz Equations Using Matlab* (Doctoral dissertation, METU).

[24] H. T. (2005). *Pseudospectral Methods Lecture Notes*. METU, Ankara.

[25] Patera, A. T. (1984). A spectral element method for fluid dynamics: laminar flow in a channel expansion. *Journal of computational Physics*, *54*(3), 468-488.

APPENDICES

Appendix A. Lobatto.m

```
function [w, y] = Lobatto(n)
% The Legendre-Lobatto points y(1:n+1) are the roots of
f(x) = (1- x^2) dP_n/dx,
% with the weights w(1:n-1) = 2/n(n+1) P_n(y(1:n-1))^-2
and w([0 n] = 2/n(n+1).
% where P_n(x) is the nth degree Legendre polynomial. %
% This routine uses Newton iteration to find the roots to
10 digit accuracy.
% Only symmetric half is computed.
% The initial estimates are the Chebyshev points
cos((pi/n)*(0:n)). %
% By using the two relations
% (1-x^2)(dP_n/dx) = n(n+1)/(2n+1) (P_(n-1) - P_(n+1))
% P_n = -1/(2n+1) (dP_(n-1)/dx - dP_(n+1)/dx)
% we identify
% f = P_(n-1) - P_(n+1) and df/dx = -(2n+1)P_n.
if n==1, w = [1 1]; y = [1 -1]; return, end
if n==2, w = [1/3 4/3 1/3]; y = [1 0 -1]; return, end
s = 2/(n*(n+1));
m = ceil(n/2) - 1; % # of half-internal points except
zero. for i=1:m
z = cos((pi/n)*i); d = 1;
while abs(d) >= 5e-11
Lnm1 = legendre(n-1,z); Lnp1 = legendre(n+1,z); Ln =
legendre(n,z);
fz = Lnm1(1,1) - Lnp1(1,1); fpz = -(2*n+1)*Ln(1,1);
    d = -(fz/fpz); z = z + d;
end
yh(i) = z;
wh(i) = 1/Ln(1,1)^2;
end
if 2*ceil(n/2)==n,
    Ln = legendre(n,0); w0 = 1/Ln(1,1)^2;
    w = s*[1 wh(:)' w0 fliplr(wh(:)') 1];
    y = [1 yh(:)' 0 -fliplr(yh(:)') -1];
else
end
```

Appendix B: processlogger.go

```
package main

import (
	"bytes"
	"fmt"
	"os"
	"os/exec"
	"regexp"
	"strconv"
	"strings"
	"time"
)

func parse_results(results string) (string, string) {
	var cpu string
	var ram string

	if results != "error" {
		r, _:= regexp.Compile(`([0-9\.]+)\s+(\d+)`)
		usage:= r.FindAllStringSubmatch(results, -1)
		cpu = usage[0][1]
		ram = usage[0][2]
	} else {
		cpu = ""
		ram = ""
	}
```

```
	return cpu, ram
}

func ps(pid string) string {
	var stdOut bytes.Buffer

	cmd:= exec.Command("ps", "-eo", ",%cpu,rss", pid)
	cmd.Stdout = &stdOut

	err:= cmd.Run()

	if err != nil {
		return "error"
	} else {
		return stdOut.String()
	}
}

func start_matlab_proc(c chan int, d chan bool) {

	cmd:= exec.Command("matlab", "-nosplash", "-nodesktop", "-r",
"sem_code")

	go func() {
		err:= cmd.Start()
		if err == nil {
			c <- cmd.Process.Pid
		}
		cmd.Wait()
		d <- true
	}()
```

```
}

func write_to_file(cpu_vals []string, mem_vals []string, t_vals []string) {

	day, month, year, hour, minute, second:= get_time_str()

	prefx:= fmt.Sprintf("%d_%d_%d_%d_%d_%d", day, month, year, hour,
minute, second)

	file, _:= open_to_write(fmt.Sprintf("cpu_%s.txt", prefx))

	fmt.Fprintf(file, fmt.Sprintf("cpu = [%s];",
strings.TrimLeft(strings.Join(cpu_vals, " "), " ")))
	fmt.Fprintf(file, fmt.Sprintf("t = [%s];", strings.TrimLeft(strings.Join(t_vals,
" "), " ")))

	file, _ = open_to_write(fmt.Sprintf("mem_%s.txt", prefx))

	fmt.Fprintf(file, fmt.Sprintf("mem = [%s];",
strings.TrimLeft(strings.Join(mem_vals, " "), " ")))
	fmt.Fprintf(file, fmt.Sprintf("t = [%s];", strings.TrimLeft(strings.Join(t_vals,
" "), " ")))
}

func open_to_write(filename string) (*os.File, error) {

	var file *os.File
	var err error

	file, err = os.Create(filename)

	if err != nil {
		panic(fmt.Sprintf("Cannot open file: %s", filename))
	}
```

```
        return file, err
}

func get_time_str() (int, int, int, int, int, int) {

        now:= time.Now()

        day:= time.Time.Day(now)
        month:= int(time.Time.Month(now))
        year:= time.Time.Year(now)

        hour:= time.Time.Hour(now)
        minute:= time.Time.Minute(now)
        second:= time.Time.Second(now)

        return day, month, year, hour, minute, second
}

func main() {

        var pid string
        var t float64
        var p int

        k:= make(chan int)
        d:= make(chan bool)

        cpu_vals:= make([]string, 1)
        mem_vals:= make([]string, 1)
        t_vals:= make([]string, 1)

        go start_matlab_proc(k, d)
```

```
p = <-k
pid = strconv.Itoa(p)

fmt.Printf("MATLAB Process has been started [pid]: %d \n", p)
fmt.Println("Process logging has been initialized...")

t = 0
res:= 200 // Set resolution

for {

        cpu, ram:= parse_results(ps(pid))

        if cpu != "" && ram != "" {

                cpu_vals = append(cpu_vals, cpu)
                mem_vals = append(mem_vals, ram)
                t_vals = append(t_vals, strconv.FormatFloat(t, 'f', 2, 64))
        }

        select {

        case done:= <-d:

                if done {
                        write_to_file(cpu_vals, mem_vals, t_vals)
                        os.Exit(0)
                }
        default:
        }
```

```
                time.Sleep(time.Duration(res) * time.Millisecond)
                t += float64(res) / 1000
        }
}
```

Appendix C: Published Article (Turk J Elec Eng & Comp Sci /DOI: 10.3906/elk-1605-6)

A spectral element method for the solution of magnetostatic fields

Ibrahim MAHARIQ[1,2,*], Atakan ERCIYAS[2]

[1] Department of Electrical and Electronics Engineering, TOBB University of Economics and Technology, Ankara 06560, Turkey

[2]Electrical & Electronics Engineering, Faculty of Engineering, University of Turkish Aeronautical Association, Ankara 06790, Turkey

*Correspondence: ibmahariq@gmail.com

Abstract: Recently, we have seen good progress in our capability to simulate complex electromagnetic systems. However, still there exist many challenges that have to be tackled in order to push limits restricting the field of computational electromagnetics upward. One of these challenges is the limitations in the available computational resources. Over several decades, the traditional computational methods, such as finite difference, finite element, and finite volume methods, have been extensively applied in the field of electromagnetics. On the other hand, the spectral element method (SEM) has been recently utilized in some branches of electromagnetics as waveguides and photonic structures for the sake of accuracy. In this paper, the numerical approximation to the set of the partial differential equations governing a typical magnetostatic problem is presented by using SEM for the first time to the best of our knowledge. Legendre polynomials and Gauss-Legendre-Lobatto grids are employed in the current study as test functions and meshing of the elements, respectively. We also simulate a magnetostatic problem in order to verify the SEM formulation adapted in the current study.

Key words: Computational electromagnetics, finite element method, magnetostatics, spectral element method.

1. Introduction

Electromagnetic problems are typically defined by Maxwell Equations which describe to us how electric and magnetic fields are generated and effect on each other. However, it is quite difficult to solve them by analytical methods owing them being part of partial differential equations [1]. Fortunately, there are some numerical methods in which Maxwell's equations are approximated to obtain the associated solutions with acceptable accuracies, thanks to computational electromagnetics that was developed in parallel with of improvement computing machines.

Numerical methods are discriminated among each other mainly according to some key points such as accuracy and requirements of computational resources (available CPU and memory). That is, a numerical method may have less computational time than another as it has more memory consumption, or vice versa [2-4]. Among these numerical methods that have been being applied intensively for several decades are the finite difference method (FDM) and the finite element method (FEM).

FEM is one of powerful numerical methods ever invented to solve partial differential and integral equations of initial and boundary-value problems (BVP) in complex geometries. In early 1960's engineers used the method in order to approximate the solution in different research areas such as fluid dynamics, heat transfer. In the late 1960's and early 1970's it became to be applied in engineering problems. Continuous quantities such as pressure, temperature can be modeled by discrete finite elements as polynomials.

Finite difference method is another approach to solve Maxwell's equations. In order to apply this method, first the problem domain should be discretized, and discretization process is done by dividing the problem domain into equi-spaced elements. This method has two computational error sources. Those are round-off error and truncation error. Round-off error based on loss of precision of decimal quantities owing to iterations on computing process. The truncation error, also known as discretization error, consists of samples which is taken from each step on computation to approximate infinite elements [5].

Many researches have been introduced in the literature over the past decades in calculating magnetic fields associated with low-frequency magnetic problems. Most of the recent work has been devoted to study the minor details such as boundary

conditions, numerical iterations and little improvements in accuracy. For instance, but not limited to, Biro [6] utilized various finite element method techniques on three-dimensional magnetostatic problems in order to improve numerical stability.

In Ref. [7], a novel analytical solution of the airgap region is derived and coupled with the FEM equations in order to solve the field in an electrical machine for both rotor and stator regions. The motivation behind that study was to naturally couple the analytical solution with the FEM equations based on the continuity of magnetic vector potentials across their boundaries. Consequently, the stiffness matrix was derived. Results and experiments shows that computational time is approximately same due to analytical computation despite the fact that it is expected to have less nodes in finite elements.

Spectral element method (SEM), on the other hand, was first introduced by Patera [8] in 1984 for computational fluid dynamics. Patera proposed a spectral element method that combines the flexibility of the finite element method with the accuracy of spectral methods.

Generally speaking, spectral element methods are considered as a family of approximation schemes based on the Galerkin method. They share common characteristics with finite-element discretizations, and this provides the reason why they can be viewed as h- or p-versions of finite element method. That is, when viewed as h-version, a Lagrangian interpolation formula on the parent element exists in both, as well as the basis functions have local support. On the other hand, spectral element methods use high-degree polynomials on a fixed geometric mesh for the sake of enhanced accuracy, and this is the fact characterizing the p-version of finite element methods [9].

In recent literature, some details regarding the application of SEM in electromagnetic wave propagation have been investigated. Martin Sjögren et al [10], the comparison of FDM and SEM over material discontinuity is studied. It is stated that FDM and SEM can simulate simple case of wave reflection and refraction in two-dimensional rectangular geometry accurately. For a particular geometry, FDM is better suited and has higher efficiency. However, in more complicated geometries SEM has more advantages due to the fact that it is easier to implement unstructured grid. Besides that, this method also suited well for parallel implementations for large computations.

Similar results were confirmed by Airiau [11] and Christoph [12] in which the discontinuous Galerkin Spectral Element Method is considered.

To the best of our knowledge, when the literature is searched, one can observe that SEM has not been applied in magnetostatic or quasi-magnetostatic problems. It is noteworthy to mention that spectral methods (but not spectral element method) were introduced in 1983 by C. Steele [13]. The author utilized a spectral method in which the magnetic fields are computed by expressing them as a linear combination of a set of orthogonal functions. The only advantage pointed by the author is the reduction in the size of the system of linear equations when compared with finite element method. However, spectral methods are not successful in solving domains involving complex geometries and/or nonhomogeneous materials. For that reason, people later on didn't extend Steele's work.

In this paper, the spectral element method is applied in modelling of time-invariant, two-dimensional magnetostatic problems. The reduced computational cost and the accuracy offered by SEM are the main motivation behind this study [2-4, 14-15]. As most of magnetostatic problems are complex in nature, the application of the SEM in low-frequency magnetic problems forms a new spot towards improving the accuracy of designs performed by engineers and specialists.

The paper is arranged as follows: Section II reviews the derivations of the governing partial differential equations in magnetostatics. In section III, the spatial approximation to these equations is presented by SEM. A typical demonstration is discussed and presented in section IV, and finally, some conclusions and future works associated with the interest of this paper is introduced in the last section.

2. Problem Formulation

Magnetostatic problems is a special case of electromagnetic problems. In a magnetostatic problem, where only magnetic fields in a given structure are solved, the currents are steady or said to be time-invariant.

Gauss's law for magnetism and Ampere's law are expressed respectively in a differential form as,

$$\nabla \cdot \vec{B} = 0 \tag{1}$$

$$\nabla \times \vec{H} = \vec{J} \tag{2}$$

in which $\vec{J}$ stands for the injected current density, $\vec{B}$ is the vector field of the magnetic flux density, and $\vec{H}$ is the field intensity, and are related as $\vec{B} = \mu\vec{H}$, with μ being the magnetic permeability. Due to helmhotz decomposition theorem, the magnetic flux density has a unique potential vector, $\vec{A}$, such that:

$$\vec{B} = \nabla \times \vec{A} \tag{3}$$

By substituting equation (3) in (2), the following differential equation is obtained:

$$\nabla \times \left(\frac{1}{\mu} \nabla \times \vec{A} \right) = \vec{J} \tag{4}$$

Since the magnetic material is assumed to be homogeneous, μ can be out of differentiation, and one can rewrite equation (4) as:

$$\nabla \left(\nabla \cdot \vec{A} \right) - \nabla^2 \vec{A} = \mu \vec{J} \tag{5}$$

in which ∇^2 stands for the vector Laplacian. With the choice of the gauge:

$$\nabla \cdot \vec{A} = 0 \tag{6}$$

equation (5) leads to Poisson equation:

$$\nabla^2 \vec{A} = \mu \vec{J} \tag{7}$$

In two dimensional Cartesian coordinates (2D), if $\vec{J} = J_z(x, y)\hat{a}_x$, then $\vec{A} = A_z(x, y)\hat{a}_z$ meaning that the solution is sought for the z-component only, i.e., let the scalars A, J be $A = A_z(x, y)$ and $J = J_z(x, y)$. Therefore, equation (7) reads as:

$$\frac{\partial^2 A}{\partial x^2} + \frac{\partial^2 A}{\partial y^2} = \mu J \tag{8}$$

and it must be satisfied in magnetic materials where currents flow, whereas the following equations:

$$\frac{\partial^2 A}{\partial x^2} + \frac{\partial^2 A}{\partial y^2} = \mu_0 J \tag{9}$$

$$\frac{\partial^2 A}{\partial x^2} + \frac{\partial^2 A}{\partial y^2} = 0 \tag{10}$$

in a coil region and in air, respectively.

The application of boundary conditions is important in order to provide unique solution of the partial differential equations. In magnetic and electrostatic problems, there are some boundary conditions that are commonly used [16]. Dirichlet boundary condition defines the value of potential explicitly on boundary. In fact, in most of magnetic problems, zero Dirichlet condition is introduced.

However, in Neumann boundary condition, the normal derivative of potential along the boundary is defined. In magnetic problems, the derivative of magnetic potential is set to zero along the boundary so that magnetic flux is forced to pass the boundary at 90˚ angle [16].

There is another boundary condition called Robin boundary condition that combines Dirichlet and Neumann boundary conditions. It describes the value of vector potential and its normal derivative at boundary. Whereas in Periodic boundary conditions, two boundaries are both joint together.

3. Spectral Element Method Formulation

Patera [8] offered a spectral element method which utilizes flexibility of finite element method and accuracy spectral method. There are mainly two techniques that are utilized in spectral element method. One depends on Chebyshev polynomials, and the other is based on Legendre polynomials. Both implementations employ Gauss-Labatto quadrature grid (GLL) in order to achieve Langrangian interpolation.

In the current study, we apply SEM based on Legendre polynomials as being test functions, and Gauss-Lobatto-Legendre quadrature grids in order to perform Lagrangian interpolation [8-9, 17].

We seek an approximate solution to the presented set of partial differential equations in the trial space

$$A = \left\{ A_z \in H \mid A_z\big|_{\partial\Omega_D} = f_{bc}, \quad \tfrac{\partial}{\partial n} A_z\big|_{\partial\Omega_N} = g \right\} \tag{11}$$

The residual resulting from the substitution of the approximate solution from the trial space into equations (8)-(10) is then projected onto the test space:

$$V = \{ v \in H \big| v\big|_{\partial\Omega_D} = 0 \} \tag{12}$$

The projection is performed by using the weighted inner product operation:

$$\left(v, A_z \right)_\omega \equiv \int_\Omega \omega \bar{v} A_z d\mathbf{x} \tag{13}$$

in the Hilbert space H where overbar denotes complex conjugation. The projection procedure

$$(\mathrm{v}, \nabla^2 A_z - \mu J_z)_\omega = 0 \tag{14}$$

and the variational (weak) form is obtained as (after integration by parts):

$$\int_\Omega \nabla(\omega \bar{\mathrm{v}}) \cdot \nabla A_z \, \mathrm{dx} - \mu J_z \int_\Omega \omega \bar{\mathrm{v}} \, \mathrm{dx} = \int_{\partial\Omega_N} \omega \bar{\mathrm{v}} \, \mathrm{g} \, \mathrm{dx} \tag{15}$$

Adapting the formulation to arbitrary domain geometry is achieved in two steps. The first involves partitioning of the domain into M-mutually disjoint elements:

$$\Omega = \Omega^1 \cup \ldots \cup \Omega^e \ldots \cup \Omega^M = \bigcup_{e=1}^{M} \Omega^e. \tag{16}$$

A typical integral in the variational form then becomes

$$\int_\Omega \omega \bar{\mathrm{v}} \, \mathrm{A}_z \, \mathrm{d}\mathbf{x} = \sum_{e=1}^{M} \int_{\Omega^e} \omega \bar{\mathrm{v}} \, \mathrm{A}_z \, \mathrm{d}\mathbf{x}, \tag{17}$$

The second step is to introduce the standard square element

$$\Omega^{\mathrm{std}} = \left\{ (\xi, \eta) \in \Re^2 \;\middle|\; -1 \le \xi \le 1, -1 \le \eta \le 1 \right\} \tag{18}$$

that will standardize and facilitate the integral operations over a general quadrilateral element Ω^e through mapping:

$$\mathrm{x} = \chi_1^e(\xi, \eta), \quad \mathrm{y} = \chi_2^e(\xi, \eta). \tag{19}$$

The operations can then be converted using the rules:

$$\begin{bmatrix} \mathrm{dx} \\ \mathrm{dy} \end{bmatrix} = \underbrace{\begin{bmatrix} \frac{\partial \chi_1^e}{\partial \xi} & \frac{\partial \chi_1^e}{\partial \eta} \\ \frac{\partial \chi_2^e}{\partial \xi} & \frac{\partial \chi_2^e}{\partial \eta} \end{bmatrix}}_{\mathbf{J}} \begin{bmatrix} \mathrm{d}\xi \\ \mathrm{d}\eta \end{bmatrix} \tag{20}$$

$$\nabla = \begin{bmatrix} \frac{\partial}{\partial \mathrm{x}} \\ \frac{\partial}{\partial \mathrm{y}} \end{bmatrix} = \frac{1}{|\mathbf{J}|} \begin{bmatrix} \frac{\partial \chi_2^e}{\partial \eta} & -\frac{\partial \chi_1^e}{\partial \eta} \\ -\frac{\partial \chi_2^e}{\partial \xi} & \frac{\partial \chi_1^e}{\partial \xi} \end{bmatrix} \begin{bmatrix} \frac{\partial}{\partial \xi} \\ \frac{\partial}{\partial \eta} \end{bmatrix}, \tag{21}$$

where $|\mathrm{J}|$ is the determinant of the Jacobian.

The associated roots ς_m as nodes provide the stable form of interpolation

$$A_z(\varsigma) = \sum_{m=0}^{N} A_z(\varsigma_m) L_m(\varsigma) \tag{22}$$

where L denotes respective Lagrange interpolants with the typical form

$$L_k(\varsigma) = \prod_{\substack{\ell=0 \\ \ell \neq k}}^{N} \frac{(\varsigma - \varsigma_\ell)}{(\varsigma_k - \varsigma_\ell)} \tag{23}$$

satisfying the cardinality property $L_k(\varsigma_\ell) = \delta_{k\ell}$. This provides the means for evaluating the derivatives,

$$\frac{d}{d\varsigma} A_z(\varsigma)\Big|_{\varsigma_k} = \sum_{m=0}^{N} A_z(\varsigma_m) L'_m(\varsigma_k) = \sum_{m=0}^{N} A_z(\varsigma_m) \underbrace{L'_m(\varsigma_k)}_{D_{km}} \tag{24}$$

where D_{km} stands for the differentiation matrix. It also provides Gauss-Legendre-Lobatto (GLL) quadrature

$$\int_{-1}^{1} A_z(\varsigma)\, d\varsigma = \sum_{k=0}^{N} \varpi_k A_z(\varsigma_k) \tag{25}$$

These can easily be extended to two dimensions over the tensor grid (ξ_k, η_ℓ) with the mapping functions $\chi_i(\xi, \eta)$ constructed by using the linear blending function approach [9, 18]. It is noteworthy to mention that MATLAB was utilized in the numerical implementation of the SEM formulation.

It is more an art experience than a science to know how to optimally place and size the mesh in the FEM. In fact, experience taught us to have more elements in the physical domain where functions change rapidly and have less elements where low gradients are expected. Mesh generation may take several trials before achieving a good mesh distribution. On the other hand, the complexity in the physical domain itself may add additional limitations on mesh generation [19].

In contrast, SEM has the flexibility of using larger elemental aspect ratio without significant deterioration in accuracy. For instance, but not limited to, S. Dong et al. [20] proposed a parallel SEM for dynamic three-dimensional nonlinear elasticity problems that provides a tolerant large elemental aspect ratio employing Jacobi

polynomial-based shape functions, as an alternative to the typical Legendre polynomial-based shape functions in solid mechanics. D. Rh. Gwynllyw et al. [21] proposed an iterative method for moving SEM applied to the journal bearing problem where they investigated the results of extremely large physical aspect ratio. In conclusion, the basis behind the mesh optimality in the case of SEM differs from that of FEM case. But yet, since this topic is an important aspect and as it doesn't lie within the scope of the current study, the authors will discuss and investigate mesh optimality by SEM in a future work because of the limitation on the paper length.

4. Simulation results

In order to verify the formulation of the spectral element method adapted in the current study, a typical magnetic problem is considered in time-invariant domain. The structure is composed of a steel core having two windows as shown in Figure 1. A coil is place on the middle leg and carries the electric current. The dimensions of the structure is chosen so that the magnetic flux flowing in the middle leg is shared equally between left leg and right leg.

As the problem is unbounded in nature, one needs to truncate it so that it becomes computationally feasible. For this purpose, we assigned Dirichlet boundary condition ($A = 0$) on the exterior boundary which is placed at a distance equals to twice of the width of an outer leg. In fact choosing $A = 0$ will not affect on the solution as the magnetic flux density is calculated based on the change in the vector potential as:

$$B_x = \frac{\partial A}{\partial y}, \text{ and } B_y = \frac{\partial A}{\partial x}. \tag{26}$$

The governing differential equations to be satisfied in each region have derived and stated in Section 2. However, in order to solve it, the problem requires interface conditions that must hold between adjacent regions (as air-core interference). This condition is satisfied by specifying the value of the normal component of

$$\hat{n}.(\frac{1}{\mu}\nabla A) \tag{27}$$

on the boundary. This is equivalent to specifying the tangential value of the magnetic field intensity on the boundary.

The computational domain as pointed earlier in this study has be discretized into elements. Figure 2 shows the elements composing the computational domain and the

Gauss-Legendre-Lobatto grids in each element. In this figure, the dark grey region represents the core, whereas the coil is represented by light grey regions. As it can be seen from the figure, meshing in spectral element method is similar to that of finite element method. In other words, the elements are getting larger and larger as we move away from the critical regions. In Figure 3, we share the solution of the vector magnetic potential in the domain. The corresponding injected current is $10\,\mathrm{A/mm^2}$ and at a core relative magnetic permeability of 2000 H/m. The associated contour plot is shown in Figure 4. As it can be clearly seen from the figure, flux density in the air is almost zero. The reason is because of the relatively high magnetic permeability defining the steel.

It is worthy to note that since our problem is symmetrical around x-axis, the computational domain is reduced to half. To account for this symmetry, Neumann boundary condition has to be applied, i.e.

$$\frac{\partial A}{\partial y} = 0 \tag{28}$$

In this work, continuous galerkin method is adapted, this means that nodes that lie on the boundaries of an element must be same as those corresponding to adjacent elements. On other hand, one can use discontinuous galerkin method, in this case Riemann solvers must be utilized in order to match the solution at the interfaces between elements [22].

For purpose of comparison, the same structure introduced in Figure 1 is solved by FEM as shown in Figure 5 in which triangular elements are used to discretize the computational domain. The contours of the magnetic vector potential are also presented on the same figure. Figure 6 presents the magnetic field density (B) as obtained by SEM and FEM across the points forming the line ab shown in Figure 5. The average of B is about 35.4 Tesla. As it can be seen from Figure 6, SEM shows smoother variation in B and symmetric around x = 0. The maximum difference between SEM and FEM results is around 1.12%. However, although this is acceptable in terms of engineering point of view, one should not forget the other advantages of SEM from the view of computational aspects. Although triangular elements can be utilized by SEM as investigated by [23], but since it adds more complexity to numerical implementation, our study is based on the application of quadrilateral elements with straight or curved sides as GLL is considered for nodal distribution. Some examples of these quadrilateral elements are shown in Figure 7. This flexibility

in the shapes of SEM elements can be utilized in meshing complex geometries where different scattering objects of arbitrary shapes are involved. Finally, we show in Figure 8 a typical GLL nodes distribution in a curved sided quadrilateral element which can also be utilized by SEM.

Based on the formulation presented in the current study, the resulting system after discretized by spectral element method is complex valued. In other words, both the real part and the imaginary part of the unknowns must be solved. This system is linear, sparse, symmetric, indefinite and relatively ill-conditioned. Hence, solving this system requires an iterative method, and to efficiently solve it, a suitable preconditioner must be applied. Conjugate Gradient (CG) method or the Generalized Minimum Residual (GMRES) can be utilized with Jacobi, ILU decomposition, or successive over relaxation as a preconditioner.

5. Conclusion

In this study, we have presented, for the first time, the formulation of a typical magnetostatic problem by the spectral element method. In addition, we have provided to the reader a typical simulation example showing the successful application of the method. Although the adapted formulation is based on continuous galerkin approach, it is also possible to utilize the discontinuous approach.

As pointed throughout the paper, the spectral element method offers higher accuracy than the traditionally applied finite element method. Moreover, it has less computational cost. The latter advantage is very valuable when dealing with large computational problems that cannot be performed sometimes because of limited available memory.

6. References

[1] Umashankar K, Allen T. Computational electromagnetics. Norwood, MA, USA, Artech House on Demand, 1993.

[2] Lee J, Xiao T, Liu QH. A 3-D spectral-element method using mixed-order curl conforming vector basis functions for electromagnetic fields. IEEE T Microw Theory 2006; 54-1: 437-444.

[3] Lee J, Liu QH. A 3-D spectral-element time-domain method for electromagnetic simulation. IEEE T Microw Theory 2007; 55-5: 983-991.

[4] Mahariq I, Kurt H, Kuzuoğlu M. Questioning degree of accuracy offered by the spectral element method in computational electromagnetics. Appl Comput Electrom 2015; 30: 698-705.

[5] Causon DM, Mingham CG. Introductory finite difference methods for pdes. Frederiksberg, Denmark, Ventus Publishing Aps, 2010.

[6] Biro O, Preis K, Richter KR. On the use of the magnetic vector potential in the nodal and edge finite element analysis of 3D magnetostatic problems. IEEE T Magn; 1996: 32: 651-654.

[7] Chau K, Jiang J, Zhang D. A finite element-analytical method for electromagnetic field analysis of electric machines with free rotation. In: IEEE 2006 International Magnetics Conference; 8-12 May 2006; San Diego, CA: IEEE. pp. 495-496.

[8] Patera AT. A spectral element method for fluid dynamics: Laminar flow in a channel expansion. J Comput Phys 1984; 54: 468-488.

[9] Deville MO, Fischer PF, Mund EH. High-order methods for incompressible fluid flow. Cambridge, UK, Cambridge University Press, 2002.

[10] Sjögren M. Comparison of spectral element and finite difference methods for electromagnetic wave propagation over a material discontinuity. Swedish Defence Research Agency Stockholm. FOI-R--0489—SE. Sci. Rep. 2002.

[11] Airiau S, Azaïez M, Belgacem FB, Guivarch R. Parallelization of spectral element methods. In: High Performance Computing for Computational Science – VECPAR; 26-28 June 2002; Porto, Portugal: Lect Notes Comput Sc. pp. 392-403.

[12] Keller R, Kramer D, Weiss JP. Facing the multicore-challenge III. Berlin, Germany: Springer, 2013.

[13] Steele CW. A spectral method for field computation. IEEE T Magn 1983; 19: 2296-2299.

[14] Mehdizadeh OZ, Paraschivoiu M. Investigation of a two-dimensional spectral element method for Helmholtz's equation. J Comput Phys 2003; 189: 111-129.

[15] Mahariq I, Kurt H, Tarman H, Kuzuoğlu M. Photonic nanojet analysis by spectral element method. IEEE Phot J 2014; 6.5: 1-14.

[16] Dede E, Ercan M, Jaewook L, Nomura T. Multiphysics simulation: electromechanical system applications and optimization. London, UK: Springer, 2014.

[17] Karniadakis G, Sherwin S. Spectral/hp elements methods for computational fluid dynamics. Oxford University Press, 2007.

[18] Gordon JW, Hall AC. Transfinite element methods: blending-function interpolation over arbitrary curved element domains. Numerische Mathematik, Germany: Springer, 1973.

[19] Pepper DW, Heinrich JC. Finite element methods: basic concepts and applications. 1st ed. Boca Raton, FL, USA: CRC Press, 1992.

[20] Dong S, Yosibash Z. A parallel spectral element method for dynamic three-dimensional nonlinear elasticity problems. Comput Struct 2012; 87: 59-72.

[21] Gwynllyw DR, Phillips TN. Iterative methods with dynamic preconditioning for moving spectral element technique applied to the journal bearing problem. In: Proceedings of the third international conference on spectral and high order methods; 5-9 June 1995; Houston, USA: Houston J Math. pp. 277-286.

[22] Lee J, Chen J, Liu Q. A 3-D discontinuous spectral element time-domain method for Maxwell's equations. IEEE T Antenn Propag 2009; 57: 2666–2674.

[23] Sherwin SJ, Karniadakis GE. A triangular spectral element method; applications to the incompressible Navier-Stokes equations. Comput Method Appl M 1995; 123: 189-229.

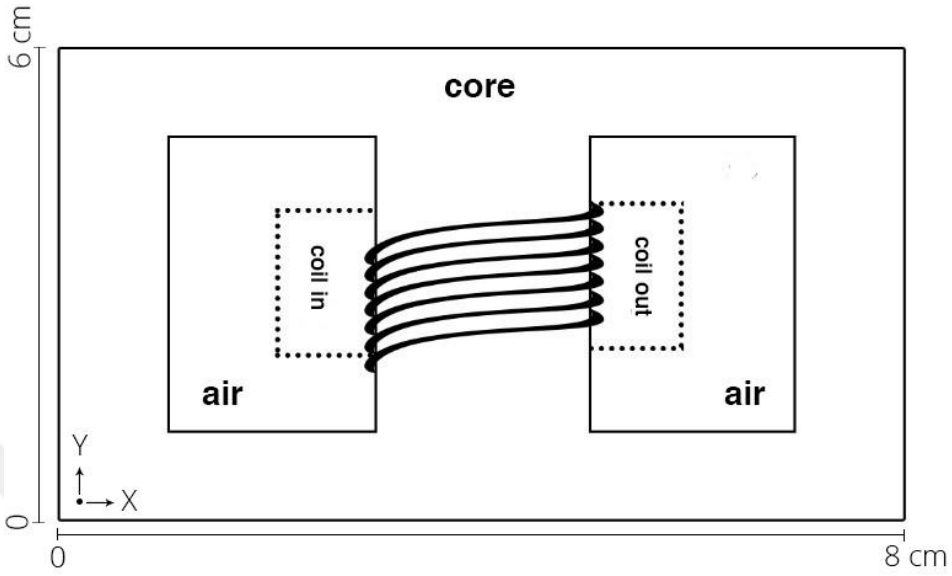

Figure C.1: The structure of the simulated problem.

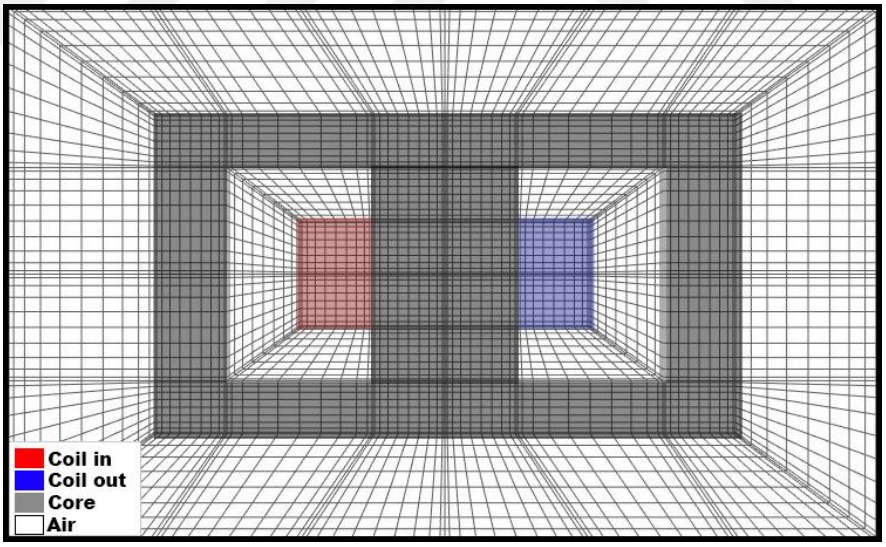

Figure C.2: Gauss-Legendre-Lobatto grids in the elements forming the computational domain.

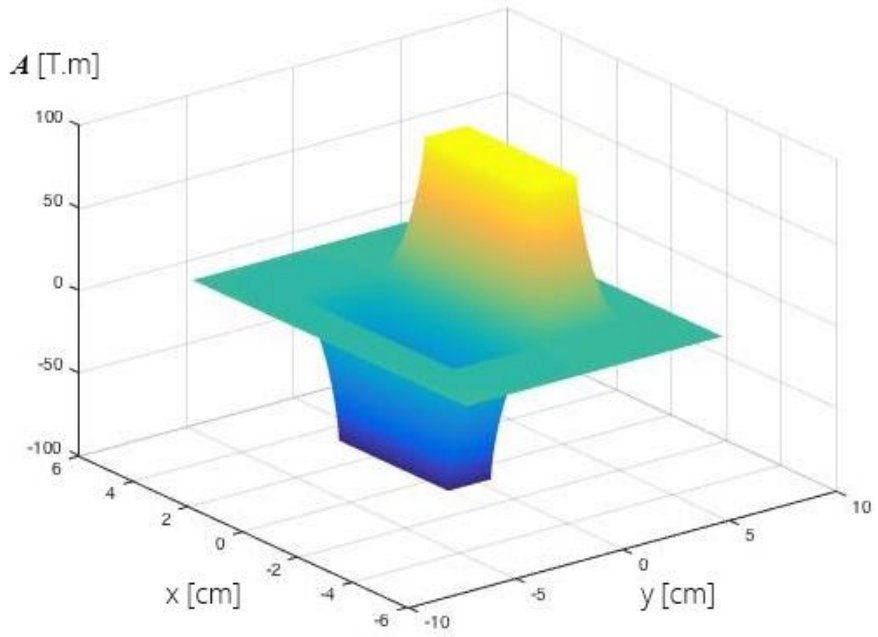

Figure C.3: The solution of the vector magnetic potential.

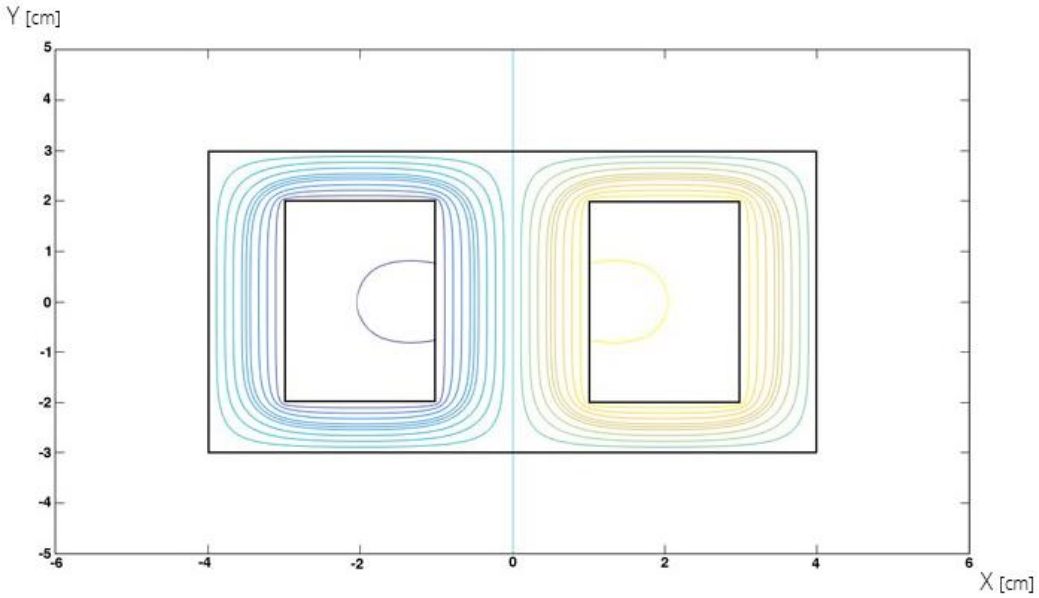

Figure C.4: The contour plot of the vector magnetic potential.

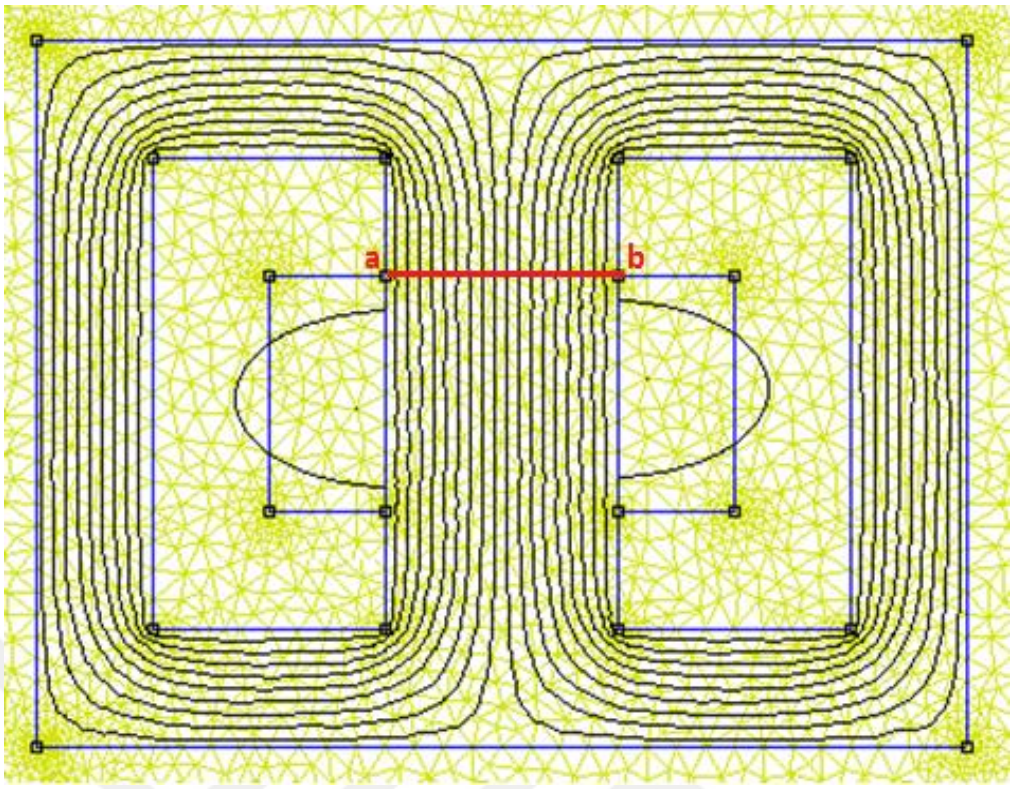

Figure C.5: Meshing and contour plots by FEM.

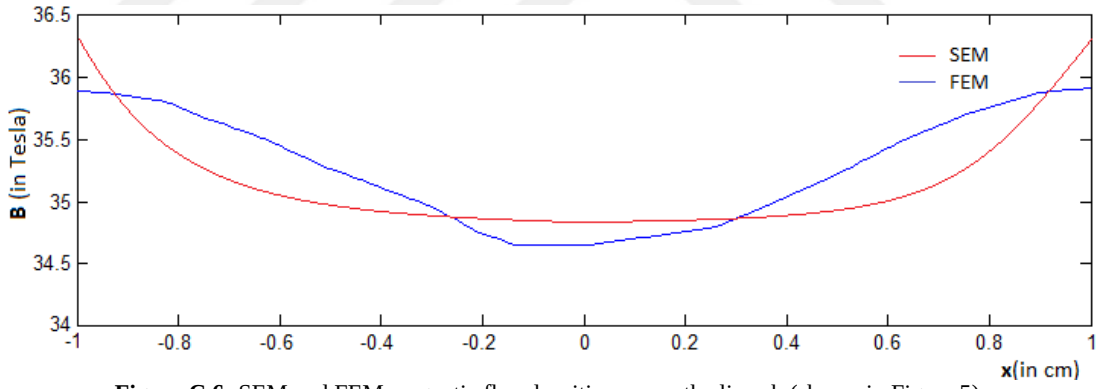

Figure C.6: SEM and FEM magnetic flux densities across the line ab (shown in Figure 5).

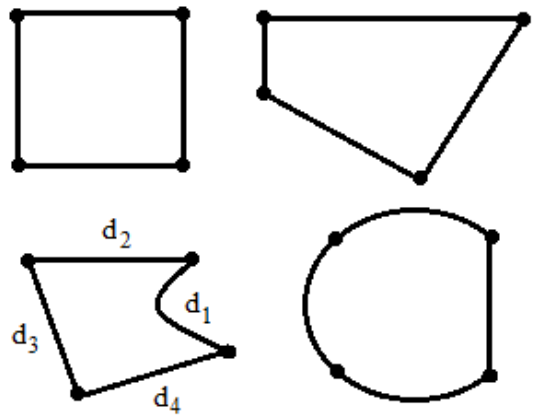

Figure C.7: Various quadrilateral elements can be utilized by SEM.

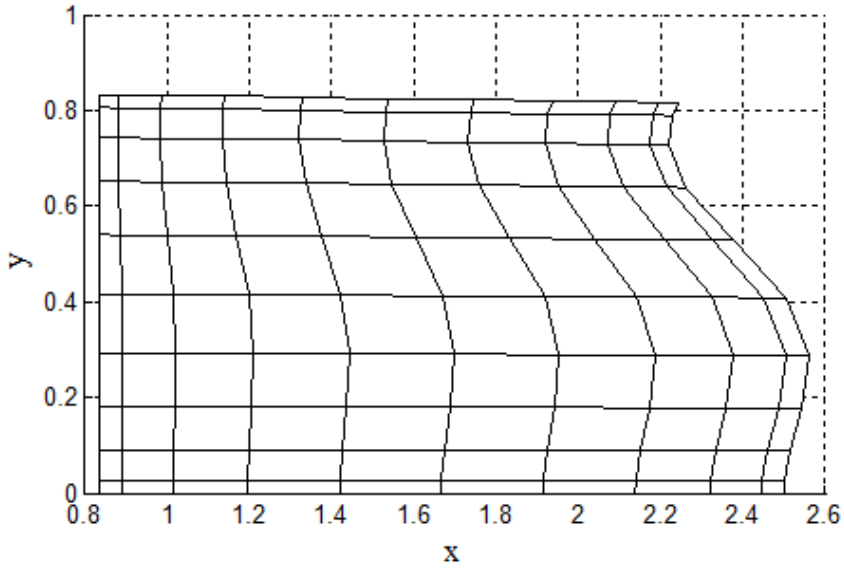

Figure C.8: Distribtuion of GLL nodes in a curved sided quadrilateral element.

CV

PERSONAL INFORMATION

First Name / Surname	Atakan ERCIYAS
E-Mail	aercys@gmail.com
Phone	0 (312) 386 01 63
Nationality	T.C.

EDUCATION

Dates	October 2013 – January 2017
Qualification Awarded	M.Sc
Principal Studies	Electrical & Electronics Engineering
Institution	University of Turkish Aeronautical Association
Dates	September 2008 – July 2013
Qualification Awarded	B.Sc
Principal Studies	Electrical & Electronics Engineering
Institution	Sakarya University

Language Spoken

English	B2
Turkish	Native

COMPUTER SKILLS

Embedded C	Moderate
Assembly (8051&AVR)	Expert
MATLAB	Moderate
GoLang	Beginner

CERTIFICATES

IELTS	Academic Training / 6.5 (Overall)	June'16
High Voltage Tech.	Gazi University	
English	Studio Cambridge	B2

WORK EXPERIENCE

COMODO Inc.

Dates	October 2013 – May 2014
Position	Malware Analyst